Mono- and Polynuclear Ferrocenyl-derived Complexes: Synthesis, Characterisation and Biological Evaluation as Antimycobacterial and Antiplasmodial Agents

Nadia Baartzes

University of Cape Town

September 2015

Mono- and Polynuclear Ferrocenyl-derived Complexes: Synthesis, Characterisation and Biological Evaluation as Antimycobacterial and Antiplasmodial Agents

A dissertation submitted to the

University of Cape Town

In fulfilment of the requirements for the degree of

Master of Science

By

Nadia Baartzes

Department of Chemistry

University of Cape Town

Supervisor: Assoc. Prof. G. S. Smith

Co-supervisors: Assoc. Prof. D. F. Warner and Dr. T. Stringer

September 2015

Declaration

I declare that "**Mono- and Polynuclear Ferrocenyl-derived Complexes: Synthesis, Characterisation and Biological Evaluation as Antimycobacterial and Antiplasmodial Agents**" is my own work and to the best of my knowledge has never been submitted for any degree or examination in any university. All sources of information are cited, acknowledged and completely referenced.

…… 07 / 09 / 2015 …….

Miss Nadia Baartzes Date

Acknowledgements

First and foremost, I would like to express my sincerest gratitude to my supervisor, Assoc. Prof. Gregory Smith, for his guidance and support, insightful comments and constructive criticisms throughout this project. Thanks to my co-supervisor, Assoc. Prof. Digby Warner, for his assistance and helpful input in the antimycobacterial studies. A heartfelt thanks to my co-supervisor and friend Dr Tameryn Stringer, for her patience, motivation and helpful discussions, in and out of the lab. Special thanks to Ms Deirdre Brooks for her administrative assistance and constant support. I would also like to thank the Organometallic Research group for their positive contribution to this project.

I would like to acknowledge the following people for their assistance: Mr P. Roberts for the recording of NMR spectra. Mr G. Benincasa for microanalytical analyses and Electron Impact Mass Spectral analyses, Dr M Stander and Mr Fletcher Hiten (University of Stellenbosch) for Electrospray Ionisation Mass Spectral analyses, Dr Carmen de Kock (UCT Department of Clinical Pharmacology) and Mr John Okombo for conducting antiplasmodial screenings and Mrs Ronnett Seldon (Institute of Infectious Disease and Molecular Medicine) for conducting antimycobacterial screenings.

I would like to thank my parents, Waleed and Aziza Baartzes, for all the encouragement and the continuous emotional support they have provided. Thanks to my brothers, Imrhan and Rafeeq Baartzes, for putting up with me and most importantly, keeping my feet on the ground. Finally, thanks to the National Research Foundation (NRF) and the Medical Research Council (MRC) for their financial support.

Table of Contents

Chapter 2: Synthesis and characterisation of mono- and polynuclear ferrocenyl-derived imino and amino complexes

Chapter 3: Synthesis and characterisation of mono- and polynuclear ferrocenylthiosemicarbazone complexes

Chapter 4: Antimycobacterial and antiplasmodial evaluation of mono- and polynuclear ferrocenyl-derived complexes

Chapter 5: Conclusions and Future Work

Conference Contributions

Poster Presentation at the 2nd H3-D Symposium 2014, Livingstone, Zambia.
Nadia Baartzes, Digby F. Warner and Gregory S. Smith, *Towards the Development of Mono- and Polynuclear Bioorganometallic Antimycobacterial Agents.*

Poster Presentation at the SACI/RSC Western Cape Young Chemists' Symposium 2014, Cape Town, South Africa.
Nadia Baartzes, Digby F. Warner and Gregory S. Smith, *Towards the Development of Mono- and Polynuclear Bioorganometallic Antimycobacterial Agents.*

Poster Presentation at the SACI Inorganic Chemistry Conference 2015, Grahamstown, South Africa.
Nadia Baartzes, Tameryn Stringer, Digby F. Warner and Gregory S. Smith, *Synthesis and Biological Evaluation of Potential Organometallic Antimicrobial Agents.*

Abstract

Ferrocene-containing precursors, vinylferrocene and (*E*)-4-vinylferrocenylbenzaldehyde were prepared, by a Wittig olefination reaction and Heck cross-coupling reaction, respectively. Mononuclear ferrocenyl-derived imino complexes were synthesised by Schiff-base condensation reactions of (*E*)-4-vinylferrocenylbenzaldehyde with various amines. This included the preparation of a silicon-containing derivative and its carbon analogue, to determine the effect of the lipophilic moiety on the biological activity. In addition, polynuclear ferrocenyl-derived imino complexes based on the tris(2-aminoethyl)amine scaffold and the polypropyleneimine (PPI) first- and second-generation scaffolds were also synthesised using Schiff-base chemistry. These polynuclear complexes were prepared using template chemical procedures to that of the mononuclear complexes. The corresponding mono- and polynuclear ferrocenyl-derived amino complexes were synthesised via reductive amination reactions from the (*E*)-4-vinylferrocenylbenzaldehyde. The imine moiety was hydrogenated in order to compare the effect on the biological activity. The imino and amino complexes were isolated in moderate to high yields.

A second series of ferrocenyl complexes was also prepared incorporating a thiosemicarbazone moiety, as this is a known pharmacophore and may confer favourable properties in terms of biological activity as well as solubility. Methyl hydrazinecarbodithioate was synthesised and reacted with the previously synthesised (*E*)-4-vinylferrocenylbenzaldehyde by a Schiff-base condensation reaction to afford a ferrocenyl dithiocarbamate. The dithiocarbamate was reacted with various amines via nucleophilic substitution reactions to give mono- and polynuclear ferrocenylthiosemicarbazone complexes. These complexes were isolated in low to moderate yields.

All compounds were unequivocally characterised using various spectroscopic and analytical techniques, such as ^{1}H, $^{13}C\{^{1}H\}$, $^{31}P\{^{1}H\}$ Nuclear Magnetic Resonance (NMR) spectroscopy, Fourier Transform-Infrared (FT-IR) spectroscopy, elemental analysis and Electron Impact (EI)- or high resolution Electrospray Ionisation (ESI)-mass spectrometry. These methods confirmed the structural integrity of the proposed precursors and complexes.

In vitro biological evaluations were carried out using the ferrocenyl-imino, ferrocenyl-amino and ferrocenylthiosemicarbazone complexes in order to investigate their potential antimycobacterial and antiplasmodial activity. Compounds were screened for their *in vitro* activity against the H37Rv strain of *Mycobacterium tuberculosis* and the chloroquine-sensitive (CQS) NF54 strain of *Plasmodium falciparum*. In the antimycobacterial evaluation, the ferrocenyl-amino complexes exhibited little to no activity compared to the ferrocenyl-imino complexes, which displayed moderate activity, giving minimum inhibitory concentration (MIC_{90}) values in the micromolar range. The trinuclear imino complex displayed the highest activity of the series, with an MIC_{90} value two-fold greater than that of

ethambutol, a clinically available anti-TB drug. The higher generation polynuclear complexes (n = 4, 8) could not be screened for antimycobacterial activity as they were not soluble at the tested concentration. The ferrocenylthiosemicarbazones, which displayed greater solubility than the imino and amino complexes, could all be tested and were also found to exhibit moderate antimycobacterial activity. The mononuclear complex and the octanuclear complex displayed the highest activity of this series. The incorporation of the pharmacologically active thiosemicarbazone moiety resulted in enhanced activity compared to the amino complexes, but decreased activity compared to the imino complexes.

In the antiplasmodial screening against the NF54 strain of *P. falciparum*, the ferrocenyl-imino complexes displayed moderate antiplasmodial activity, with the octanuclear ferrocenyl-imino complex showing the best activity of the series. The mononuclear ferrocenylthiosemicarbazone complex displayed enhanced activity compared to the imino complexes. The ferrocenyl-amino complexes exhibited the best activity in the antiplasmodial screening, displaying IC_{50} values in the low micromolar range. The most active complex was the silicon-containing mononuclear derivative, which showed enhanced activity compared to its carbon analogue. The ferrocenylthiosemicarbazone complexes were also moderately active against *P. falciparum*, the mono- and trinuclear complexes exhibiting the highest activity of the series. As seen in the antimycobacterial screening, the thiosemicarbazone complexes were not the most active in the antiplasmodial screening. These complexes exhibited enhanced activity compared to the imino complexes and decreased activity compared to the amino complexes.

Abbreviations

%	percent
°C	degrees Celsius
ACT	artemisinin-based combined therapy
ATR	Attenuated Total Reflection (infrared spectroscopy)
br	broad (NMR)
cm^{-1}	reciprocal centimeters
COD	1,5-cyclooctadiene
COSY	Correlation Spectroscopy
CQ	chloroquine
CQR	chloroquine-resistant
CQS	chloroquine-sensitive
d	doublet (NMR)
DCM	dichloromethane
dd	doublet of doublets
Dd2	CQR *P. falciparum* strain
DMF	dimethylformamide
DMSO	dimethylsulfoxide
EA	elemental analysis
EI	Electron Impact
EMB	Ethambutol
ESI	Electrospray Ionisation
Fc	ferrocenyl
FT-IR	Fourier Transform-Infrared
HPLC	high pressure liquid chromatography
Hz	hertz
IC_{50}	compound concentration causing 50% inhibition of parasitemia
IR	infrared
INH	Isoniazid
J	coupling constant
KBr	Potassium bromide
Lit	Literature

m	multiplet (NMR)
M.p.	melting point
m/z	mass-charge ratio
mM	millimolar
MS	mass spectrometry
ND	Not Determined
NF54	CQS *P. falciparum* strain
NMR	Nuclear Magnetic Resonance
PAMAM	poly(amidoamine)
POT	tri-*o*-tolylphosphine
PPh_3	triphenylphosphine
PPI	poly(propylene)imine
ppm	parts per million
PZA	Pyrazinamide
r.t.	room temperature
s	singlet (NMR)
t	triplet (NMR)
TMS	tetramethylsilane
µg	microgram
µM	micromolar
W2	CQR *P. falciparum* strain

Chapter 1

Introduction and brief overview of metal-based antimycobacterial and antiplasmodial chemotherapies

1.1 Problem Identification

Microorganisms or microbes refer to single or multicellular microscopic organisms such as bacteria, viruses, fungi and the protozoa. Microbial diseases are caused (in humans or animals) by the introduction of one of these four organisms. Examples of such infectious diseases are tuberculosis (bacterial), malaria (protozoan), HIV/AIDS (viral), meningococcal meningitis (bacterial) and cholera (bacterial), which are all high priority diseases of the World Health Organisation (WHO) due to their worldwide burden.[1] Malaria and tuberculosis remain a major global health problem affecting the developing world, causing an estimated 2 million deaths worldwide in 2012.[2, 3]

Effective antituberculosis (anti-TB) and antimalarial treatments are known and are currently in use. However, the nature of microbes, by which they undergo random and specific mutations in order to survive, allows them to develop resistance to these treatments. This diminishes the efficacy of current treatments and these diseases remain prevalent and continue to spread. The emergence and spread of drug-resistant parasites is a major threat to disease control and new drug therapies and drug design strategies are required to overcome this resistance and combat microbial diseases.

1.2 Tuberculosis

1.2.1 Transmission and Worldwide Burden

Tuberculosis (TB) is an infectious bacterial disease caused by the bacillus *Mycobacterium tuberculosis* (*M. tuberculosis*), typically infecting the lungs in the form of pulmonary TB. This bacterial pathogen caused 8.6 million new TB cases and 1.3 million TB deaths globally in 2012, and remains a major global health problem of great importance to the World Health Organisation (WHO).[3] Fig. 1.1 shows the estimated TB incidence rates in 2012.

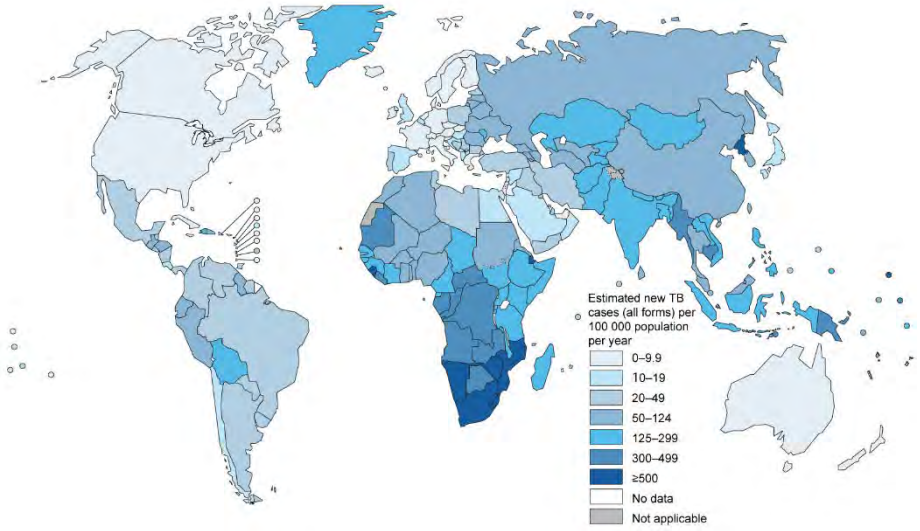

Fig. 1.1: Estimated TB incidence rates in 2012.[3]

1.2.2 TB Disease Pathogenesis

Tuberculosis spreads with great ease, through the air, when people who are infected with active pulmonary TB expel bacteria. Inhalation of as little as a few droplet nuclei, 2 – 5 μm in diameter, containing as few as 1 – 3 tubercle bacilli is enough to result in the spread of TB infection.[4] Infection occurs when these tubercle bacilli reach the alveoli of the lungs, where alveolar macrophages ingest the bacilli.[5] An immune response is triggered and other white blood cells kill or encapsulate bacilli, forming a barrier shell called a granuloma, which keeps the bacilli under control. The majority of tubercle bacilli are then destroyed or inhibited.[5] This process of inhibition of multiplication of the bacilli and halting of disease progression results in latent tuberculosis infection (LBTI).[4, 5] However, if the immune system cannot keep the tubercle bacilli under control, some of the bacilli begin to multiply rapidly inside the macrophage (intracellularly), and TB disease has commenced. Ultimately the granuloma ruptures and spills many viable and infectious bacilli.[5] Some of these bacilli may enter the lymphatic channels or the bloodstream and spread throughout the body to distant tissues and organs, particularly to the lymph nodes, apex of the lung, kidneys, brain and bone, where TB disease is most likely to develop.[5] This process of dissemination triggers a further immune response and granulomas form at the tissues and organs where the bacilli have spread, allowing LTBI to be reestablished. Nevertheless, TB disease pathogenesis can occur at these areas as well in response to an inadequate immune response.

1.2.3 Standard anti-TB drugs

The first effective drug in the treatment of tuberculosis infections was the aminoglycoside antibiotic streptomycin. Initially used in monotherapy, streptomycin was quickly rendered less effective due to mycobacterial resistance to the drug. Other drugs, such as the antibiotic para-aminosalicylic acid and

the nicotinamide analogue isoniazid, were also discovered to be active against *Mycobacterium tuberculosis*. Thus, 'triple therapy' was introduced, incorporating all three drugs in one regimen, over a period of twenty-four months. Over time, new classes of antimycobacterial drugs have been incorporated into the combination therapy in order to overcome resistance and shorten the duration of treatment. In addition, there are a number of other effective anti-TB drugs which are used as second-line treatments or as cheaper alternatives. These include cycloserine, fluoroquinolones and the thiosemicarbazone-based thiacetazone.

The current and most effective anti-TB therapy for drug-susceptible (DS)-TB comprises a six-month four-drug regimen.[3, 4] Treatment involves the use of isoniazid, rifampicin, pyrazinamide and ethambutol as an initial phase for the first two months.[3, 4] This is followed by a continuation phase of only isoniazid and rifampicin for the last four months.[3, 4] All four drugs, whose structures are shown in Fig. 1.2, have different mechanisms of action, and all inevitably inhibit the growth of *M. tuberculosis*.[4, 6] Isoniazid and pyrazinamide are prodrugs, which means that they are administered in an inactive or less active form, and converted to the active form (activated) internally through a normal metabolic process. [4, 6]

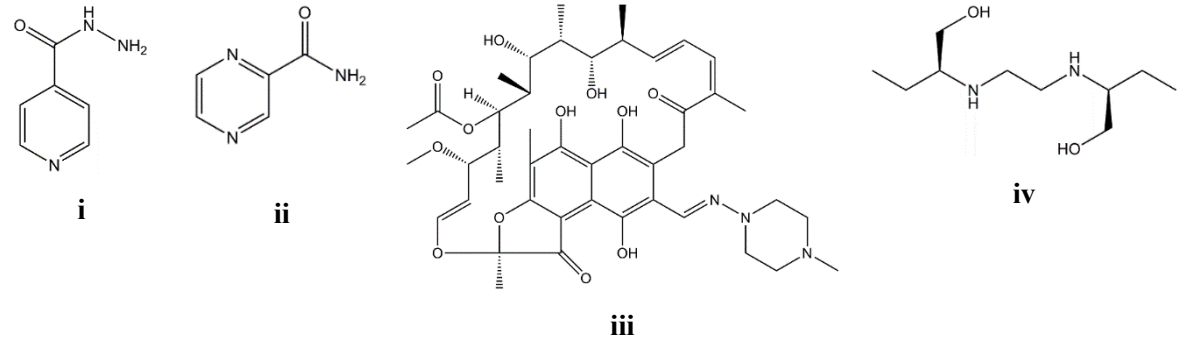

Fig. 1.2: Structures of drugs used in tuberculosis treatment i) isoniazid ii) pyrazinamide iii) rifampicin iv) ethambutol.

Isoniazid (INH) enters the mycobacterial cell by passive diffusion through small water-filled pores in the cell membrane.[7, 8] Here, INH undergoes oxidative activation by a catalase peroxidase to an isonicotinoyl radical, the active metabolite.[7-10] These radicals react with co-factors to give INH-adducts, which inhibit the synthesis of nucleic acids, phospholipids and most importantly and mycolic acids.[7-10] Pyrazinamide (PZA), which is structurally similar to INH, gains access to the cell through passive diffusion as well as via ATP-dependent transport systems.[8, 10] PZA is converted to its active form, pyrazinoic acid, by the pyrazinamidase enzyme. The mechanism of action of PZA is poorly understood, however, it is known to target semi-dormant tubercle bacilli present in acidic environments, resulting in reduced relapse rates in TB infections.[8, 10]

Rifampicin, being highly lipophilic in nature, easily diffuses across the cell membrane.[8] The drug then binds to the mycobacterial DNA-dependent RNA polymerases with high affinity, thus inhibiting mRNA

synthesis.[8, 10] Ethambutol (EMB) is known to inhibit many cellular pathways of *M. tuberculosis*, such as mycolic acid transport, phospholipid synthesis, RNA metabolism and spermidine biosynthesis.[8, 10] However, the target crucial to its antimycobacterial activity is the inhibition of arabinogalactan biosynthesis, an important structural component of the cell wall. This is achieved by prevention of arabinan polymerisation.[8, 10]

1.2.4 Mycobacterial drug-resistance

The four-drug regimen of isoniazid, pyrazinamide, rifampicin and ethambutol as an anti-TB treatment is highly effective, however, due to the ability of bacteria to undergo minor mutations coupled with the misuse of drug therapies, *M. tuberculosis* has developed resistance to some of these drugs. Thus, there are different strains of *M. tuberculosis* with varying levels of resistance. Multidrug-resistant (MDR)-TB is a strain which is resistant to the two most important first-line anti-TB drugs, isoniazid and rifampicin.[4] Extensively drug-resistant tuberculosis is resistant to isoniazid, rifampicin, all fluoroquinolones and all second-line injectable drugs.[4]

The mechanism of resistance development in *M. tuberculosis* strains against current anti-TB agents has a genetic basis.[11] An approach of gene sequencing and analysis of specific drug-resistant TB strains was used in order to determine the reason for resistance.[11] The mutated genes or mutations that are associated with resistance to specific anti-TB drugs are shown in Table 1.1.

Table 1.1: Summary of the molecular mechanisms of drug-resistance.[11]

Drug	Associated mutated gene or mutation
Isoniazid	*katC*, *inhA*, *oxyR*, *ahpC*, *furA*
Rifampicin	*rpoB*
Pyrazinamide	*pncA*, IS*6110* insertion
Ethambutol	*embB*
Streptomycin	*rrs*, *rpsL*
Fluoroquinolones	*gyrA*, *gyrB*

1.3 Malaria

1.3.1 Parasite strains and life cycle

Malaria is an infectious parasitic disease caused by protists of the Plasmodium genus and transmitted by the female Anopheles mosquito. There are five Plasmodium species that cause malaria; *P. falciparum*, *P. vivax*, *P. ovale*, *P. malariae* and *P. knowlesi*, which cause malaria of varying severities.[12-14] The life cycle of the malaria parasite requires two hosts for completion,[13] as represented in Fig. 1.3. It involves a continuous cycle of red blood cell invasion, parasite replication, cell rupture, and reinvasion. Of these different stages, the parasite is only pathogenic when it is in the host's bloodstream, known as the blood stage, which is responsible for the symptoms and deadly consequence of the disease.[13, 14]

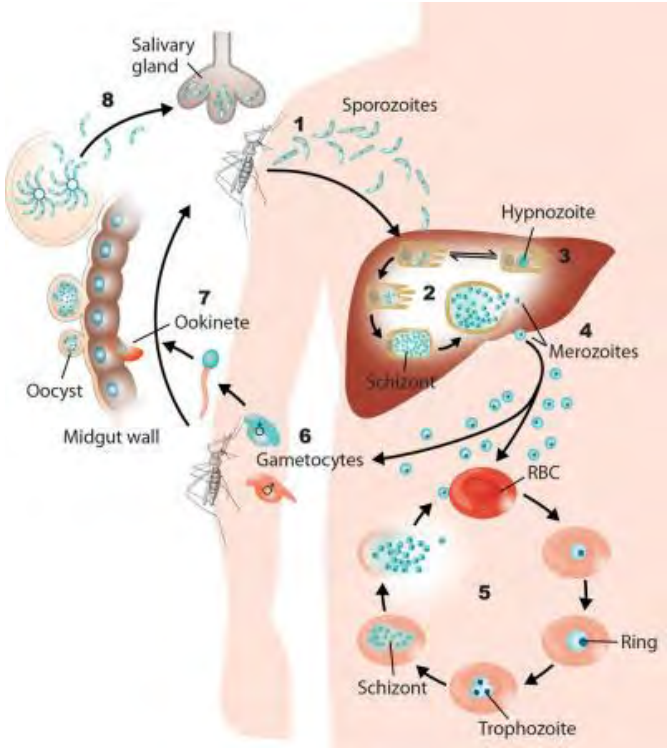

Fig. 1.3: Life cycle of the malaria parasite.[14]

1.3.2 Malaria disease pathogenesis

During the blood stage, the malaria parasites invade erythrocytes and ingest large amounts (60 – 80 %) of host cell haemoglobin in order to complete its life and survive.[13, 14] By a phagocytosis-like mechanism, the trophozoite and early shizont parasite forms ingest and transport the haemoglobin to the digestive food vacuole.[13, 14] This acidic, proteolytic organelle with a pH in the range 5.0 – 5.4 and containing a wide range of proteases, is thought to be specialised for the purpose of haemoglobin degradation.[13, 14] The proteases can be divided into four groups: aspartic proteases, cysteine proteases,

a histoaspartic protease, and a zinc metalloprotease. These enzymes catabolise the haemoglobin tetramer in a systematic manner to produce peptide fragment and ultimately generating amino acids essential for parasite survival.[13, 14] The process of haemoglobin degradation and haem detoxification is shown in Fig. 1.4.

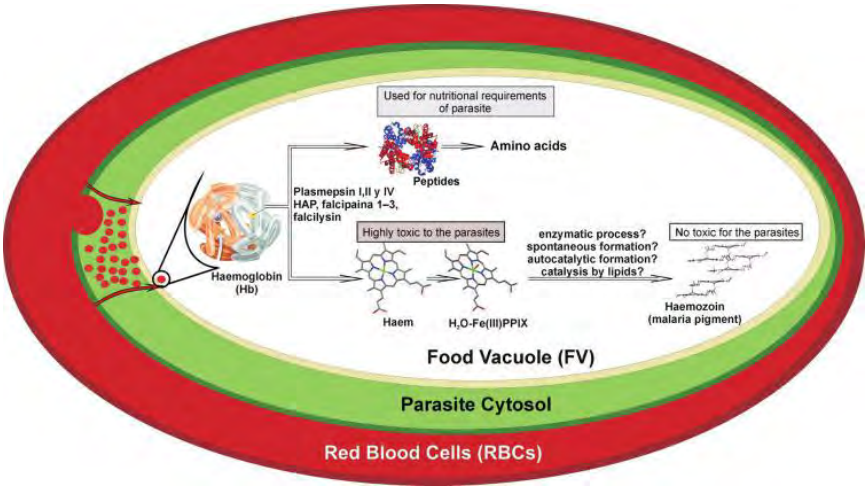

Fig. 1.4: Haemoglobin degradation and haem detoxification process by the malaria parasite.[12]

This catabolism of haemoglobin also generates free haem, the iron centre of which is oxidized from Fe^{2+} to Fe^{3+} to give aquaferriprotoporphyrin IX (H_2O-Fe(III)PPIX) as a by-product, which is toxic to the malaria parasite.[13, 14] This haem species is harmful to the parasite as it may cause enzyme inhibition, peroxidation of membranes, production of free oxygen radicals and impaired leukocyte function.[13, 14] Thus, *Plasmodium* species have developed haem detoxification mechanisms or pathways. The most important of these mechanisms is the biocrystallisation of haem to form a highly insoluble, chemically inert substance called haemozoin or malaria pigment, which accumulates in the food vacuole.[13, 14]

1.3.3 Quinoline-based drugs

In the past, treatment of malaria involved the use of quinoline-based organic drugs, with few side effects and toxicity. This includes drugs such as quinine, chloroquine, amodiaquine, piperaquine, primaquine and mefloquine (Fig. 1.5).[12-14] Within the parasite's life-cycle, quinoline-based antimalarials target the process of host cell haemoglobin catabolism to haemozoin, an important target in current antimalarial research, which takes place in the parasite's acidic food vacuole.[13, 14] Specifically, these drugs inhibit haemozoin formation, resulting in the accumulation of aquaferriprotoporphyrin IX which is toxic to the parasite.[13, 14]

However, due to widespread resistance displayed by *P. falciparum*, which causes severe malaria, these drugs have been rendered ineffective. An example of this plasmodial resistance can be seen in the

resistance to the once most effective antimalarial, chloroquine, which began to fail ten years after being put to use.[13] Though the mechanism of resistance-development is not well characterised, what is known is that the chemoresistance mechanisms generally involve chromosomal mutations.[13]

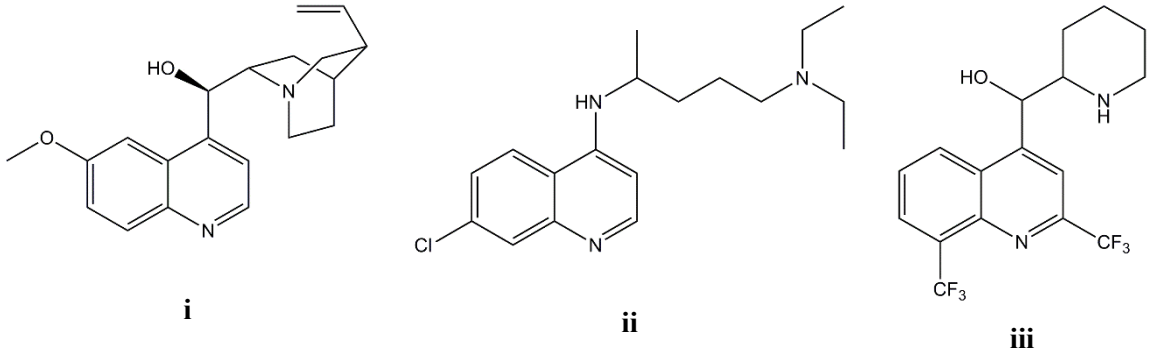

Fig. 1.5: Organic compounds used as antimalarials i) quinine ii) chloroquine iii) mefloquine.[13, 14]

1.3.4 Antifolate drugs

Another class of antimalarial drugs are the antifolates, which are formed by combinations or drug pairs composed of a sulfa drug (sulfadoxine, sulfalene or dapsone) and either pyrimethamine, proguanil or chlorproguanil, used in fixed ratio combinations.[13, 14] Antifolate drug combinations (Fig. 1.6) interfere with parasite metabolism, by specifically inhibiting the formation of folate, a substance vital for malaria parasite survival. The drug combinations incorporate a drug which is a dihydrofolate reductase (DHFR) inhibitor and another which is a dihydropteroate synthase (DHPS) inhibitor, which in turn impedes the different steps in the folate biosynthesis pathway and ultimately interferes with parasite DNA synthesis.[13-15]

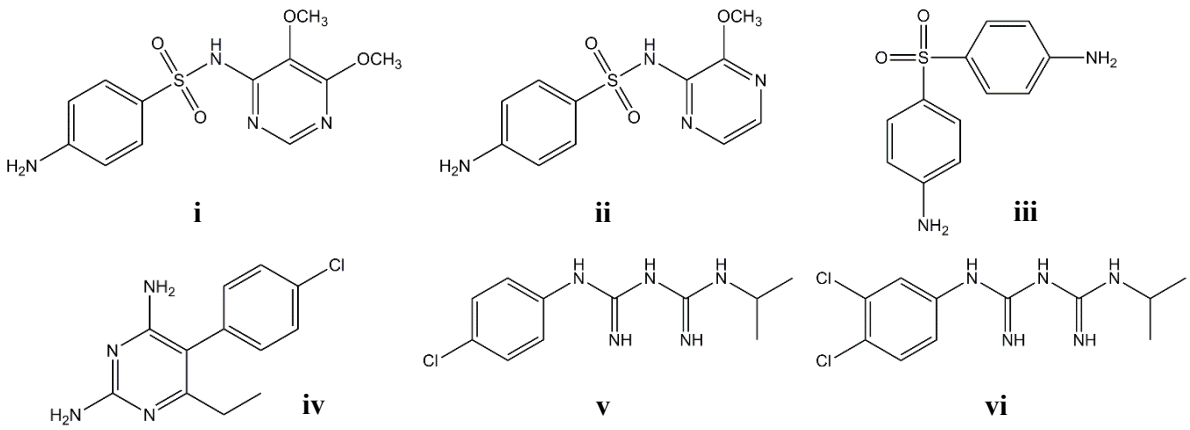

Fig. 1.6: Antifolate drugs i) sulfadoxine ii) sulfalene iii) dapsone iv) pyrimethamine v) proguanil vi) chlorproguanil.[13, 14]

These antifolate drugs have also shown susceptibility to resistant malaria parasite strains. The mechanism of resistance by the parasite is the development of point mutations in the two antifolate drug target enzymes in the folate biosynthetic pathway, DHFR and DHPS.[13, 16]

1.3.5 Artemisinin-based combination therapy

The most effective antimalarial treatment currently in use for *P. falciparum* infections is artemisinin-based combination therapy (ACT).[14, 17] Artemisinin is isolated from the Chinese sweet wormwood plant, which was traditionally used to treat fever. Artemisinin and its derivatives (Fig. 1.7) are a group of highly effective drugs, capable of rapid elimination of malaria parasites.[14, 18] ACT is therapy incorporating artemisinin or an artemisinin derivative and a second drug with a different mechanism of action, the combination of which gives enhanced efficacy, while decreasing the risk of resistance developing.[14, 18]

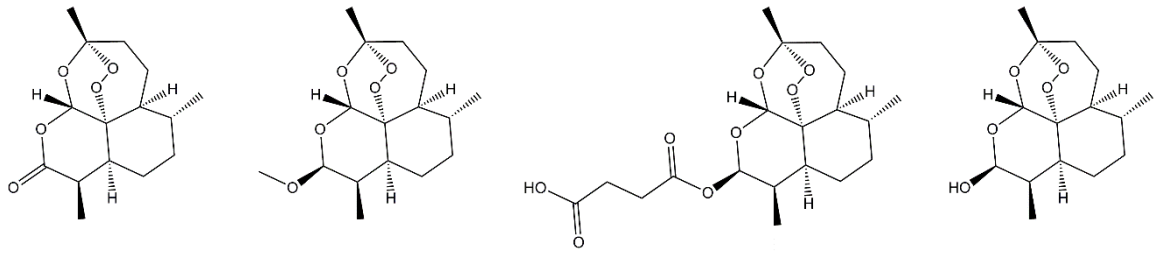

Fig. 1.7: The structures of artemisinin and derivatives used in ACT, i) artemisinin ii) artemether iii) artesunate iv) dihydroartemisinin.[14]

In contrast to quinoline-based antimalarials, artemisinin and its derivatives show antiparasitic activity at all stages of the parasite's life cycle.[19] These drugs show antiplasmodial effects in the liver stages (asexual pre-erythrocytic) and blood stages (erythrocytic), as well as in the sexual stages (by killing gametes), decreasing transmission of infection.[19] The multifaceted mode of action of these drugs may be the key to their efficiency. The exact mechanism of action is not fully understood, but the unusual peroxide bridge is thought to be essential to their antimalarial activity.[19, 20] ACT is the most widely used antimalarial treatment; however, there have recently been reports of resistance and suspected resistance to these drugs.[21-24]

1.4 Metal-based chemotherapy

1.4.1 History and Motivation

Medicinal inorganic chemistry is an interdisciplinary research field which has recently gained great interest, and involves the use of metal-based compounds as chemotherapeutic agents. Thought to have started with the discovery of Salvarsan (Arsphenamine), an arsenic-based chemotherapeutic agent used to treat syphilis,[25] the field has grown significantly due to the success of the platinum-based anticancer drug cisplatin (*cis*-diamminedichloroplatinum(II)),[26] shown in Fig. 1.8.

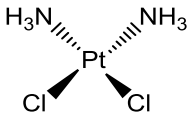

Fig. 1.8: Structure of anticancer drug, cisplatin.

Cisplatin and its second generation mononuclear derivatives, carboplatin and oxaliplatin, remain the most widely used drugs in cancer treatments, however, there are some drawbacks to their use.[27] Their high toxicity, side effects and appearance of resistance in some cell lines has led to new approaches to make compounds with unique pharmacological properties.[28-31] One such approach is the development of multinuclear complexes and an example of one such compound is Farrel's BBR3464 (Fig. 1.9).[32, 33] This complex displayed higher *in vitro* cytotoxity than cisplatin and a mechanism of action different to that of cisplatin,[32, 33] supporting the idea that multinuclearity may result in enhanced biological activity. However, BBR3464 was found to be highly toxic and phase IIb clinical trials were ceased.[33]

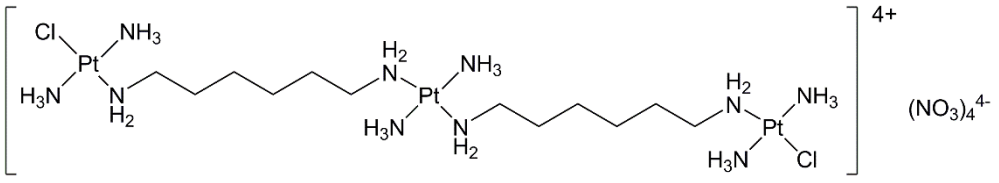

Fig. 1.9: Structure trinuclear platinum complex, BBR3464.

Other drug design approaches include ligand modification and the use of alternative metals to platinum (to decrease toxicity).[29, 30, 34] Complexes incorporating transition metals such as the Platinum Group Metals (PGMs) – ruthenium, rhodium, palladium, osmium and iridium – are of particular interest as they are likely to show similar activity and lower toxicity to platinum. Metal-based chemotherapy has thus been well explored in anticancer research and current research has shown the application of these strategies in antimalarial research and more recently in antimycobacterial studies.

1.4.2 Metal-based antimalarial agents

Based on the increased activity of organic compounds incorporating metals, Wasi *et al*. synthesised and evaluated the antimalarial activity of metal complexes of amodiaquine and primaquine, however this did not enhance their activity.[35] Following on from this, Sanchez-Delgado *et al*. designed metal-chloroquine conjugates, aiming to increase antimalarial activity and overcome widespread resistance shown by *P. falciparum*.[36, 37] Chloroquine (CQ) was modified with transition metals specifically because of their binding capability and reactivity brought about by the d orbitals.[36, 37]

i) Rhodium conjugate

A rhodium-chloroquine conjugate [RhCl(COD)CQ] (COD = 1,5-cyclooctadiene), shown in Fig. 1.10, was the first to be synthesised, characterised and biologically tested. CQ binds to Rh through the heteroaromatic (quinoline) nitrogen atom to form a 16 electron, square-planar complex. This complex exhibited *in vitro* antiplasmodial activities similar to that of chloroquine diphosphate (CQDP), while *in vivo* experiments showed that it caused a reduction in parasitemia of 94 % at a concentration at which CQDP caused 50 % reduction of parasitemia.[36, 37]

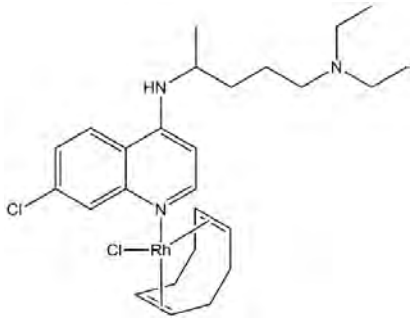

Fig. 1.10: Structure of a rhodium-chloroquine conjugate, RhCl(COD)CQ.[37]

These significant results demonstrated the potential of incorporation of metals into drugs of known therapeutic value, and the design was extended to incorporate a different metal centre, ruthenium, into the chloroquine organic scaffold.

ii) Ruthenium-arene conjugates

With the aim to increase biological activity, a Ru(II) binuclear chloroquine conjugate and Ru(η^6-arene) chloroquine conjugates, shown in Fig. 1.11, were synthesised. In these complexes, ruthenium is bound to chloroquine in the η^1-N mode, through the quinoline nitrogen, similar to the Rh-chloroquine conjugate (Fig. 1.10) These metal-chloroquine derivatives were tested and showed *in vitro* activity against CQ-sensitive and CQ-resistant strains of *P. falciparum*.[36, 37] The complexes displayed

consistently higher activity than CQDP in the sensitive strain, and enhanced activity in the resistant strain.[36, 37]

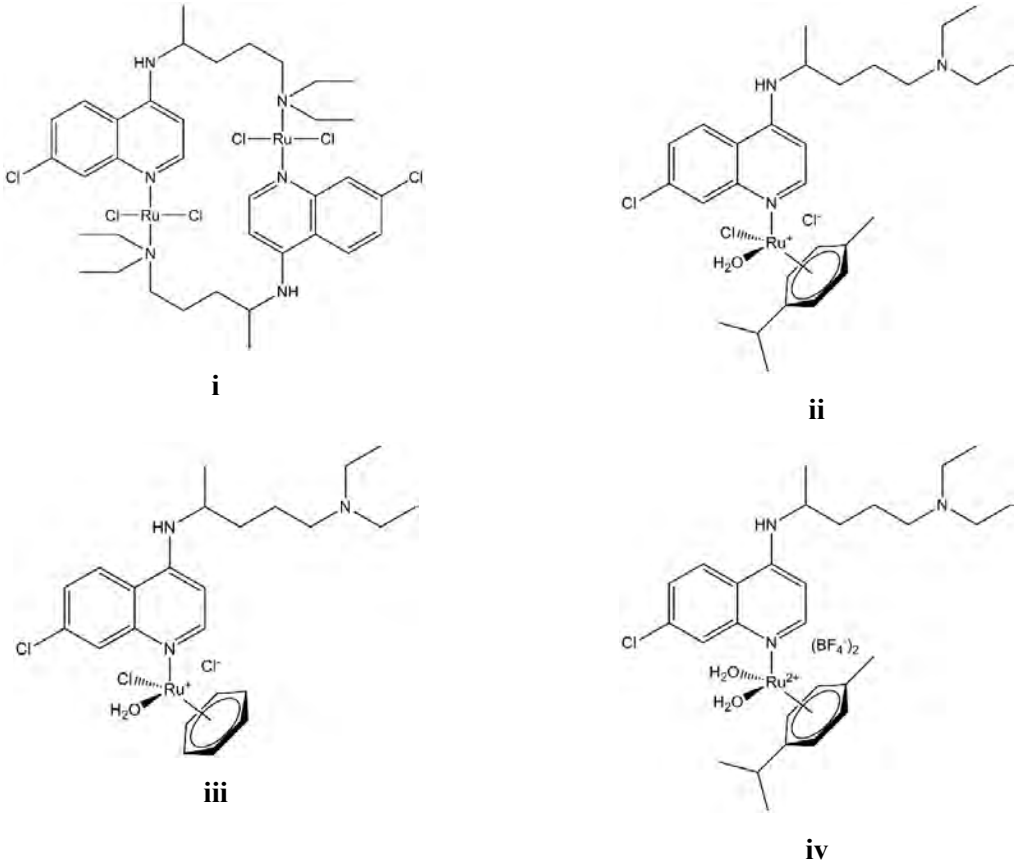

Fig. 1.11: Ruthenium(II) conjugates of chloroquine.[12, 37]

iii) Ferroquine and ferrocenyl analogues

In the continued search to increase biological activity through organometallic derivatisation, attention was turned to ferrocene, a small and rigid sandwich structure, for incorporation into known drug compounds. Ferrocene is a highly robust, neutral and chemically stable compound with low toxicity that can be easily derivatised and functionalised.[38, 39] In general, metallocenes are known to exhibit a diverse array of biological activity and so it is not surprising that the ferrocenyl compounds are afforded interesting anti-tumour, antimalarial, antifungal and DNA-cleaving activity.[38, 40] Ferrocene also has highly lipophilic properties, having the ability to interact with or effectively penetrate biological membranes, and exhibits unique electrochemical properties.[38-40]

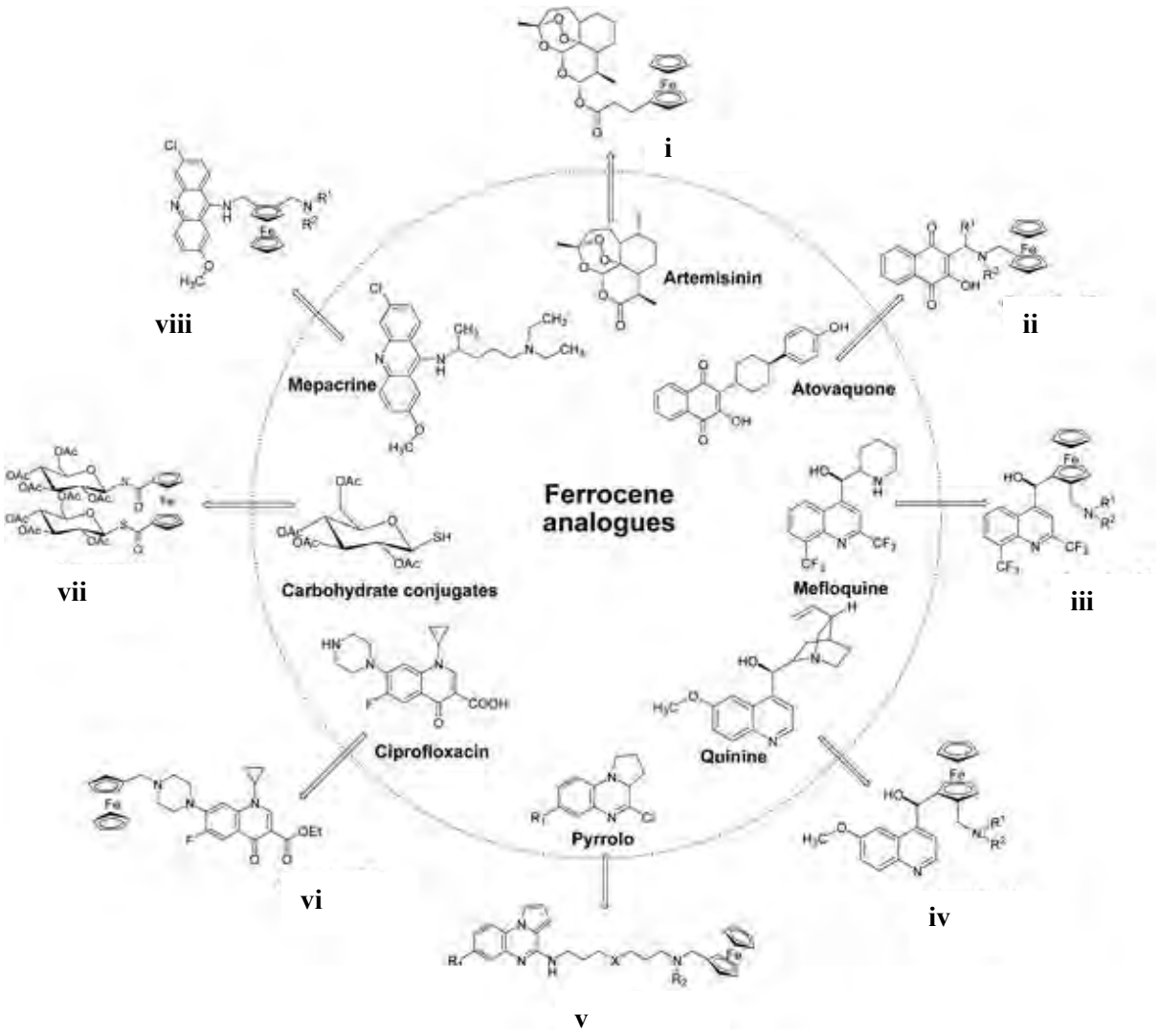

Fig. 1.12: Ferrocenyl analogues of known organic antimalarial agents.[13]

Many ferrocenyl analogues of known organic antimalarial drugs, examples of which are shown in Fig. 1.12, have been prepared and evaluated for their *in vitro* biological activity compared to the organic parent drug.[13] Of these ferrocenyl analogues, the only significant result was seen in the case of the ferrocene-ciprofloxacin conjugate (Fig. 1.12, **vi**), where its activity exceeded that of the parent drug (ciprofloxacin) in CQ-resistant strains.[13]

Following on from the important metal-chloroquine conjugate work by Sanchez-Delgado *et al*.,[36, 37] came the discovery, by Biot *et al*.,[41] of ferroquine (7-chloro-4-[[[2-[N,N-dimethylamino)methyl]-N-ferrocenyl]-methyl]amino]quinoline), a chloroquine derivative incorporating ferrocene into the lateral side chain.[41] Ferroquine (FQ), shown in Fig. 1.13, has high *in vitro* activity in both the CQ-sensitive and CQ-resistant *P. falciparum* strains.[41] In the CQ-sensitive strain, FQ proved as effective as CQDP (IC_{50} = 3.5 – 218 nM), while it was up to twenty times more effective than CQDP in the CQ-resistant strain (IC_{50} = 5 – 241 nM).[12-14, 41] This compound also showed good *in vivo* activity in mice infected

with various Plasmodium strains.[13, 41] The mechanism of antimalarial action is similar to that of chloroquine, involving the inhibition of haemazoin formation.[12, 42] Ferroquine reached phase IIb clinical trials,[43] being examined in malaria patients in an artemisinin-combined therapy (ACT) with artesunate.[14] It was thus shown that this organometallic derivatisation significantly increased the biological activity compared to the parent drug/compound.

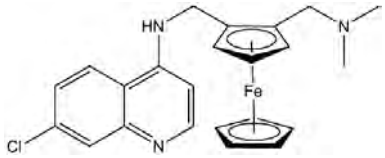

Fig. 1.13: Ferroquine, a ferrocenyl analogue of chloroquine.

1.4.3 Metal-based antimycobacterial agents

i) Ferrocene-containing compounds

Owing to the success of ferroquine, ferrocenyl conjugation or modification as a drug design strategy is currently being applied and developed in the preparation of new antimycobacterial agents. Pelinski and co-workers reported the synthesis and antimycobacterial activity of ferrocenyl analogues of ethambutol and isoniazid, two important anti-TB drugs.[44-46] In these studies, testing the *in vitro* activity against the H37Rv *M. tuberculosis* strain, two ferrocenyl diamines and two ferrocenyl acylhydrazones were found to be most active.[44-46] The structures and minimum inhibitory concentration (MIC) values of these ferrocenyl compounds are shown in Fig. 1.14.

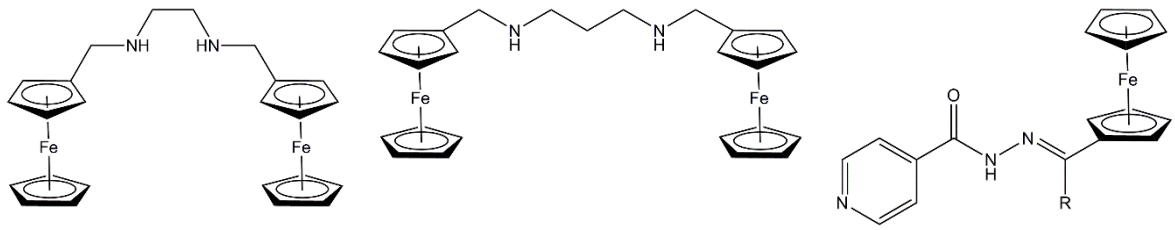

i: MIC = 17.54 μM

ii: MIC = 17.01 μM

iii: R = H, MIC = 0.75 μM

iv: R = CH_3, MIC = 0.72 μM

Fig. 1.14: Ferrocene-containing anti-TB agents and corresponding MIC values.[44-46]

In the case of the ferrocenyl acylhydrazones, the antimycobacterial activity is similar to that of isoniazid (MIC > 0.43 μM) and superior to that of ethambutol (MIC = 9.8 μM).[46] This indicates that compounds based on the ferrocenyl polyamine scaffold may be of great significance in anti-TB research.

ii) PGM-containing compounds

Inorganic medicinal chemistry has also seen the introduction of PGM-based compounds as part of antimycobacterial therapeutic research. Historically, palladium compounds have previously been used in the treatment of tuberculosis. In the 1940s, doses of $PdCl_2$ were administered daily with no apparent adverse effects in TB patients, but was found to be ineffective.[47] More recently, Mauro and co-workers have reported several interesting examples of novel inorganic palladium(II) compounds,[48-51] shown in Fig. 1.15.

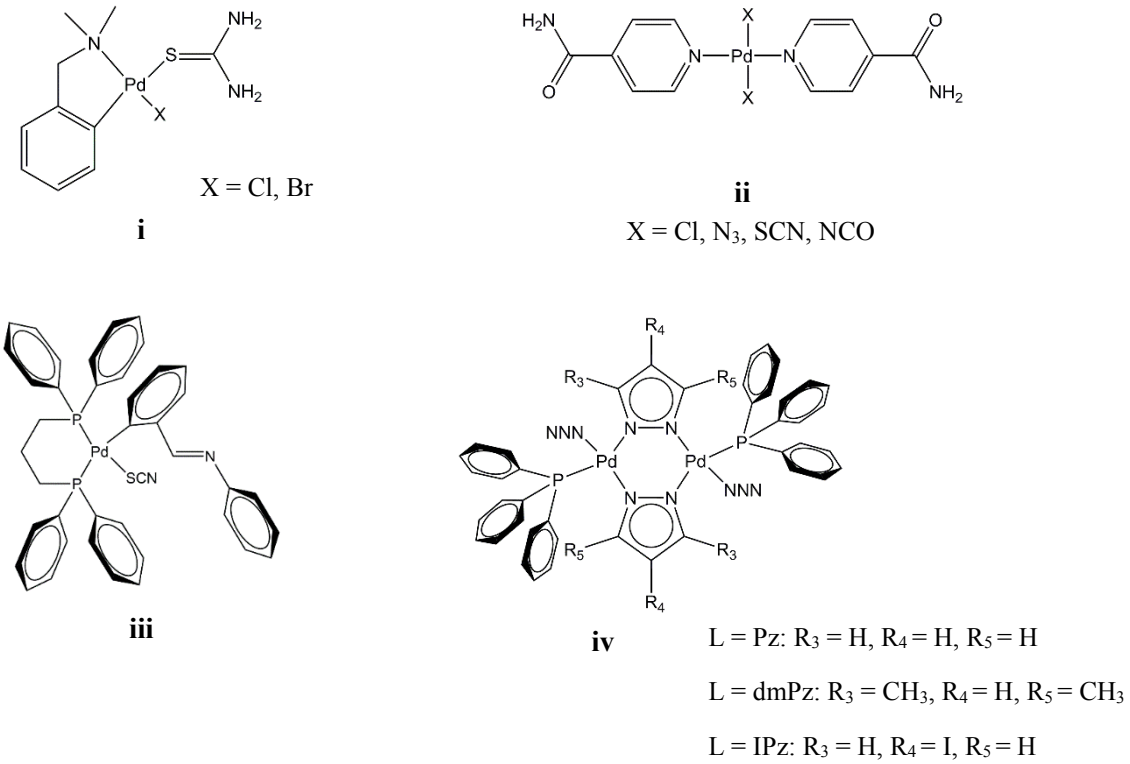

Fig. 1.15: Novel palladium(II) compounds i) [Pd (C^2, N-dmba)(X)(tu)] ii) $[Pd(X)_2(isn)_2]$ iii) [Pd(C-bzan)(SCN)(dppp)] iv) $[Pd(\mu\text{-}L)(N_3)(PPh_3)]_2$

In an evaluation of these compounds' antimycobacterial activity against the H37Rv *M. tuberculosis* strain, all displayed minimum inhibitory concentrations (MIC) in the micromolar range. With respect to the thiourea complexes (Fig. 1.15, **i**), the bromide analogue (MIC = 57.99 μM) proved more potent than the chloride analogue (MIC = 88.74 μM).[48] The isonicotinamide complexes (Fig. 1.15, **ii**), displayed quite a broad MIC range (35.89 – 296.5 μM), with the azide analogue showing the highest activity.[49] In comparison, the phosphine-containing palladium(II) complexes exhibited much higher activity, displaying MIC values of 5.15 μM for the mononuclear Pd(II)-phosphine complex (Fig. 1.15, **iii**)[50] and 8.16 μM for the binuclear complex (Fig. 1.15, **iv**, L=Pz)[51]. These activities are similar or better than the MIC values of some commonly used anti-TB drugs, shown in Table 1.2. The higher

antimycobacterial activitiy of these compounds could be attributed to their increased lipophilicity, brought about by the presence of lipophilic phosphine groups, as well as the chelating coordination of the other ligands.[50-52]

Table 1.2: MIC values of some anti-TB drugs in the H37Rv strain.[53]

Drug	MIC range (μM)
Gentamicin	4.14 – 8.38
Tobramycin	8.56 – 17.11
Clarithromycin	10.70 – 21.40
Cycloserine	122.4 – 489.7

Based on the clinical success of cisplatin (Fig. 1.8) and the great promise shown by the trinuclear analogue, BBR3464 (Fig. 1.9),[32] research has shown several examples in which polynuclearity enhances biological activity.[54-58] This may be due to increased biological interactions or more optimal chemical and physical properties. The 'polynuclear' approach can be applied to both organic- and metallodrugs and can be achieved by conjugating known pharmacophores onto dendritic scaffolds.[54-58]

1.5 Dendrimer chemistry

Dendrimer chemistry was first explored by Fritz Vogtle in 1978, dendrimers were then known as 'cascade molecules'.[59] The term 'dendrimer' was first introduced in 1985, by Donald Tomalia, who synthesised the first family of such compounds.[60] The word is derived from two Greek words, *dendros* meaning tree and *meros* meaning part, due to the resemblance of these molecules to the structure of a tree. In chemistry, dendrimers are defined as synthetic macromolecules with a repetitively branched molecular structure.[61, 62] These molecules are monodisperse nanoscale polymers with defined molecular weights. Their hyperbranched nature results in highly multivalency, exposing a large number of functional groups on the surface of the molecule.

1.5.1 Organic-based dendrimers

Over the years, many different types of organic-based dendrimers (Fig. 1.16) have been developed:[61, 62]

- Polyamido amino or PAMAM-dendrimers prepared by Tomalia,
- Newkome's arborols,
- Frechet's polyether dendrimers,
- Poly (propylene imine) or PPI-dendrimers prepared by Meijer and Mulhaupt,
- Moore's phenylacetylene dendrimers.

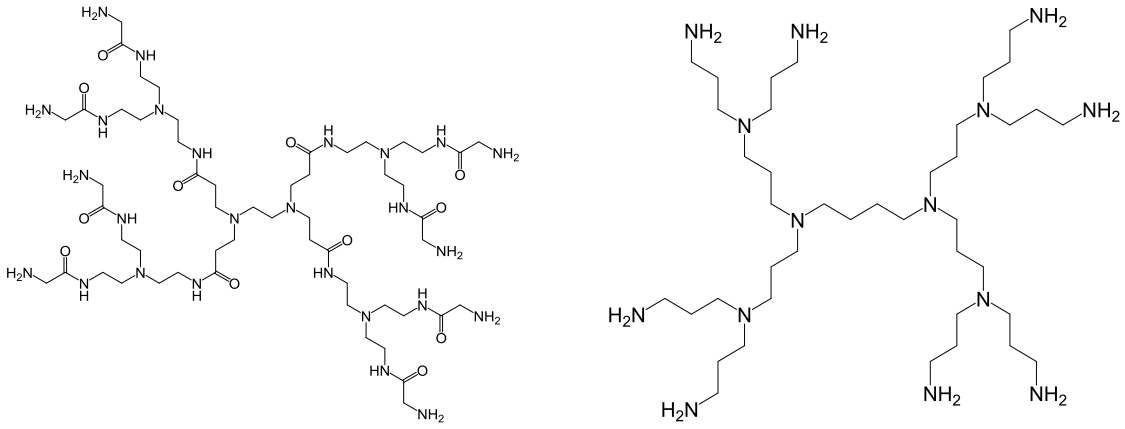

PAMAM dendrimer (G1) PPI dendrimer (G2)

Fig. 1.16: Two most common dendrimer types, PAMAM- and PPI-dendrimers.

These different dendrimer structures are synthesised in an algorithmic step-by-step manner using either divergent or convergent methods (Fig. 1.17).[62] Divergent methods involve the assembly of the dendrimer from an internal multifunctional core, extending it outward to the eventual periphery (usually by a series of Michael additions). In convergent methods, the dendrimer is built from a starting monomer that ends up at the periphery and the structure is built inward to the internal core. Each

repeated sequence of reactions producing a higher generation of the dendrimer.[61, 63] With each increase in generation, the molecular weight of the dendrimer and the number of functional end groups are practically doubled. The multiple functional end-groups can be easily modified through simple organic reactions, which, in combination with the general properties of dendrimers affords them numerous applications in chemistry and biology.[61, 62]

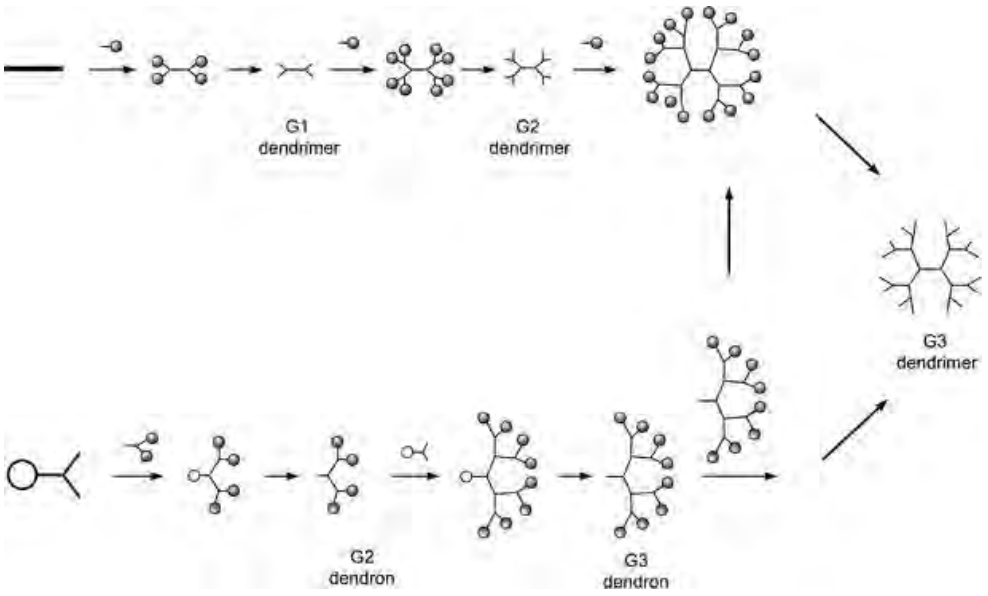

Fig. 1.17: Divergent (top) and convergent (bottom) dendrimer synthesis.

1.5.2 Dendrimers in biology

The property of dendrimers that makes them significant in biological systems is its multivalent surface (high concentration of functional groups on the periphery), which allows for maximum interaction with biological surroundings (e.g. substrates and receptors).[62] Many dendrimers have also proven biologically compatible as they are non-toxic, non-immunogenic, biopermeable, target specific, and able to stay in biological circulation long enough to illicit the required clinical response.[62] For these reasons, research has seen the application of dendrimers in medicinal chemistry and a number of these organic scaffolds have been studied as antiviral, antibacterial and antitumour dendrimers as well as dendrimer-based vaccines.[61-63]

1.5.3 Metallodendrimers

Transition metal derivatisation of organic-based dendrimers gives rise to metallodendrimers. In the past, research has been focused on the synthesis and characterisation of dendrimers, but more recently there has been a shift in focus to the various applications possible for these macromolecules.[64] The incorporation of transition metals onto dendrimer scaffolds modifies its properties and functionality and thus opens up new areas of application such as catalysis,[65] host-guest chemistry[66] and extends the application in medicinal chemistry.[67] There have been advances in biomedical sensing, photothermal sensing, photodynamic therapy and particularly their use as metal-based drugs.[64]

Dendrimers as drugs offer a number of advantages with respect to control of effects within biological systems such as a high degree of molecular definition, versatility of drug design and multivalency of active motifs.[62] In metallodendrimers, these effects may be compounded as the incorporation of metals increases reactivity and binding and has often been seen to increase biological activity in general.[64, 68] It has been observed that polynuclear complexes often display enhanced biological activity compared to their mononuclear analogues. This trend has been reported for metallodendrimers in the literature, and suggests that biological activity increases with molecular size.[69, 70] There are numerous examples in the literature of the synthesis and antitumour activity of metallodendrimers, particularly those containing platinum, as a result of the success of cisplatin.[64] The application of these macromolecules in antimalarial research is also on-going, but to a lesser extent in antibacterial research. There are currently no examples of metallodendrimers in the application of antimycobacterial studies reported in literature.

With regards to metallodendrimers in antiplasmodial studies, Khanye and co-workers[71] reported on the synthesis and antimalarial activity of ferrocenylthiosemicarbazones conjugated to the periphery of PPI-dendritic scaffolds (Fig. 1.18).[71] The ferrocenyl ligands and tetranuclear metallodendrimers were evaluated for antiplasmodial activity against a CQ-resistant strain of *P. falciparum*. The ferrocenyl thioester ligands displayed no antiplasmodial activity, while the two metallodendrimers (R = H, CH_3) displayed good activity in the low micromolar range (IC_{50} = 2 – 7 μM).[71]

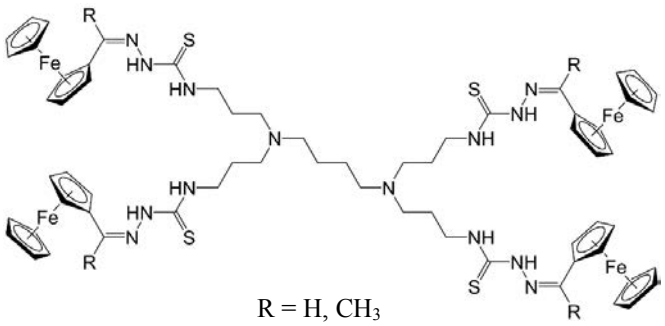

Fig. 1.18: A tetranuclear ferrocenylthiosemicarbazone metallodendrimer.

1.6 Summary

New and growing resistance to past and current antiplasmoadial and antimycobacterial treatments has resulted in the need for new drug therapies and drug design strategies. The ferrocenyl moiety has proven a promising modification in the design of potential anticancer and antiplasmodial drug candidates. The use of ferrocene in medicinal chemistry is widespread and growing, however, its application in antimycobacterial research is in its infancy. With the use of metallodendrimers being relatively new in the fields of antiplasmodial and antimycobacterial research, this study aims to incorporate a number of chemical moieties with favourable properties onto macromolecular scaffolds, and evaluate these complexes as potential antimicrobial agents. This includes the ferrocene moiety, hydrophobic spacers, polyamines and thiosemicarbazones. The effect of the different chemical functionalities, as well as the nuclearity of the metallodendrimers, on the biological activity and properties are explored.

1.7 Aims and Objectives

1.7.1 General Aims

The main aim of this project was to develop transition metal containing complexes based on polyamine (dendritic) macromolecular scaffolds, to complete full characterisation and evaluate their biological activity as potential antimycobacterial and antimalarial agents.

1.7.2 Specific objectives

In order to achieve this aim, this project had five main objectives:

i) To synthesise ferrocenyl precursors; [72, 73]

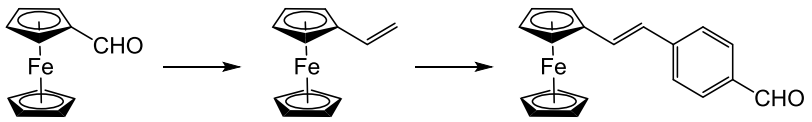

Scheme 1.1: Structures of ferrocenyl precursors.

ii) To prepare a series of novel polynuclear ferrocenyl-imino and -amino complexes as well as the corresponding mononuclear complexes;

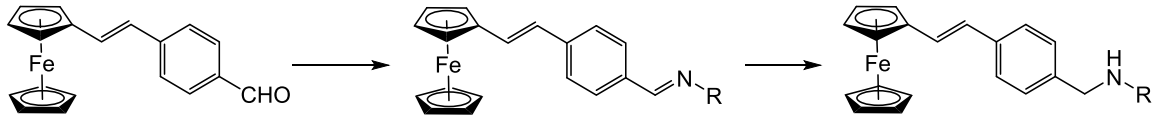

R = $CH_2CH_2CH_3$ or $CH_2C(CH_3)_3$ or $CH_2Si(CH_3)_3$

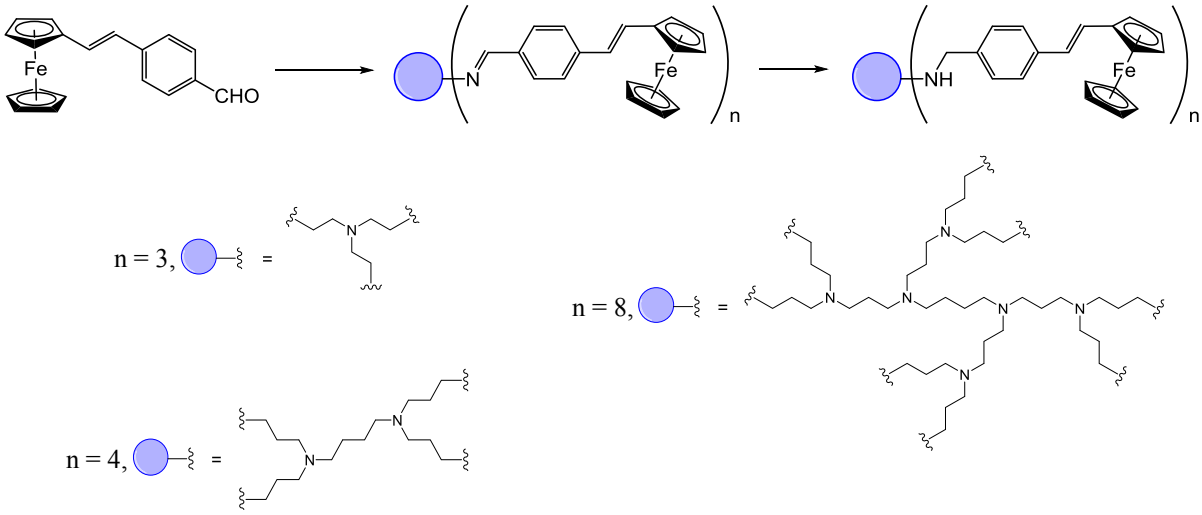

Scheme 1.2: Mono- and polynuclear ferrocenyl-imino and -amino complexes investigated in this project.

iii) To synthesise a series of ferrocenylthiosemicarbazone complexes;

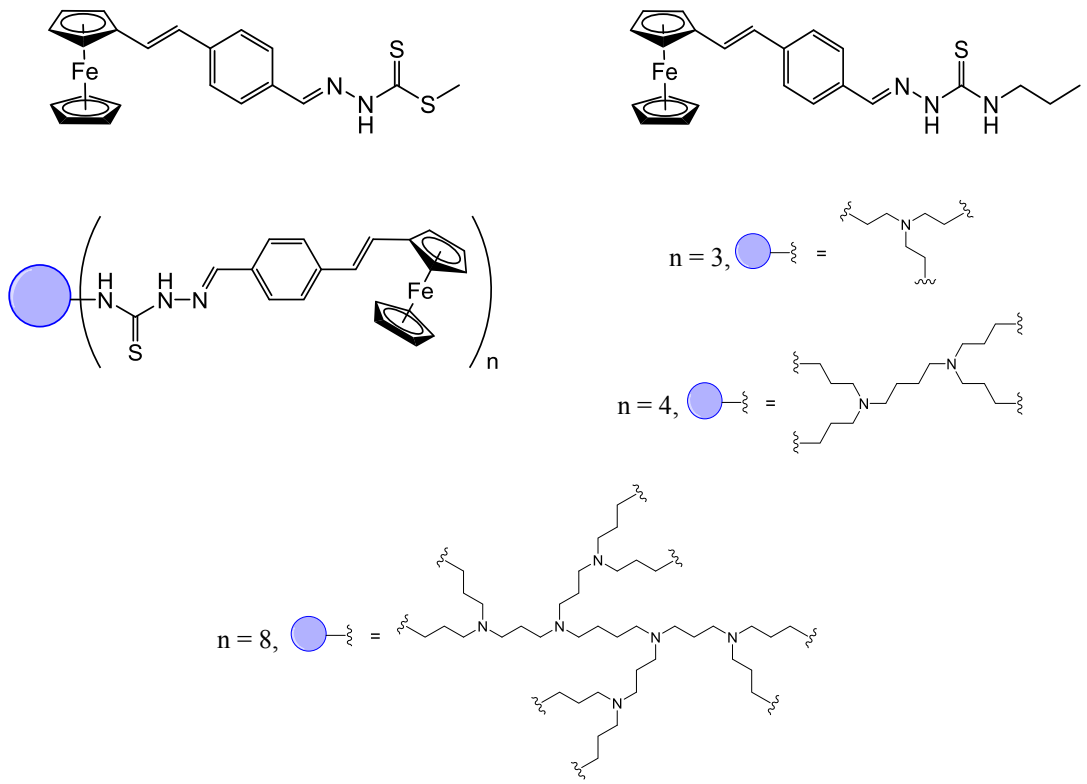

Scheme 1.3: Mono- and polynuclear ferrocenylthiosemicarbazones investigated in this project.

iv) To fully characterise all compounds using ^{1}H and $^{13}C\{^{1}H\}$ Nuclear Magnetic Resonance and Infrared spectroscopy, mass spectrometry, elemental analysis or High Pressure Liquid Chromatography and determination of melting points.

v) To investigate the utility of these polyamine/dendrimer-bound metal complexes as antimycobacterial and antimalarial agents against *M. tuberculosis* (H37Rv) and *P. falciparum* (NF54) strains, respectively.

1.8 References

1. World Health Organisation, *World Health Statistics 2013*, WHO Press, Geneva, 2013.
2. World Health Organisation, *World Malaria Report 2011*, WHO Press, Geneva, 2011.
3. World Health Organisation, *Global tuberculosis report 2013*, World Health Organization, WHO Press, Geneva, 2013.
4. A. Koul, E. Arnoult, N. Lounis, J. Guillemont and K. Andries, *Nature,* 2011, **469**, 483-490.
5. I. Smith, *Clin. Microbiol. Rev.,* 2003, **16**, 463-496.
6. J. van den Boogaard, G. S. Kibiki, E. R. Kisanga, M. J. Boeree and R. E. Aarnoutse, *Antimicrob. Agents Chemother.,* 2009, **53**, 849-862.
7. G. S. Timmins and V. Deretic, *Mol. Microbiol.,* 2006, **62**, 1220-1227.
8. P. C. Karakousis, *Antimicrobial drug resistance,* Springer, 2009, pp.271-291.
9. V. Bernardes-Genisson, C. Deraeve, A. Chollet, J. Bernadou and G. Pratviel, *Curr. Med. Chem.,* 2013, **20**, 4370-4385.
10. I. Chopra and P. Brennan, *Tubercle Lung Dis.,* 1998, **78**, 89-98.
11. S. H. Gillespie, *Antimicrob. Agents Chemother.,* 2002, **46**, 267-274.
12. M. Navarro, W. Castro and C. Biot, *Organometallics,* 2012, **31**, 5715-5727.
13. C. Biot, W. Castro, C. Y. Botté and M. Navarro, *Dalton Trans.,* 2012, **41**, 6335-6349.
14. P. F. Salas, C. Herrmann and C. Orvig, *Chem. Rev.,* 2013, **113**, 3450-3492.
15. P. Winstanley and S. Ward, *Adv. Parasitol.,* 2006, **61**, 47-76.
16. A. Dieckmann and A. Jung, *Parasitology,* 1986, **93**, 275-278.
17. World Health Organisation, *Guidelines for the Treatment of Malaria*, 2nd ed., WHO Press, Geneva, 2010.
18. World Health Organisation, *Global Report of Antimalarial Drug Efficacy and Drug Resistance: 2000-2010*, WHO Press, Geneva, 2010.
19. R. N. Price, *Exp. Opin. Invest. Drugs,* 2000, **9**, 1815.
20. T. T. Hien, N. J. White, *Lancet,* 1993, **341**, 603.

21. M. Enserink, *Science,* 2010, **328**, 842-842.
22. H. Noedl, Y. Se, K. Schaecher, B. L. Smith, D. Socheat and M. M. Fukuda, *N. Engl. J. Med.,* 2008, **359**, 2619-2620.
23. A. M. Dondorp, F. Nosten, P. Yi, D. Das, A. P. Phyo, J. Tarning, K. M. Lwin, F. Ariey, W. Hanpithakpong and S. J. Lee, *N. Engl. J. Med.,* 2009, **361**, 455-467.
24. N. Gargano, F. Cenci and Q. Bassat, *Trop. Med. Int. Health,* 2011, **16**, 1466-1473.
25. K. Strebhardt and A. Ullrich, *Nat. Rev. Cancer,* 2008, **8**, 473-480.
26. B. Rosenberg and L. Vancamp, *Nature,* 1969, **222**, 385-386.
27. M. Gordon and S. Hollander, *J. Med.,* 1993, **24**, 209-265.
28. E. Wong and C. M. Giandomenico, *Chem. Rev.,* 1999, **99**, 2451-2466.
29. M. A. Jakupec, M. Galanski, V. B. Arion, C. G. Hartinger and B. K. Keppler, *Dalton Trans.,* 2008, **2**, 183-194.
30. C. G. Hartinger and P. J. Dyson, *Chem. Soc. Rev.,* 2009, **38**, 391-401.
31. P. J. Dyson and G. Sava, *Dalton Trans.,* 2006, **16**, 1929-1933.
32. C. Billecke, S. Finniss, L. Tahash, C. Miller, T. Mikkelsen, N. P. Farrell and O. Bogler, *Neuro. Oncol.,* 2006, **8**, 215-226.
33. D. Jodrell, T. Evans, W. Steward, D. Cameron, J. Prendiville, C. Aschele, C. Noberasco, M. Lind, J. Carmichael and N. Dobbs, *Eur. J. Cancer,* 2004, **40**, 1872-1877.
34. A. F. Peacock and P. J. Sadler, *Chem. Asian J.,* 2008, **3**, 1890-1899.
35. N. Wasi, H. Singh, A. Gajanana and A. Raichowdhary, *Inorg. Chim. Acta,* 1987, **135**, 133-137.
36. R. A. Sánchez-Delgado, M. Navarro, H. Pérez and J. A. Urbina, *J. Med. Chem.,* 1996, **39**, 1095-1099.
37. R. A. Sánchez-Delgado, A. Anzellotti and L. Suarez, *Met. Ions Biol. Syst.,* 2004, **41**, 379-420.
38. M. F. Fouda, M. M. Abd-Elzaher, R. A. Abdelsamaia and A. A. Labib, *Appl. Organomet. Chem.,* 2007, **21**, 613-625.
39. N. Lease, V. Vasilevski, M. Carreira, A. de Almeida, M. Sanau, A. Casini and M. Contel, *J. Med. Chem.,* 2013, **56**, 5806-5818.
40. C. Biot, N. François, L. Maciejewski, J. Brocard and D. Poulain, *Bioorg. Med. Chem. Lett.,* 2000, **10**, 839-841.
41. C. Biot, G. Glorian, L. A. Maciejewski, J. S. Brocard, O. Domarle, G. Blampain, P. Millet, A. J. Georges, H. Abessolo and D. Dive, *J. Med. Chem.,* 1997, **40**, 3715-3718.
42. C. Biot, D. Taramelli, I. Forfar-Bares, L. A. Maciejewski, M. Boyce, G. Nowogrocki, J. S. Brocard, N. Basilico, P. Olliaro and T. J. Egan, *Mol. Pharmaceut.,* 2005, **2**, 185-193.
43. G. Mombo-Ngoma, C. Supan, M. P. Dal-Bianco, M. A. Missinou, P. Matsiegui, C. L. Ospina Salazar, S. Issifou, D. Ter-Minassian, M. Ramharter and M. Kombila, *Malar. J.,* 2011, **10**, 53.
44. D. Razafimahefa, D. A. Ralambomanana, L. Hammouche, L. Pélinski, S. Lauvagie, C. Bebear, J. Brocard and J. Maugein, *Bioorg. Med. Chem. Lett.,* 2005, **15**, 2301-2303.

45. D. Andrianina Ralambomanana, D. Razafimahefa-Ramilison, A. C. Rakotohova, J. Maugein and L. Pélinski, *Bioorg. Med. Chem.,* 2008, **16**, 9546-9553.
46. G. M. Maguene, J. Jakhlal, M. Ladyman, A. Vallin, D. A. Ralambomanana, T. Bousquet, J. Maugein, J. Lebibi and L. Pélinski, *Eur. J. Med. Chem.,* 2011, **46**, 31-38.
47. C. E. Garrett and K. Prasad, *Adv. Synth. Catal.,* 2004, **346**, 889-900.
48. A. C. Moro, A. E. Mauro, A. V. Netto, S. R. Ananias, M. B. Quilles, I. Z. Carlos, F. R. Pavan, C. Q. Leite and M. Hoerner, *Eur. J. Med. Chem.,* 2009, **44**, 4611-4615.
49. R. A. de Souza, A. Stevanato, O. Treu-Filho, A. V. Netto, A. E. Mauro, E. E. Castellano, I. Z. Carlos, F. R. Pavan and C. Q. Leite, *Eur. J. Med. Chem.,* 2010, **45**, 4863-4868.
50. J. G. Ferreira, A. Stevanato, A. M. Santana, A. E. Mauro, A. V. Netto, R. C. Frem, F. R. Pavan, C. Q. Leite and R. H. Santos, *Inorg. Chem. Commun.,* 2012, **23**, 63-66.
51. C. da Silva, J. Ferreira, A. Mauro, R. Frem, R. Santos, P. da Silva, F. Pavan, L. Marino, C. Leite and A. Netto, *Inorg. Chem. Commun.,* 2014, **48**, 153-155.
52. P. B. Pansuriya, M. N. Patel, M. R. Chhasatia, P. Dhandhukia and V. Thakkar, *J. Coord. Chem.,* 2008, **61**, 3336-3349.
53. S. G. Franzblau, R. S. Witzig, J. C. McLaughlin, P. Torres, G. Madico, A. Hernandez, M. T. Degnan, M. B. Cook, V. K. Quenzer, R. M. Ferguson and R. H. Gilman, *J. Clin. Microbiol.,* 1998, **36**, 362-366.
54. D. Astruc, E. Boisselier and C. Ornelas, *Chem. Rev.,* 2010, **110**, 1857-1959.
55. G. R. Newkome and C. Shreiner, *Chem. Rev.,* 2010, **110**, 6338-6442.
56. G. R. Newkome, E. He and C. N. Moorefield, *Chem. Rev.,* 1999, **99**, 1689-1746.
57. S. Hwang, C. D. Shreiner, C. N. Moorefield and G. R. Newkome, *New J. Chem.,* 2007, **31**, 1192-1217.
58. I. Angurell, O. Rossell and M. Seco, *Inorg. Chim. Acta,* 2014, **409**, 2-11.
59. E. Buhleier, W. Wehner and F. Vogtle, *Synthesis-Stuttgart,* 1978, 155-158.
60. D. Tomalia, H. Baker, J. Dewald, M. Hall, G. Kallos, S. Martin, J. Roeck, J. Ryder and P. Smith, *Polym. J.,* 1985, **17**, 117-132.
61. B. V. Manalan, A. E. Prabahar, A. B. Adi and R. R. Nadendla, *Int. J. Bio. Pharmaceut. Res.*, 2013, **4**, 1000-1009.
62. U. Boas, J. B. Christensen and P. M. Heegaard, *Dendrimers in medicine and biotechnology: new molecular tools*, Royal Society of Chemistry, 2006.
63. M. A. Mintzer, E. L. Dane, G. A. O'Toole and M. W. Grinstaff, *Mol. Pharmaceut.,* 2011, **9**, 342-354.
64. P. Govender, B. Therrien and G. S. Smith, *Eur. J. Inorg. Chem.,* 2012, 2853-2862.
65. D. Astruc, *Pure Appl. Chem.,* 2003, **75**, 461-481.
66. R. E. Bauer, C. G. Clark Jr and K. Müllen, *New J. Chem.,* 2007, **31**, 1275-1282.
67. H. Yang and W. J. Kao, *J. Biomat. Sci-Polym. E.,* 2006, **17**, 3-19.

68. C. Gorman, *Adv Mater,* 1998, **10**, 295-309.
69. P. Govender, N. C. Antonels, J. Mattsson, A. K. Renfrew, P. J. Dyson, J. R. Moss, B. Therrien and G. S. Smith, *J. Organomet. Chem.,* 2009, **694**, 3470-3476.
70. P. Govender, A. K. Renfrew, C. M. Clavel, P. J. Dyson, B. Therrien and G. S. Smith, *Dalton Trans.,* 2011, **40**, 1158-1167.
71. S. D. Khanye, J. Gut, P. J. Rosenthal, K. Chibale and G. S. Smith, *J. Organomet. Chem.,* 2011, **696**, 3296-3300.
72. M. Gallei, R. Klein and M. Rehahn, *Macromolecules,* 2010, **43**, 1844-1854.
73. M. I. Reyes Valderrama, R. A. Vasquez García, T. Klimova, E. Klimova, L. Ortiz-Frade and M. Martinez García, *Inorg. Chim. Acta,* 2008, **361**, 1597-1605.

Chapter 2

Synthesis and characterisation of mono- and polynuclear ferrocenyl-derived imino and amino complexes

2.1 Introduction

In addition to incorporating metals into organic-based compounds as a drug design strategy as mentioned in chapter 1, the organic scaffolds of known drugs can also be further derivatised in order to enhance their potency. In this regard, in terms of antimycobacterial research, organic and organometallic analogues of the anti-TB drug ethambutol (Fig. 2.1) have been explored to some extent. Derivatisation of ethambutol (EMB) specifically has gained interest due to its low toxicity and chemical simplicity, as well as its quite efficient clinical anti-TB activity, which proves that the diamine backbone is a favourable framework.[1] Thus far, studies that focused on the organic modification of EMB have seen the preparation of diamine and diaminoalcohol analogues thereof (Fig. 2.1), which have shown enhanced activities compared to EMB.[2-7]

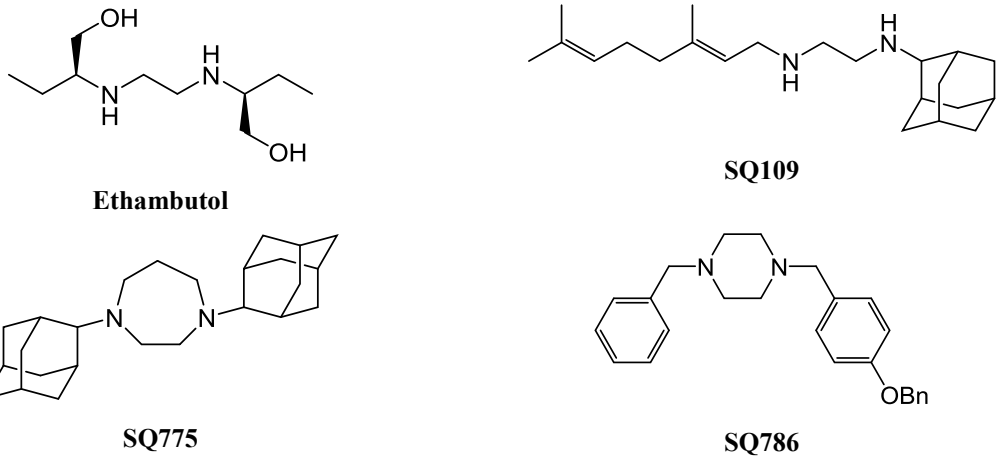

Fig. 2.1: Structure of ethambutol and three organic analogues.

Based on the promising increased efficiency of these compounds, Pelinski and coworkers prepared a series of organometallic derivatives of EMB, employing different strategies to insert the ferrocene moiety as shown in Fig. 2.2.[8, 9] Two of these analogues, in which ferrocenes replace the alcohol moieties, exhibited promising antitubercular activity, comparable to that of EMB.[8, 9]

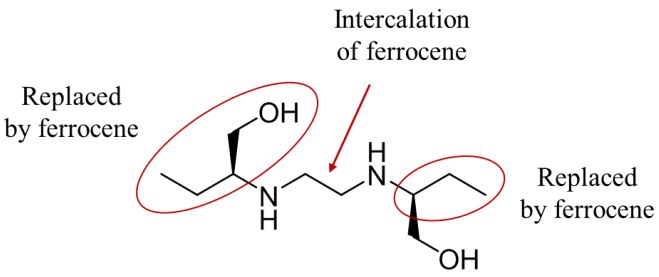

Fig. 2.2: Chemical modifications of EMB.

Polyamines are compounds containing two or more primary amino groups, which show potential as drug delivery systems. Polyamines such as putrescine, spermidine and spermine are naturally occurring biomolecules essential for cellular growth and proliferation.[10-13] Molecules of this kind enter the cell via a polyamine transporter (PAT), which also allows modified polyamines to pass through. Therefore, drug-polyamine conjugates are able to enter these cells, a strategy which has been used to penetrate tumour cells in anticancer research.[14] However, polyamines as drug delivery scaffolds are also applicable in parasitic diseases, as they also show selective uptake in erythrocytes infected by the *Plasmodium* parasite.[15, 16] Edwards and co-workers prepared a series of tetraamines of the general formula $RNH(CH_2)_xNH(CH_2)_yNH(CH_2)_xNHR$, which were evaluated for their antimalarial activity against *Plasmodium falciparum*.[17] The dibenzyl analogues (R = benzyl) with optimum chain lengths (x = 3, y = 7) exhibited low micromolar IC_{50} values.[17]

Thus, polyamines can be used as drug delivery systems in a similar way to some dendrimers. Dendrimers are highly branched, mono-disperse macromolecules with high multivalency, exposing a large number functional groups of the periphery of the molecule. One way in which dendrimers can act as drug delivery scaffolds is by covalent conjugation to drug compounds or active species.[18-22] The dendrimer aids in transporting the drug into the cell or to the target site, where it is then degraded and the drug is released.[18-22]

In this chapter, the synthesis and characterisation of a series of mono- and polynuclear ferrocenyl-derived imino and amino complexes, based on the tris(2-aminoethyl)amine and polypropyleneimine (PPI) dendritic scaffolds, is described. All compounds were characterised using a range of spectroscopic and analytical techniques.

2.2 Preparation of Ferrocene-containing precursors (2.2 – 2.3)

2.2.1 Synthesis

Two ferrocene-containing precursors (**2.2** and **2.3**) were prepared using literature methods[23, 24] as shown in Scheme 2.1. Vinylferrocene (**2.2**) was synthesised via a Wittig olefination reaction, as described by Gallei *et al.*,[23] in anhydrous tetrahydrofuran under inert conditions, and was isolated in 91 % yield as a bright orange crystalline solid. A Wittig olefination reaction allows for the preparation of an alkene by reaction of an aldehyde (or ketone) with a phosphonium ylide generated from the phosphonium salt.

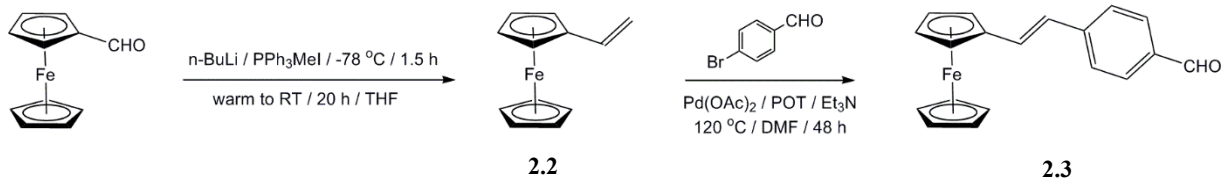

2.2 **2.3**

Scheme 2.1: Preparation of ferrocene-containing precursors.

The first step of the Wittig olefination reaction involves the *in situ* generation of the phosphonium ylide by deprotonation of the methyl group of the phosphonium salt. In the second step, the nucleophilic carbon of the ylide attacks the electrophilic carbonyl carbon of ferrocenecarboxaldehyde. The reaction then proceeds via a four-membered heterocyclic ring intermediate to produce the alkene (the vinyl group of **2.2** in this case) as shown in Fig. 2.3. The melting point of **2.2** agrees with the range reported in literature.[23]

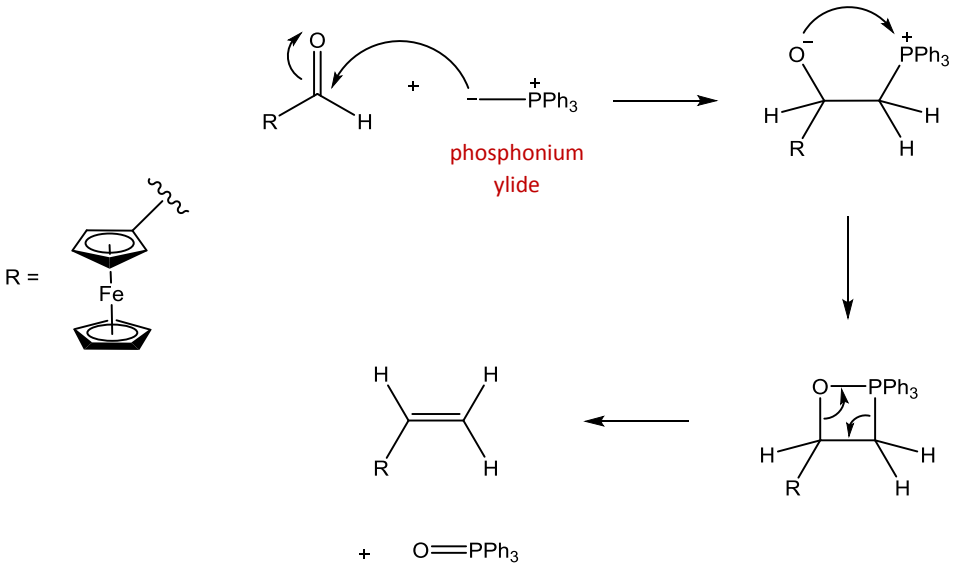

Fig. 2.3: Mechanism of the Wittig olefination reaction.[25]

Ferrocenyl-conjugate, (*E*)-4-vinylferrocenylbenzaldehyde (**2.3**), was prepared via a Heck cross-coupling reaction of **1** with 4-bromobenzaldehyde, using a method utilised by Reyes Valderrama *et al.*[24] The reagents were refluxed in *N*,*N*-dimethylformamide and triethylamine under inert conditions for 48

hours, and **2.3** was isolated in 52 % yield. However, the yield of this reaction was significantly improved by modifying the method and reagents, replacing 4-bromobenzaldehyde with 4-iodobenzaldehyde, as iodides are generally better leaving groups compared to bromides. The reagents were refluxed in acetonitrile and triethylamine under inert conditions for 24 hours (a reduced time) and afforded an improved 72 % yield. Compound **2.3** was isolated as a red crystalline solid and displays solubility in organic solvents as well as alcoholic solvents.

The Heck cross-coupling reaction involves a catalytic cycle (Fig. 2.4) in which a Pd(0) active species catalyses a series of structural changes, ultimately producing the alkene product. In the cycle shown below, palladium acetate is reduced by tri-o-tolylphosphine to bis(tri-o-toylphosphine)palladium(0), the active species. Step A of the cycle is an oxidative addition reaction in which the palladium species inserts into the aryl-bromide bond of 4-bromobenzaldehyde. This is followed by formation of a pi-complex of palladium with the alkene, vinylferrocene (**2.2**). In step B, by *syn* addition the alkene inserts into the Pd-C bond, which is followed by beta-hydride elimination in step C to give a new Pd-alkene pi-complex. Step D is reductive elimination by a base (triethylamine) to regenerate a Pd(0) species and the desired coupled product **2.3**.

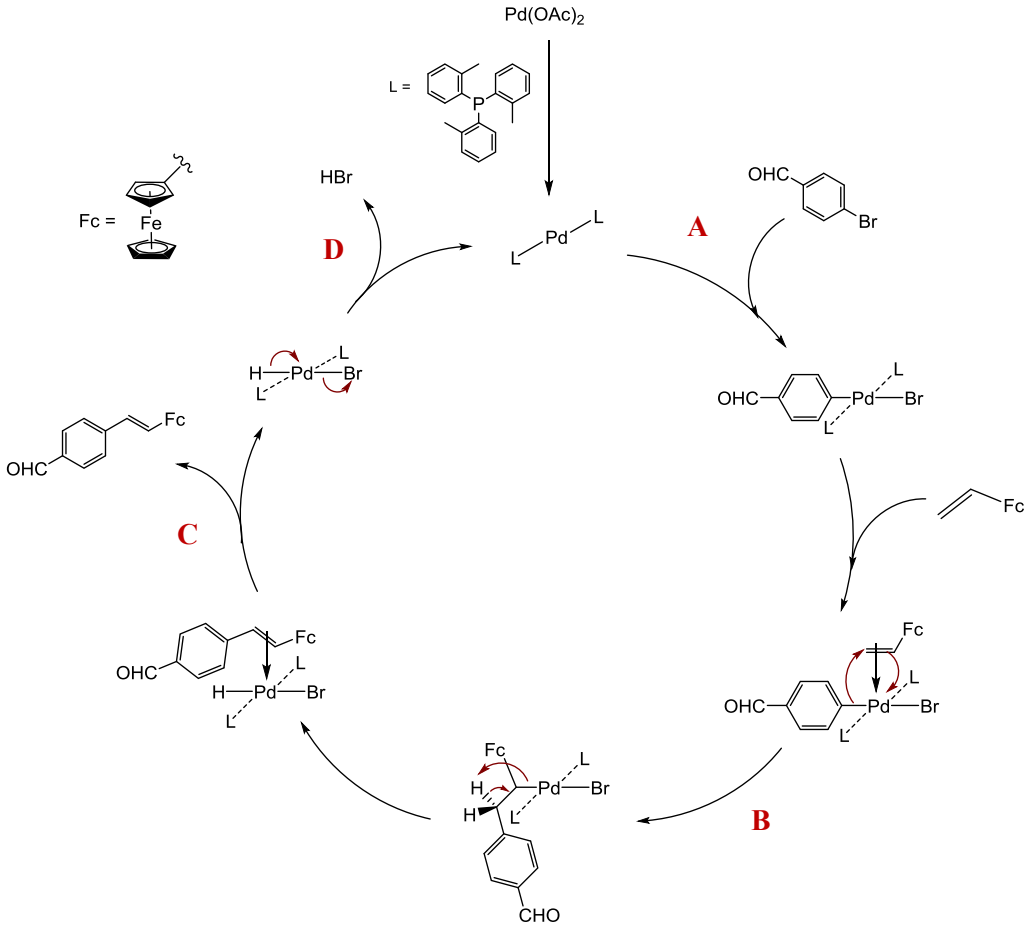

Fig. 2.4: Heck cross-coupling catalytic cycle.[26]

2.2.2 Characterisation

^{1}H Nuclear Magnetic Resonance Spectroscopy

The ^{1}H NMR spectrum of **2.2** (Fig. 2.5) displays peaks corresponding to the ferrocenyl protons; a singlet at 4.11 ppm, corresponding to the 5 protons of the unsubstituted cyclopentadienyl ring, and two triplets (4.21 and 4.36 ppm) for the protons of the monosubtituted cyclopentadienyl ring, as they are in different chemical environments. The spectrum shows a doublet-of-doublets at 6.46 ppm integrating for one proton, which corresponds to the alkenyl proton adjacent to the cyclopentadienyl ring. The two terminal alkenyl protons each give rise to a doublet-of-doublets (at 5.35 and 5.04 ppm respectively). This multiplicity is due to geminal and vicinal coupling experienced by these protons.

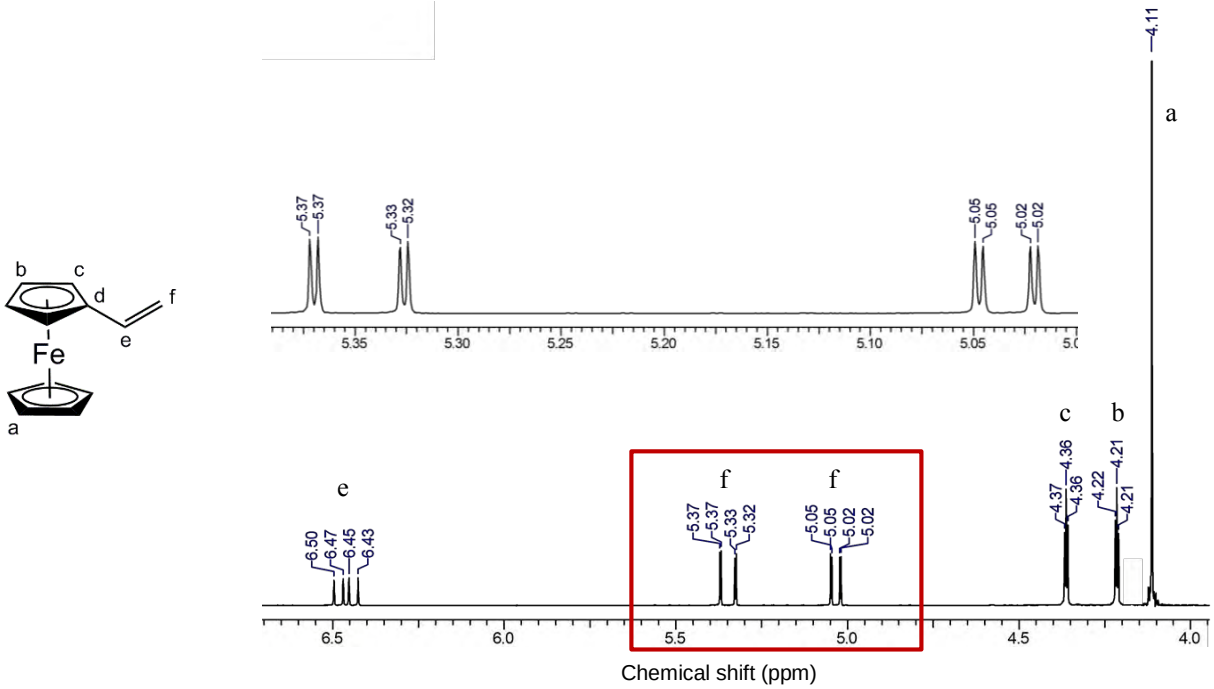

Fig. 2.5: ^{1}H NMR spectrum of **2.2** in $CDCl_3$.

The ^{1}H NMR spectrum of **2.3** confirms the formation of the aldehyde with the presence of a singlet at 9.97 ppm corresponding to the aldehyde proton. The four protons of the 1,4-substitiuted aromatic ring give rise to two doublets at 7.83 and 7.56 ppm respectively, with coupling constants of $J \sim 8$ Hz (Fig. 2.6).

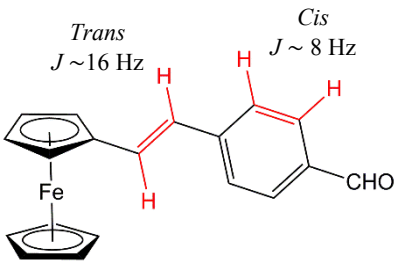

Fig. 2.6: *Cis* and *trans* configurations and coupling constants observed in **2.3**.

Evidence of C-C bond formation is shown in the absence of three alkenyl doublet-of-doublets (as observed for the vinyl protons in the ^{1}H NMR spectrum of **2.2**, Fig 2.5), and the presence of two doublets (at 7.07 and 6.73 ppm respectively) corresponding to the two protons of the alkene moiety. There are two stereoisomers possible for this structure, that with *cis* or *trans* configuration about the alkene group. However, the alkenyl doublets have vicinal coupling constants $J \sim 16$ Hz, confirming a *trans* configuration at the double bond (Fig. 2.6). The ^{1}H NMR spectrum of **2.3** (Fig. 2.7) displays a pattern of peaks similar to that of **2.2** for the ferrocenyl protons. There are two triplets (4 protons of substituted Cp ring) and a singlet (5 protons of unsubstituted Cp ring) shifted slightly downfield compared to that of **2.2**.

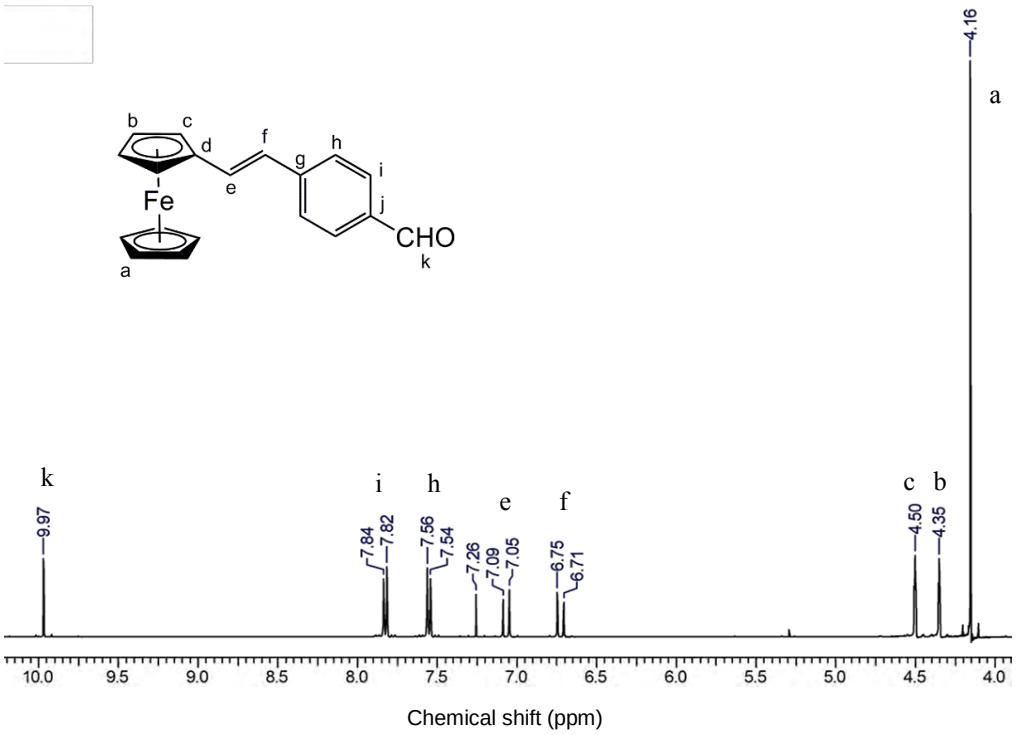

Fig. 2.7: ^{1}H NMR spectrum of **2.3** in $CDCl_3$.

$^{13}C\{^{1}H\}$ Nuclear Magnetic Resonance Spectroscopy

The $^{13}C\{^{1}H\}$ NMR spectra of **2.2** and **2.3** each display the expected number of carbon signals, giving further evidence for their chemical structures. The spectrum of **2.2** displays signals at 134.82 and 111.19 ppm corresponding to the carbon atoms of the vinyl group, with the carbon adjacent to the Cp ring lying most downfield. The ferrocenyl carbon atoms give rise to three signals, similar to the pattern seen in the ^{1}H NMR spectrum of **2.2**. The unsubstituted Cp carbon atoms give rise to one peak at 69.36 ppm, while the carbon atoms of the monosubstituted Cp ring give rise to two peaks (68.79 and 66.83 ppm). Furthermore, the spectrum shows a signal for the quaternary carbon atom of the substituted Cp ring at 83.74 ppm, which is significantly deshielded compared to the other ferrocenyl carbon atoms.

The $^{13}C\{^{1}H\}$ NMR spectrum of **2.3** displays a peak corresponding to the carbonyl carbon atom at 191.67 ppm, further confirming the presence of the aldehyde moiety. The spectrum also displays peaks at 131.52 and 124.60 ppm for the carbon atoms of the alkene moiety. Further to this, the ferrocenyl Cp carbon atoms again give rise to three signals (at 69.99, 69.50 and 67.49 ppm respectively) and a fourth at 82.36 for the quarternary Cp carbon. The six aromatic carbon atoms are observed as four signals in the range 144 – 126 ppm, one signal for each quarternary carbon and another for each pair of equivalent carbons of the 1,4-disubstituted aromatic ring.

Infrared Spectroscopy

Infrared (IR) spectral analysis provides further evidence supporting the synthesis of these ferrocenyl precursors (**2.2** and **2.3**). The different absorption bands observed attest to the composition of the compounds and are in accordance with literature data. Figure 2.8 shows the region from 1600 – 1700 cm^{-1} is important for **2.2** and **2.3**. The presence of a ν(C=C) absorption band at 1630 cm^{-1} in the IR spectrum of **2.2** confirms the alkene moiety of the vinyl group. In the IR spectrum of **2.3**, the ν(C=C) band for the alkene is retained at 1630 cm^{-1}, while the ν(C=O) absorption band for the aldehyde moiety is observed at 1693 cm^{-1} for **2.3**.

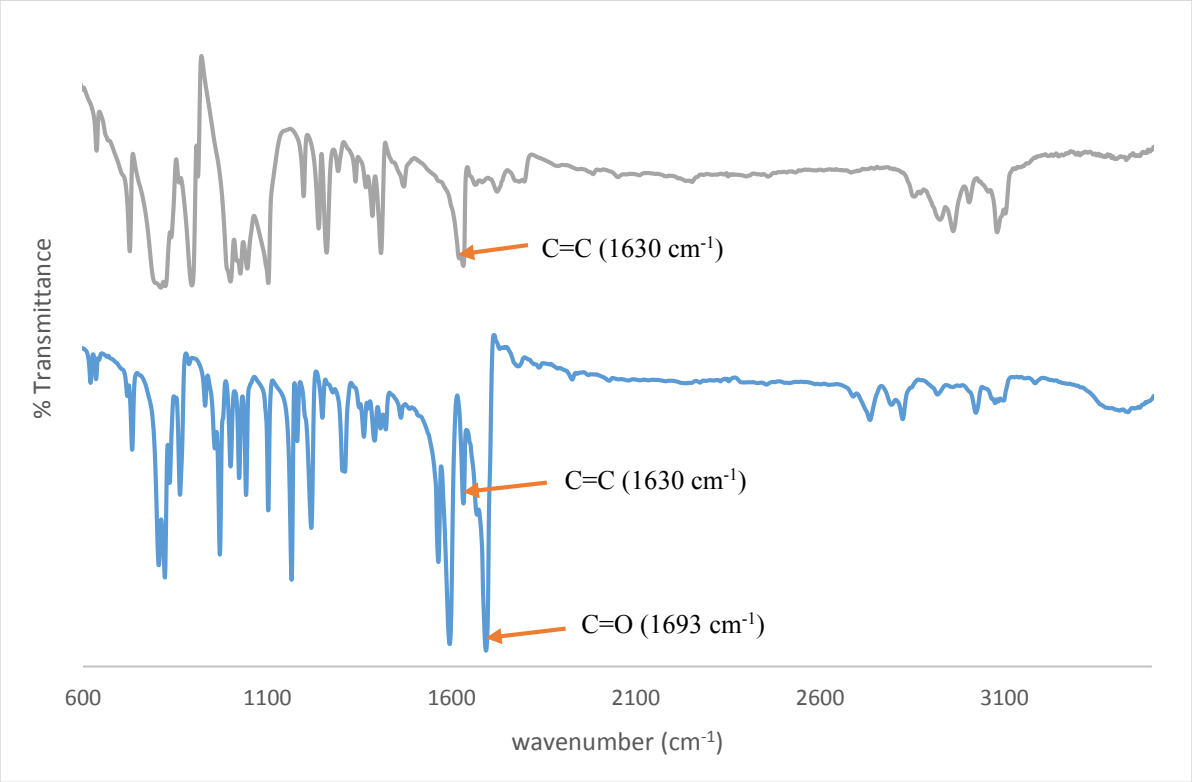

Fig. 2.8: IR spectra of **2.2** (top) and **2.3** (bottom).

Mass Spectrometry

Furthermore, the Electron Impact (EI)-mass spectra of **2.2** and **2.3**, each shows a base peak corresponding to $[M]^+$, 212 *m/z* for **2.2** and 316 *m/z* for **2.3**, further confirming that the desired compounds were obtained.

2.3 Synthesis of Mono- and Polynuclear Ferrocenyl-derived imino complexes (2.4 – 2.9)

2.3.1 Mononuclear complexes (2.4 – 2.6)

2.3.1.1 Synthesis

(*E*)-4-vinylferrocenylbenzaldehyde (**2.3**) was then used in the synthesis of mononuclear ferrocenyl-imino complexes (**2.4** – **2.6**). This was achieved by Schiff-base condensation reactions of **2.3** with various amines in methanol at 40 °C (Scheme 2.2). Compounds **2.4** – **2.6** were isolated as red powders in good yields (83 – 95 %). These complexes display solubility in a range of polar and non-polar solvents, as well as alcoholic solvents.

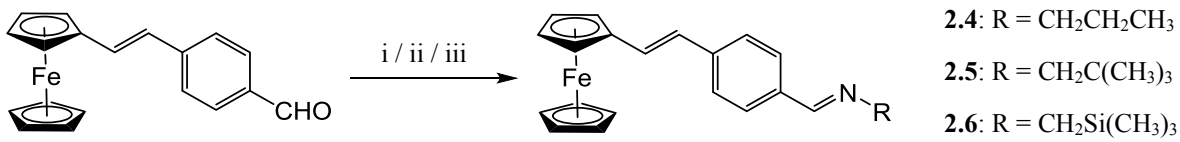

Scheme 2.2: Preparation of mononuclear ferrocenyl imino complexes. (i) n-Propylamine / MeOH / 40 °C / 24 h; (ii) 2,2-Dimethyl-1-propanamine / MeOH / 40 °C / N_2 / 48 h; (iii) (Trimethylsilyl)methylamine / MeOH / 40 °C / N_2 / 48 h.

A Schiff-base condensation reaction, the mechanism of which is shown in Fig. 2.9, involves the nucleophilic addition of an amine to a carbonyl group (aldehyde moiety of **2.3**), followed by dehydration to give the Schiff-base or imine product.

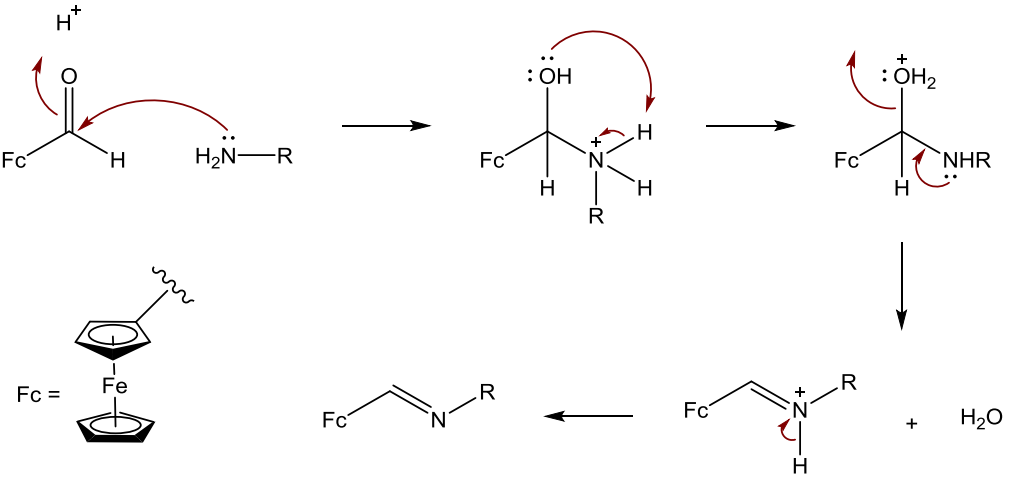

Fig. 2.9: Mechanism of a Schiff-base condensation reaction.

2.3.1.2 Characterisation

^{1}H Nuclear Magnetic Resonance Spectroscopy

The ^{1}H NMR spectra of complexes **2.4** – **2.6**, recorded in $CDCl_3$, all displayed similar trends and patterns upon comparison. A representative example of a typical mononuclear imino complex is shown in Fig 2.10. The most important signal to note is the sharp singlet integrating for one proton, corresponding to the imine proton, in the region 8.25 – 8.11 ppm. This, along with the absence of the singlet corresponding to the aldehyde (at 9.97 ppm), gives evidence of complete imine bond formation (Schiff-base condensation). The two pairs of chemically identical aromatic protons each give rise to a doublet (region 7.71 – 7.45 ppm), while the two protons of the alkene moiety are each observed as a doublet between 6.95 and 6.71 ppm. Furthermore the spectra of **2.4** – **2.6** all display three signals for the ferrocenyl protons; a singlet integrating for the 5 protons of the unsubstituted Cp ring as well as two triplets for the two pairs of chemically equivalent protons of the substituted Cp ring. All of these signals occur at similar chemical shifts and with similar multiplicities and coupling constants to that of compound **2.3**.

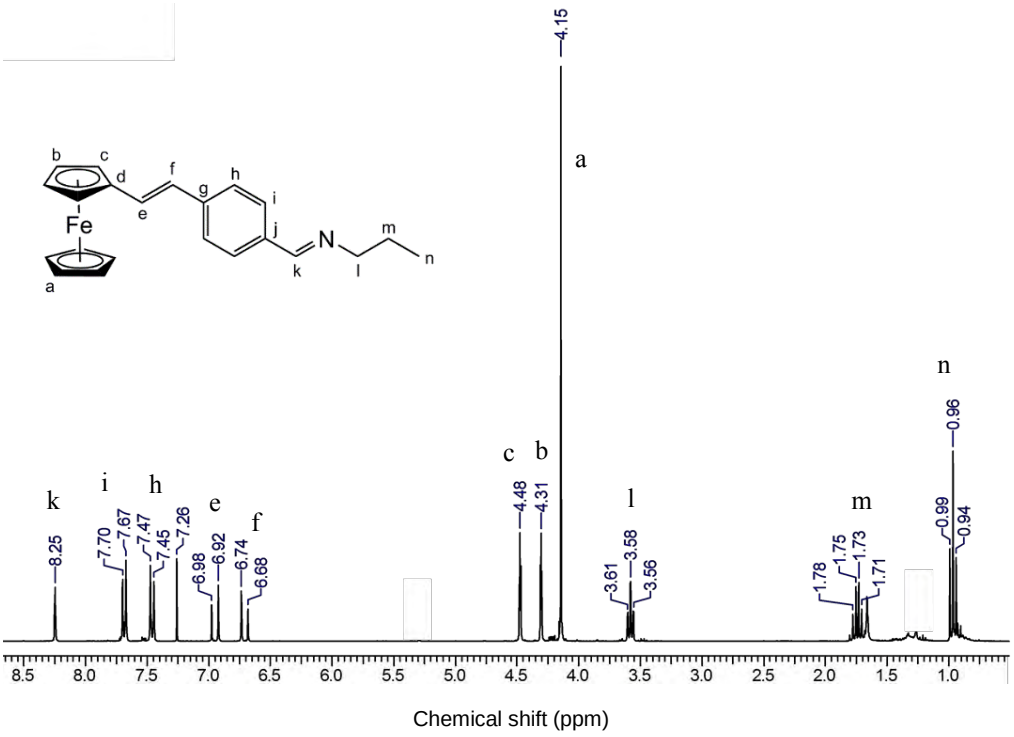

Fig. 2.10: ^{1}H NMR spectrum of **2.4**, a representative example, in $CDCl_3$.

The aliphatic region for **2.4** – **2.6** differ slightly due to their varied alkyl chains. In the spectrum of **2.4** (Fig. 2.10), the two groups of methylene protons of the propyl group are observed as a triplet (3.58 ppm) and a multiplet (1.74 ppm) respectively, while the terminal methyl protons give rise to a triplet at 0.96 ppm. Compounds **2.5** and **2.6** each have one group of methylene protons (adjacent to the imine

bond), which give rise to doublets integrating for two protons at 3.37 and 3.42 ppm respectively. The spectra of **2.5** and **2.6** also display a sharp singlet for the nine protons of the terminal trimethyl moiety. For **2.6**, this singlet is significantly shielded (0.08 ppm compared to 0.99 ppm for **2.5**, the carbon analogue), which is expected as the silicon atom is considerably more electron-donating than a carbon atom.

$^{13}C\{^{1}H\}$ Nuclear Magnetic Resonance Spectroscopy

The imine carbon atoms of **2.4** – **2.6** give rise to signals between 160.68 and 158.04 ppm in the $^{13}C\{^{1}H\}$NMR spectra of these complexes. In addition, the spectra display peaks for the carbon atoms of the ferrocenyl Cp rings, the alkene and the aromatic groups, at similar chemical shift to that of **2.3**. Signals for the alkyl carbon atoms are also seen between 29.70 and 1.03 ppm.

Infrared Spectroscopy

Further evidence for the presence of an imine bond is shown in the IR spectra of **2.4** – **2.6**, which displays the characteristic imine ν(C=N) absorption band at 1628 cm^{-1} for all three complexes. In addition, the carbonyl ν(C=O) of the aldehyde moiety is not present in these spectra. The alkenyl ν(C=C) stretch is present at 1598 cm^{-1}, a significantly lower wavenumber compared to the aldehyde precursor **2.3**. This is expected due to the electron-withdrawing nature of the new imine group.

Mass Spectrometry

The structures of **2.4** – **2.6** were further confirmed using EI-MS. The mass spectra of **2.4** – **2.6** each displays peak corresponding to the molecular ion $[M^+]$ at 357, 385 and 401 *m/z* respectively.

2.3.2 Polynuclear complexes (2.7 – 2.9)

2.3.2.1 Synthesis

Polynuclear ferrocenyl-imino complexes (**2.7** – **2.9**) were subsequently synthesised by Schiff-base condensation reactions of **2.3** with various amines (tris-(2-aminoethyl)-amine or DAB-Am-4 or DAB-Am-8) in methanol at 40 °C (Scheme 2.3), using a similar procedure to that for the preparation of **2.4** – **2.6**. Compounds **2.7** – **2.9** were isolated as orange powders in moderate to high yields (48 – 93 %), displaying solubility in polar organic solvents such as dichloromethane, chloroform and ethyl acetate.

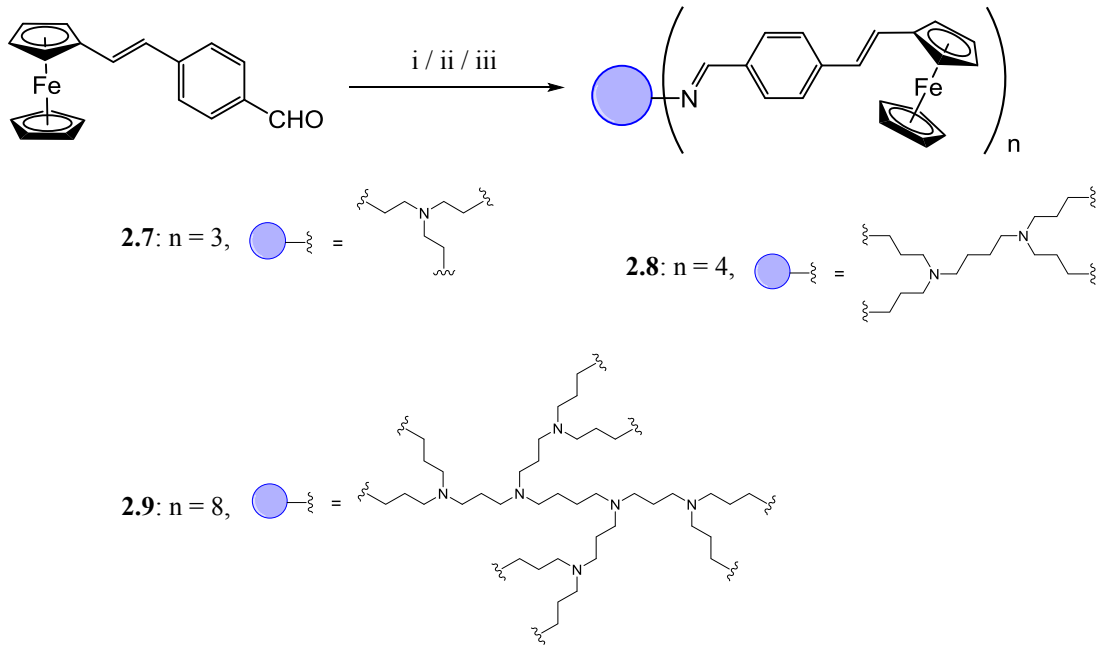

Scheme 2.3: Preparation of polynuclear ferrocenyl imino complexes. (i) Tris-(2-aminoethyl)-amine / MeOH / 40 °C / 22 h; (ii) DAB-Am-4 / MeOH / 40 °C / 36 h; (iii) DAB-Am-8, MeOH / 40 °C / 36 h.

2.3.2.2 Characterisation

^{1}H Nuclear Magnetic Resonance Spectroscopy

The ^{1}H NMR spectra of **2.7** – **2.9** all display peaks corresponding to protons of the ferrocenyl cyclopentadienyl (Cp) rings, alkenyl moeity and the aromatic ring with similar multiplicities, coupling constants and similar chemical shifts to that of compounds **2.4** – **2.6**. All the ^{1}H NMR spectra display a singlet in the range 8.07 – 8.24 ppm, corresponding to the imine protons of **2.7** – **2.9**. The aliphatic region of the ^{1}H NMR spectra of **2.7** – **2.9** due to their different dendritic cores. The protons of the three ethylene branches of **2.7** are observed as two triplets (3.69 and 2.94 ppm) in the spectrum (Fig. 2.11), each integrating for the six protons that are in the same chemical environment.

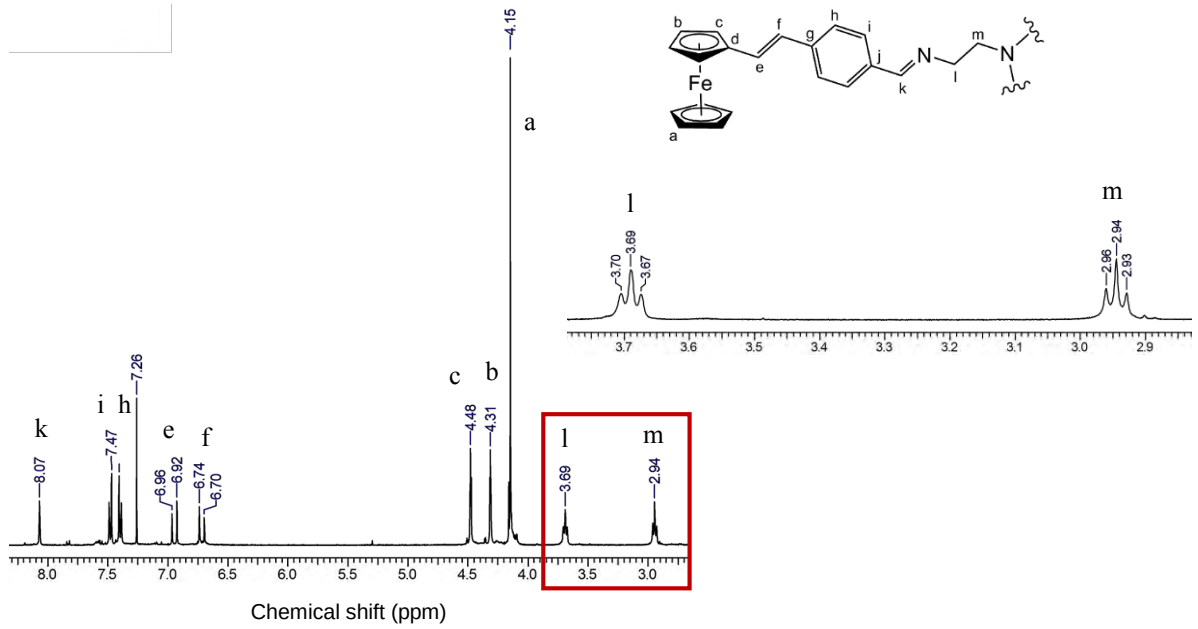

Fig. 2.11: ^{1}H NMR spectrum of **2.7** in $CDCl_3$.

In the ^{1}H NMR spectrum of the first generation metallodendrimer **2.8** (Fig. 2.12), the protons of the aliphatic core and four aliphatic branches give rise to five signals in the region 1.44 – 3.63 ppm and are assigned as shown in the spectrum below. The ^{1}H NMR spectrum of **2.9** displays six peaks in the region 1.43 – 3.61 ppm, corresponding to the 88 protons of the dendritic branches and core.

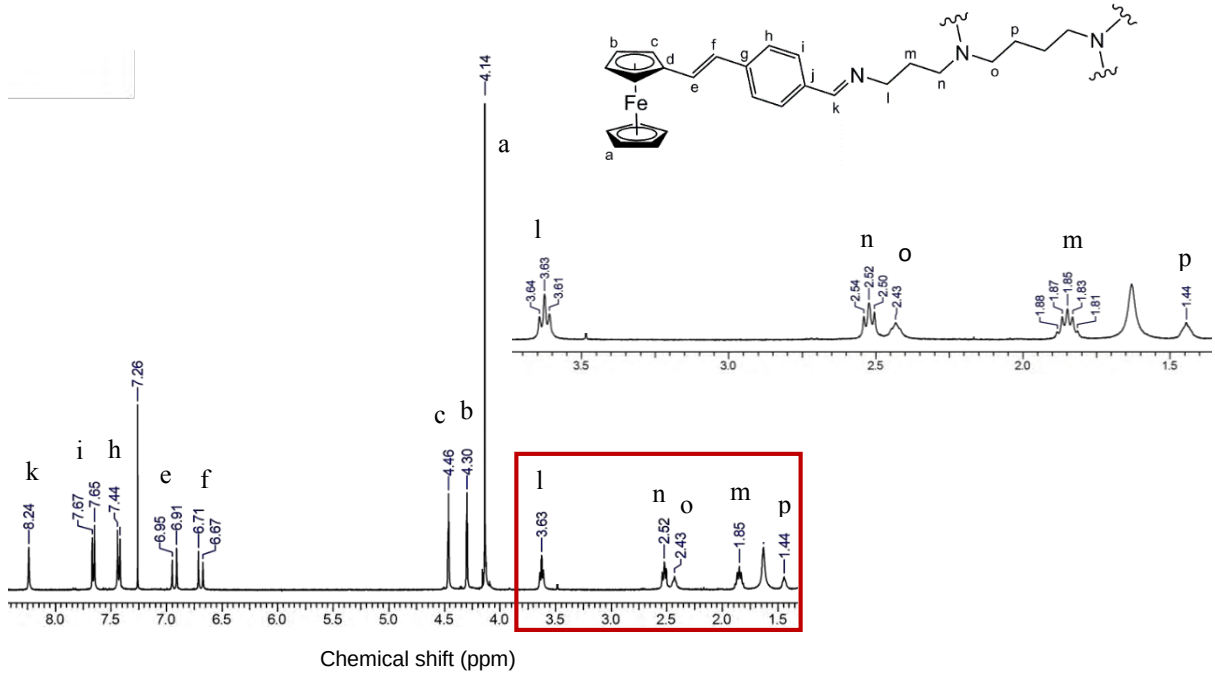

Fig. 2.12: ^{1}H NMR spectrum of **2.8** in $CDCl_3$.

$^{13}C\{^{1}H\}$ Nuclear Magnetic Resonance Spectroscopy

The $^{13}C\{^{1}H\}$ NMR spectra of **2.7** – **2.9** display peaks corresponding to the ferrocenyl carbon atoms, alkenyl carbon atoms and aromatic carbon atoms. The signal for the imine carbon atoms are observed between 161.74 and 160.74 ppm. Furthermore, the carbon atoms of the various aliphatic/dendritic branches and cores are also observed in the spectrum in the range 60.46 – 25.28 ppm.

Infrared Spectroscopy

The IR spectra of **2.7** – **2.9** display further evidence of the presence of the imine bond with the presence of an imine ν(C=N) absorption band at ~1630 cm^{-1} for all three complexes. An alkenyl ν(C=C) stretch for the alkene moiety is also observed in these spectra, at 1598 cm^{-1} for **2.7** and 1600 cm^{-1} for **2.8** and **2.9**.

Mass Spectrometry

High resolution Electrospray Ionisation (ESI) mass spectral analysis was used to confirm the structures of **2.7** – **2.9**. The mass spectrum of **2.7** displays peaks at *m/z* 1041.2966 ($[M+H]^{+}$), *m/z* 521.1527 ($[M+2H]^{2+}$) and *m/z* 347.7709 ($[M+3H]^{3+}$), confirming its structure. In the mass spectrum of **2.8**, a peak corresponding to $[M+2CH_3CN+4H]^{4+}$ is observed at *m/z* 399.2807. Furthermore, the spectrum of **2.9** displays a peak at *m/z* 1061.3795 for $[M+2H+Na]^{3+}$.

2.4 Synthesis of Mono- and Polynuclear Ferrocenyl-derived amino complexes (2.10 – 2.15)

2.4.1 Mononuclear complexes (2.10 – 2.12)

2.4.1.1 Synthesis

The next synthetic step was the preparation of the corresponding amines of compounds **2.4** – **2.9**. Mononuclear amino complex **2.10** was initially synthesised by reduction of the imine bond of mononuclear complex **2.4**. This was achieved via hydrogenation, by reacting **2.4** with sodium borohydride in methanol (Scheme 2.4). Compound **2.10** was isolated as an orange solid, differing in colour compared to the corresponding dark red imine precursor, in 50 % yield.

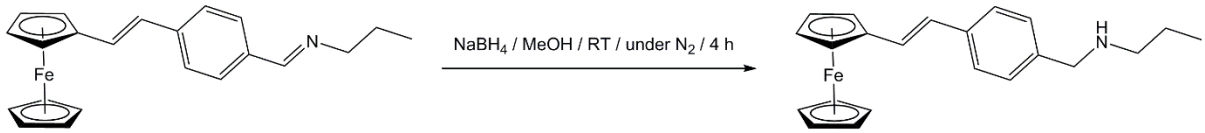

Scheme 2.4: Synthetic route to mononuclear complex **2.10**.

In efforts to improve the low yield of this reaction, all subsequent reactions to produce the amine complexes were performed in a one-pot reductive amination from the aldehyde (**2.3**), without isolating the intermediate imine complex as shown in Scheme 2.5. Compounds **2.10** – **2.12** were synthesised in a one-pot reaction in which a ferrocenyl-aldehyde (**2.3**) underwent a Schiff-base condensation reaction with various amines to give the corresponding ferrocenyl-imine (not isolated), followed by reduction with sodium borohydride to afford the ferrocenyl-amines (**2.10** – **2.12**). All mononuclear complexes were isolated as red or orange solids, displaying solubility in a range of polar and non-polar solvents.

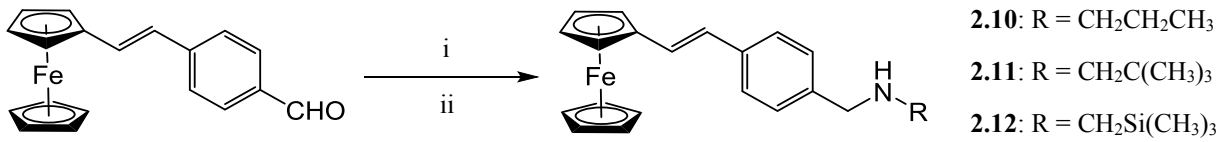

Scheme 2.5: One-pot synthesis of mononuclear ferrocenyl-derived amino complexes. (i) Propylamine or 2,2-Dimethyl-1-propanamine or Trimethylsilyl-1-methanamine / MeOH / 24 hr; (ii) $NaBH_4$ / MeOH: DCM (1:5).

2.4.1.2 Characterisation

^{1}H Nuclear Magnetic Resonance Spectroscopy

The ^{1}H NMR spectra of **2.10** – **2.12** (Fig. 2.13) display peaks corresponding to the protons of the ferrocenyl Cp rings, the alkene group and the aromatic protons with similar multiplicities and coupling constants to their corresponding imino complexes (**2.4** – **2.6**). However, these peaks are all shifted slightly upfield (protons are more shielded) compared to the ferrocenyl-imino complexes (**2.4** – **2.6**). This is due to the relative electron-withdrawing effects of the imine bond compared to the amine bond. The imino moiety is more electron-withdrawing than the amino moiety, resulting in a more deshielding effect on the protons in complexes **2.4** – **2.6**.

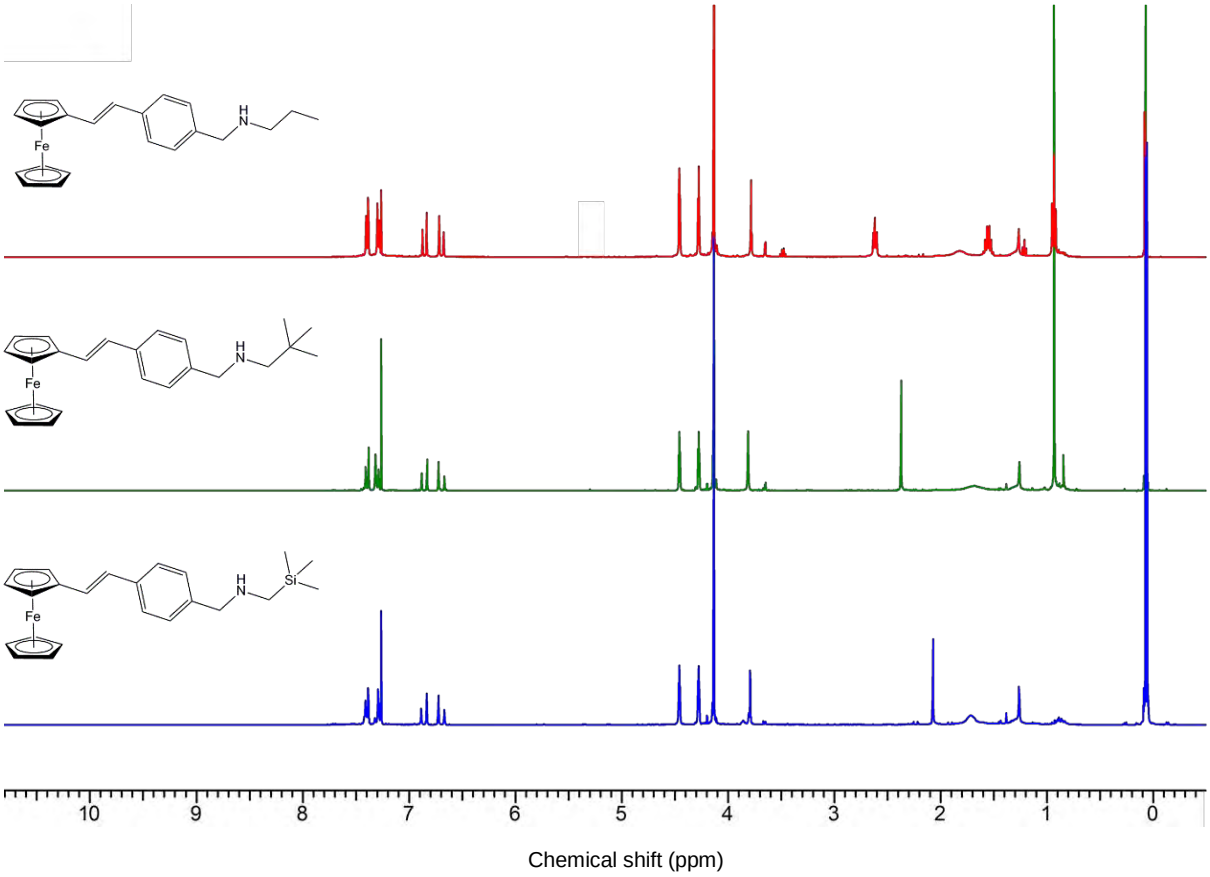

Fig. 2.13: Stacked ^{1}H NMR spectra of **2.10** – **2.12** in $CDCl_3$.

Evidence of reductive amination is displayed in the ^{1}H NMR spectra of **2.10** – **2.12**. The spectra do not display a peak (singlet) corresponding to an aldehyde proton (~10 ppm) or an imine proton (~8 ppm), indicating successful and complete conversion to the amine. Furthermore, the two new methylene protons, adjacent to the aromatic ring and the new amine nitrogen, are observed as a singlet at between 3.81 – 3.79 ppm, confirming hydrogenation of the imine. These trends are consistent for all mononuclear complexes **2.10** – **2.12**.

In the ^{1}H NMR spectrum of **2.10**, the methylene protons of the propyl group give rise to a triplet (2.62 ppm) and a multiplet (1.55 ppm), while the methyl protons are observed as a triplet at 0.93 ppm. These three signals are shifted significantly upfield compared to the imine precursor. This is expected due to the inductive effects of the different functional groups; the imine moiety is more electron-withdrawing than the amine moiety.

For **2.11**, the signal for the two methylene protons adjacent to the amine nitrogen and quaternary carbon is seen at 2.37 ppm (singlet), while the nine terminal methyl protons give rise to a singlet at 0.93 ppm. In the ^{1}H NMR spectrum of **2.12**, the methylene protons adjacent to the silicon atom give rise to a singlet at 2.08 ppm, while the spectrum displays a singlet at 0.07 ppm corresponding to the protons of the methyl group. These protons are significantly shielded (upfield) compared to its carbon analogue (**10**), as a result of the electron-donating effect of the silicon atom.

$^{13}C\{^{1}H\}$ Nuclear Magnetic Resonance Spectroscopy

The $^{13}C\{^{1}H\}$ spectra of **2.10** – **2.12** display all the expected peaks for the aromatic, ferrocenyl and alkene carbon atoms, at similar chemical shifts to that in the corresponding imino complexes **2.4** – **2.6**. In the $^{13}C\{^{1}H\}$ spectrum of **2.4**, the carbon atom between the aromatic ring and the new amine nitrogen gives rise to a significantly deshielded peak at ~161 ppm, which is not present in that of **2.10** – **2.12**. Instead, in the spectra of **2.10** – **2.12**, this carbon atom is now a methylene carbon and is observed as a relatively shielded peak in the region 70.74 – 50.35 ppm. These two observations confirm the presence of an amine moiety.

Infrared Spectroscopy

The infrared spectra of **2.10** – **2.12** give further evidence of reductive amination. The ν(C=O) and ν(C=N) absorption bands of the precursor (**2.3**) and intermediates (**2.4** – **2.6**) respectively, are not present in these spectra. In addition, a ν(N-H) stretching vibration is displayed between 3298 – 3279 cm^{-1} and a ν(N-H) bending vibration around 1633 – 1631 cm^{-1}, confirming the presence of the amine group. A ν(C=C) absorption band is observed for the alkene moiety between 1611 – 1607 cm^{-1}, shifted to slightly higher wavenumbers (compared to **2.4** – **2.6**) as a result of the electron-donating nature of the new amine moiety.

Mass Spectrometry

Electron Impact mass spectrometry was used to confirm the structures of **2.10** – **2.12**. The base peak in the mass spectra of **2.10** – **2.12** each corresponds to the molecular ion [M^+]. These occur at 359, 387 and 403 *m/z* respectively.

2.4.2 Polynuclear Complexes (2.13 – 2.15)

2.4.2.1 Synthesis

Compounds **2.13** – **2.15** were each synthesised in a one-pot reaction in which the ferrocenyl-aldehyde (**2**) underwent a Schiff-base condensation reaction with various amines (tris-(2-aminoethyl)-amine or DAB-Am-4 or DAB-Am-8) to give the corresponding ferrocenyl-imine (not isolated), followed by a reduction with sodium borohydride to afford the ferrocenyl-amine (**2.13** – **2.15**). All polynuclear complexes were isolated as orange powders in moderate yields, displaying solubility in a range of relatively polar solvents such as dichloromethane, ethyl acetate and chloroform.

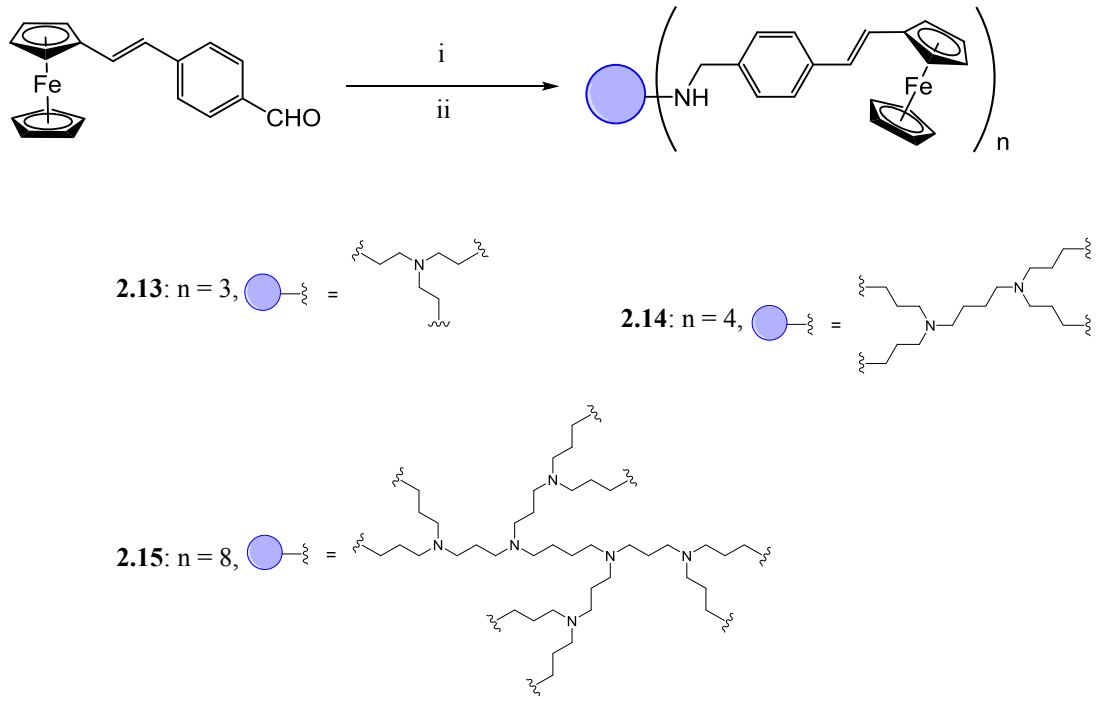

Scheme 2.6: One-pot synthesis of polynuclear ferrocenyl-derived amino complexes. (i) Tris-(2-aminoethyl)-amine / MeOH / 40 °C / 22 h or DAB-Am-4 / MeOH / 40 °C / 36 h or DAB-Am-8, MeOH / 40 °C / 36 h. (ii) $NaBH_4$ / MeOH: DCM (1:5).

2.4.2.2 Characterisation

^{1}H Nuclear Magnetic Resonance Spectroscopy

As with the mononuclear complexes **2.10** – **2.12**, the ^{1}H NMR spectra of **2.13** – **2.15** display peaks corresponding to the protons of the ferrocenyl Cp rings (4.45 – 4.13 ppm), the alkene group (6.90 – 6.65 ppm) and the aromatic protons (7.40 – 7.25 ppm) with similar multiplicities and coupling constants to their imine precursors (**2.7** – **2.9**). Again, the peaks are shifted upfield compared to the imine precursors as a result of the lessened electron-withdrawing nature of the amine group. The ^{1}H NMR spectrum of **2.14** is shown in Fig. 2.14 as a representative example. The spectra of **2.13** – **2.15** do not display a singlet corresponding to an aldehyde proton (~10 ppm) or an imine proton (~8 ppm) of the precursors. Furthermore, all spectra display a broad singlet assigned to the methylene protons adjacent to the amine nitrogen and aromatic ring (region 3.74 – 3.73 ppm), confirming hydrogenation/reduction.

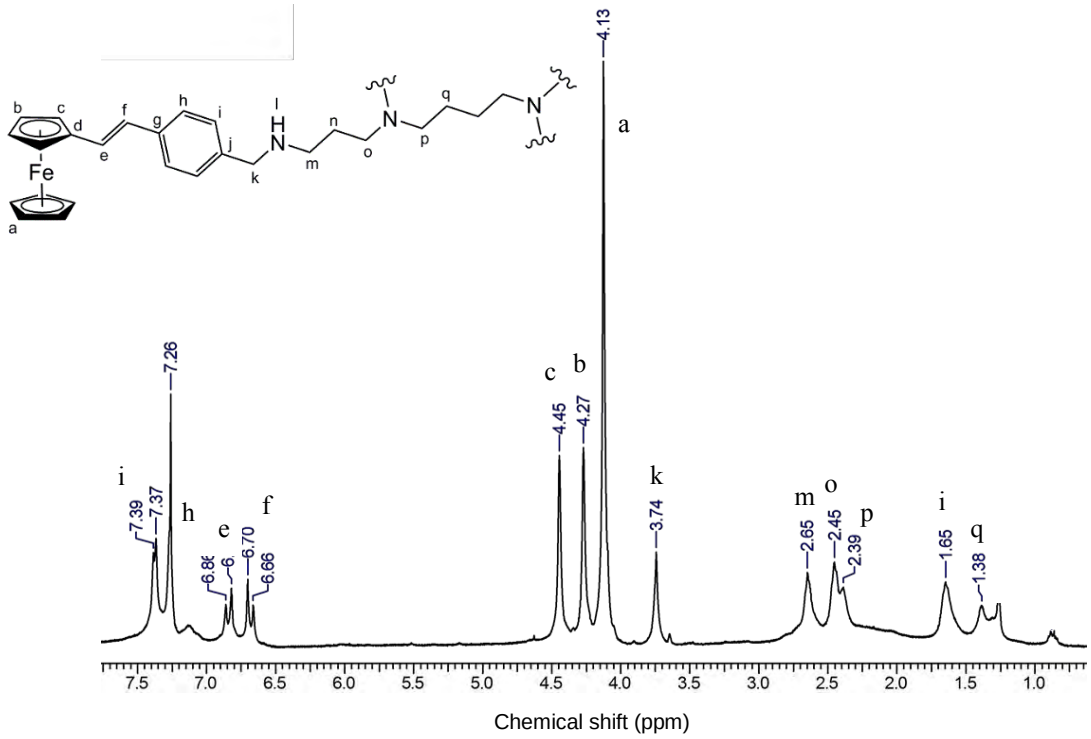

Fig. 2.14: ^{1}H NMR spectrum of **2.14**, a first generation ferrocenyl dendrimer, in $CDCl_3$.

The ^{1}H NMR spectra of **2.13** – **2.15** display broadening and overlapping signals, which is characteristic of dendritic ligands of this type. The signals for the protons of the aliphatic core and branches of **2.13** – **2.15** appear in the regions 2.69 – 2.61, 2.64 – 1.38 and 2.63 – 1.41 ppm, respectively. The ^{1}H and ^{13}C{^{1}H} NMR signals were assigned using 2D NMR methods, Correlation Spectroscopy (COSY) and Heteronuclear Single-Quantum Correlation Spectroscopy (HSQC).

$^{13}C\{^{1}H\}$ Nuclear Magnetic Resonance Spectroscopy

The $^{13}C\{^{1}H\}$ spectra of **2.13 – 2.15** display the expected number of signals corresponding to the carbons of the aromatic group, ferrocenyl moiety and the alkene group in the expected regions. The singlet observed at ~160 ppm in the $^{13}C\{^{1}H\}$ spectra of ferrocenyl-imines **2.7 – 2.9**, assigned to the imine carbon atom, is not observed in the spectra of **2.13 – 2.15**. The presence of peaks between 53.99 – 53.97 ppm for the newly hydrogenated carbon, adjacent to the aromatic ring and the amine nitrogen, further confirms that reductive amination has taken place.

Infrared Spectroscopy

The infrared spectra of the polynuclear complexes **2.13** – **2.15** are similar to that of the mononuclear complexes **2.10** – **2.12**. A alkenyl ν(C=C) absorption band is observed at 1609 cm^{-1} as well as a ν(N-H) stretching and bending vibration at 3302 – 3283 cm^{-1} and 1607 – 1609 cm^{-1} respectively.

Mass Spectrometry

Mass spectral data of **2.13** – **2.15** further confirms the structures of these complexes. The high resolution ESI-mass spectrum of **2.13** displays a peak corresponding to $[M+CH_3OH+H]^+$ at *m/z* 1079.3688. The mass spectra of **2.14** and **2.15** display peaks at *m/z* 759.2933 ($[M+2H]^{2+}$) and *m/z* 318.0697 ($[M+10H]^{10+}$), respectively.

2.5 Summary

Two ferrocene-containing precursors, vinylferrocene (**2.2**) and (*E*)-4-vinylferrocenylbenzaldehyde (**2.3**) were prepared, by a Wittig olefination reaction and Heck cross-coupling reaction, respectively. Using the aldehyde **2.3**, mononuclear ferrocenyl-derived imino complexes (**2.4** – **2.6**) were synthesised by Schiff-base condensation reactions with various amines. A silicon-containing derivative and its carbon analogue were also synthesised, in order to determine the effect of the lipophilic moiety on the biological activity compared to its organic analogue. Polynuclear ferrocenyl-derived imino complexes (**2.7** – **2.9**) based on the tris(2-aminoethyl)amine scaffold and the polypropyleneimine (PPI) first- and second-generation scaffolds were also synthesised using Schiff-base chemistry. These polynuclear complexes were prepared using similar chemical procedures to that of the mononuclear complexes. These afforded tri-, tetra- and octanuclear ferrocenyl complexes. The corresponding mono- and polynuclear ferrocenyl-derived amino complexes (**2.10** – **2.15**) were synthesised via reductive

amination reactions from the aldehyde **2.3**. The imine moiety was hydrogenated in order to compare the effect on the biological activity.

The synthesised imino and amino complexes were isolated in moderate to high yields and were found to be stable in air and in solution. The mononuclear complexes were readily soluble in organic and alcoholic solvents, while the solubility of the polynuclear complexes was limited to organic solvents such as DCM, chloroform and ethyl acetate, as well partial solubility in DMSO. All complexes were characterised ^{1}H, $^{13}C\{^{1}H\}$, COSY and HSQC NMR spectroscopy, IR spectroscopy, elemental analysis and EI- or high-res ESI-mass spectrometry.

2.6 Experimental

2.6.1 Materials

n-Butyllithium, ferrocenecarboxaldehyde, *n*-propylamine, tris(2-aminoethyl)-amine and DAB-Am-4 were purchased from Sigma Aldrich. DAB-Am-8 was purchased from SymoChem. Solvents were purchased from Kimix and Merck and THF was dried by distillation. Methyltriphenylphosphonium iodide (**2.1**)[27] and vinylferrocene (**2.2**)[23] were prepared using modified literature procedures.

2.6.2 Spectroscopic and Analytical Techniques

Infrared (IR) absorptions were measured on a Perkin-Elmer Spectrum 100 FT-IR Spectrometer as KBr pellets or using Attenuated Total Reflectance (ATR). Nuclear Magnetic Resonance (NMR) Spectra were recorded on a Varian Unity XR400 MHz (^{1}H at 399.95 MHz, ^{13}C at 100.58 MHz, ^{31}P at 161.90 MHz), Varian Mercury XR300 MHz (^{1}H at 300.08 MHz, ^{13}C at 75.46 MHz, ^{31}P at 121.47 MHz) or a Bruker Biospin GmbH (^{1}H at 400.22 MHz, ^{13}C at 100.64 MHz, ^{31}P at 162.01 MHz) spectrometer at 30 °C. Chemical shifts are reported using tetramethylsilane (TMS) as the internal standard. Elemental analysis for C, H and N were carried out using a Thermo Flash 1112 Series CHNS-O Analyser. Mass spectrometry determinations were carried out using Electron Impact (EI) on a JEOL GC Matell instrument or Electrospray Ionisation (ESI) on a Waters API Quattro Micro triple quadrupole mass spectrometer with data recorded using both the positive. Melting points were determined using a Reichert-Jung Thermovar or a Büchi Melting Point Apparatus B-540. Compound **2.10** was analysed by HPLC using an Xbridge C18 (4.6 × 150 mm) 5 µm column; 2.0 µL injection volume; flow 0.7 mL min^{-1}; gradient: 30–100% B in 15 min (hold 2 min) (Mobile phase A: 10 nM NH_4OAc in H_2O and Mobile phase B: 10 nM NH_4OAc in methanol) with a Thermo Separation Products (TSP), Spectra SERIES P200 pump UV100 detector set at 254 nm.

2.6.3 Synthesis of precursors

2.6.3.1 Methyltriphenylphosphonium iodide (2.1)[27]

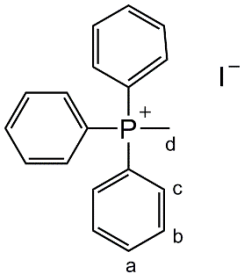

Iodomethane (1.32 mL, 21.1 mmol) dissolved in 20 mL of diethyl ether was added to a stirring solution of triphenylphosphine (5.61 mL, 21.4 mmol) in 30 mL of diethyl ether and the reaction mixture was stirred at room temperature for 12 hours. The desired product **2.1** formed as a white precipitate, which was collected by suction filtration and washed with diethyl ether. Yield: 8.21 g, 95.0 %. **^{1}H NMR (400.22 MHz, $CDCl_3$)**: δ (ppm) = 7.76 (m, 6H, H_b), 7.75 (m, 3H, H_a), 7.73 (m, 6H, H_c), 3.11(m, 3H, H_d). **^{31}P{^{1}H} NMR (162.01 MHz, $CDCl_3$)**: δ (ppm) = 22.61 (s, 1P).

2.6.3.2 Vinylferrocene (2.2)[23]

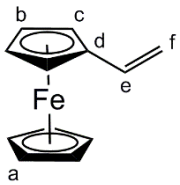

n-Butyllithium (3.79 mL, 9.48 mmol) was added dropwise to a stirring solution of **2.1** (2.55 g, 6.32 mmol) in dry THF (80 mL) at -78 °C. The resulting bright yellow suspension was then warmed to room temperature and stirred for 2 hours. A solution of ferrocenecarboxaldehyde (1.00 g, 4.67 mmol) in dry THF (20 mL) was added dropwise to the suspension at -78 °C and the resulting dull red reaction mixture was warmed to room temperature and stirred for 20 hours. Following stirring, the reaction mixture was quenched with a saturated solution of ammonium chloride (50 mL) at 0 °C. The organic layer was separated and the aqueous layer was washed with diethyl ether (3 x 50 mL). The organic fractions were combined, stirred over anhydrous magnesium sulfate and filtered by gravity. The solvent of the filtrate was reduced and excess diethyl ether was added. A brown precipitate was observed and filtered by gravity. The solvent was then removed to give a bright orange-red residue. The product was then purified by column chromatography using 100 % petroleum ether (40 – 60 °C) as the eluent, with the desired product eluted first. The fractions containing the desired product were combined, the solvent removed and the pure product **2.2** was left to dry under vacuum. The desired product was isolated as an orange crystalline solid. Yield: 0.903 g, 91.2 %. Mp: 49 – 51 °C (lit. 48 – 50 °C). **^{1}H NMR (400.22**

MHz, $CDCl_3$): δ (ppm) = 6.46 (dd, 1H, ^3J = 17.5, ^3J = 10.7 Hz, H_e), 5.35 (dd, 1H, ^3J = 17.5, ^2J = 1.6 Hz, H_f), 5.03 (dd, 1H, ^3J = 10.7, ^2J = 1.6 Hz, H_f), 4.36 (t, 2H, ^3J = 1.8 Hz, H_c), 4.21 (t, 2H, ^3J = 1.8 Hz, H_b), 4.11 (s, 5H, H_a). **$^{13}C\{^1H\}$ NMR (100.64 MHz, $CDCl_3$)**: δ (ppm) = 134.69 (C_e), 111.06 (C_f), 83.61 (C_d), 69.2 (C_a), 68.7 (C_b), 66.7 (C_c). **IR (KBr, cm^{-1})** ν = 1630 (C=C). **Elemental Analysis** for $C_{12}H_{12}Fe$: Found C, 67.6; H, 6.03 %; Calculated C, 68.0; H, 5.70 %. **EI-MS**: m/z 212 ($[M]^+$, 100%).

2.6.3.3 (*E*)-4-vinylferrocenylbenzaldehyde (2.3)

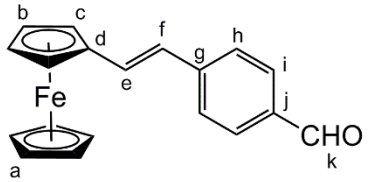

Compound **2.2** (1.50 g, 7.07 mmol), 4-iodobenzaldehyde (0.684 g, 2.95 mmol), palladium(II) acetate (0.0331 g, 0.147 mmol) and tri-*o*-tolyl-phosphine (0.224 g, 0.767 mmol) were dissolved in a 1:10 solution of triethylamine and acetonitrile (30 mL). The dark red reaction mixture was stirred under N_2 at 82 °C for 24 hours. After cooling, the solvent removed and resulting red residue was dissolved in 25 mL of DCM and 25 mL of water added. The organic layer was separated and the aqueous layer washed with DCM (3 x 25 mL). The organic (DCM) fractions were combined, stirred over anhydrous $MgSO_4$ and filtered by gravity. The solvent was removed to give a dark red residue. The product was purified by column chromatography, initially using a solvent system of 100% petroleum ether, followed by 50:50 mixture of petroleum ether (40 – 60 °C) and DCM. The desired product **2.3** was isolated as a dark red powder. Yield: 0.680 g, 72.9 %. Mp: decomposition without melting, onset at 110 °C. **^1H NMR (400.22 MHz, $CDCl_3$)**: δ (ppm) = 9.97 (s, 1H, H_k), 7.83 (d, 2H, ^3J = 8.3 Hz, H_i), 7.56 (d, 2H, ^3J = 8.4 Hz, H_h), 7.07 (d, 1H, ^3J = 16.1 Hz, H_e), 6.73 (d, 1H, ^3J = 16.1 Hz, H_f), 4.51 (t, 2H, ^3J = 1.8 Hz, H_c), 4.35 (t, 2H, ^3J = 1.8 Hz, H_b), 4.16 (s, 5H, H_a). **$^{13}C\{^1H\}$ NMR (100.64 MHz, $CDCl_3$)**: δ (ppm) = 191.55 (C_k), 144.07 (C_j), 134.67 (C_g), 131.52 (C_e), 130.32 (C_i), 126.07 (C_h), 124.60 (C_f), 82.25 (C_d), 69.76 (C_b), 69.38 (C_a), 67.37 (C_c). **IR (KBr, cm^{-1})** ν = 1693 (C=O), 1630 (C=C). **Elemental Analysis** for $C_{19}H_{16}FeO{\cdot}0.5H_2O$: Found C, 70.3; H, 5.07 %; Calculated C, 70.18; H, 5.27 %. **EI-MS**: m/z 316 ($[M]^+$, 100%).

2.6.4 Synthesis of Mononuclear Ferrocenyl-imino Complexes

2.6.4.1 (*E*,*E*)-1-propyl-4-vinylferrocenylbenzaldimine (2.4)

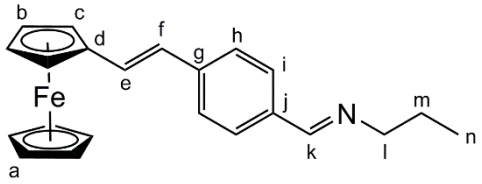

n-Propylamine (0.0953 g, 1.61 mmol) dissolved in 10 mL of methanol was added dropwise to a solution of **2.3** (0.0509 g, 0.158 mmol) in 20 mL of methanol. The red suspension was stirred at room temperature for 24 hours. The solvent of the resulting red solution was reduced to dryness, the residue dissolved in DCM and washed using a DCM/water extraction. The organic (DCM) fractions were combined, stirred over $MgSO_4$ and filtered by gravity. The solvent of the filtrate was removed to afford the desired product **2.4** as a dark red solid residue, which was dried under vacuum. Yield: 0.0468 g, 82.8 %. M.p: 127.7 – 129.8 °C. **^{1}H NMR (400.22 MHz, $CDCl_3$)**: δ (ppm) = 8.25 (s, 1H, H_k), 7.68 (d, 2H, ^3J = 8.3 Hz, H_i), 7.46 (d, 2H, ^3J = 8.3 Hz, H_h), 6.95 (d, 1H, ^3J = 16.1 Hz, H_e), 6.71 (d, 1H, ^3J = 16.1 Hz, H_f), 4.48 (t, 2H, ^3J = 1.8, H_c), 4.30 (t, 2H, ^3J = 1.8, H_b), 4.15 (s, 5H, H_a), 3.58 (td, 2H, ^3J = 7.0, ^4J = 1.2, H_l), 1.74 (m, 2H, H_m), 0.97 (t, 3H, ^3J = 7.4, H_n). **^{13}C{^{1}H} NMR (100.64 MHz, $CDCl_3$)**: δ (ppm) = 160.68 (C_k), 140.10 (C_j), 134.79 (C_g), 128.66 (C_e), 128.59 (C_i), 126.02 (C_h), 125.58 (C_f), 83.15 (C_d), 69.41 (C_a and C_b), 67.18 (C_c), 63.75 (C_l), 24.26 (C_m), 11.99 (C_n). **IR (KBr, cm^{-1})** ν = 1628 (C=N), 1598 (C=C). **Elemental Analysis** for $C_{22}H_{23}FeN{\cdot}1.5H_2O$: Found C, 69.10; H, 6.90; N, 2.29 %; Calculated C, 68.76; H, 6.82; N, 3.64 %. **EI-MS**: m/z 357 ($[M]^+$, 100%).

2.6.4.2 (*E*,*E*)-1-(2,2-dimethyl-1-propyl)-4-vinylferrocenylbenzaldimine (2.5)

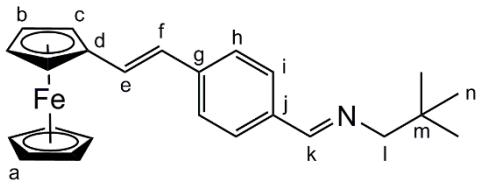

2,2-Dimethyl-1-propanamine (0.0266 g, 0.316 mmol) was added dropwise to a solution of **2.3** (0.0503 g, 0.158 mmol) in 40 mL of methanol. The dark red suspension was stirred under nitrogen at room temperature for 48 hours. The solvent of the resulting red solution was reduced to dryness, the residue dissolved in DCM and separated by DCM/water extraction, the aqueous layer was washed with DCM (3 x 20 mL). The organic (DCM) fractions were collected, stirred over $MgSO_4$, filtered by gravity and the solvent of the filtrate removed to afford the desired product **25** as a dark red solid, which was dried under vacuum. Yield: 0.0929 g, 95.3 %. Mp: 141.4 – 142.9 °C. **^{1}H NMR (400.22 MHz, $CDCl_3$): δ (ppm)** = 8.20 (s, 1H, H_k), 7.71 (d, 2H, ^3J = 8.3 Hz, H_i), 7.46 (d, 2H, ^3J = 8.3 Hz, H_h), 6.95 (d, 1H, ^3J = 16.1 Hz, H_e), 6.72 (d, 1H, ^3J = 16.1 Hz, H_f), 4.48 (t, 2H, ^3J = 1.7, H_c), 4.31 (t, 2H, ^3J = 1.7 Hz, H_b), 4.15

(s, 5H, H_a), 3.37 (d, 2H, ^4J = 1.5 Hz, H_l), 1.00 (s, 9H, H_n). **$^{13}C\{^1H\}$ NMR (100.64 MHz, $CDCl_3$)**: δ (ppm) = 160.60 (C_k), 140.17 (C_j), 135.09 (C_g), 128.66 (C_e), 128.57 (C_i), 126.00 (C_h), 125.64 (C_f), 83.18 (C_d), 74.22 (C_m), 69.41 (C_a and C_b), 67.19 (C_c), 32.80 (C_l), 28.16 (C_n). **IR (KBr, cm^{-1})** ν =1628 (C=N), 1598 (C=C). **Elemental Analysis** for $C_{24}H_{27}FeN{\cdot}0.7H_2O$: Found C, 72.41; H, 7.27; N, 2.70 %; Calculated C, 72.44; H, 7.19; N, 3.52 %. **HPLC**: > 95 %, t_r = 4.94 min. **EI-MS**: m/z 385 ($[M]^+$, 100%).

2.6.4.3 (*E*,*E*)-1-(trimethylsilyl-methyl)-4-vinylferrocenylbenzaldimine (2.6)

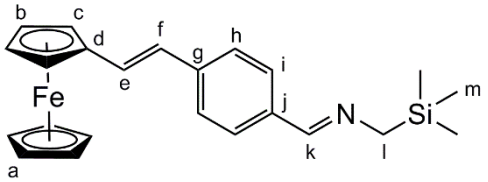

(Trimethylsilyl)methylamine (0.131 g, 1.27 mmol) was added dropwise to a solution of **2.3** (0.0812 g, 0.253 mmol) in 40 mL of methanol. The dark red suspension was stirred under nitrogen at room temperature for 48 hours. The solvent of the resulting red solution was reduced to dryness, the residue dissolved in DCM and washed using a DCM/water extraction. The organic (DCM) fractions were collected and the solvent reduced to afford the desired product **2.6** as a dark red solid, which was dried under vacuum. Yield: 0.0905 g, 89.2 %. Mp: 110.4 – 113.2 °C. **^1H NMR (400.22 MHz, $CDCl_3$)**: δ (ppm) 8.11 (s, 1H, H_k), 7.65 (d, 2H, ^3J = 8.3 Hz, H_i), 7.45 (d, 2H, ^3J = 8.3 Hz, H_h), 6.93 (d, 1H, ^3J = 16.1 Hz, H_e), 6.71 (d, 1H, ^3J = 16.1 Hz, H_f), 4.48 (t, 2H, ^3J = 1.7 Hz, H_c), 4.30 (t, 2H, ^3J = 1.7 Hz, H_b), 4.14 (s, 5H, H_a), 3.42 (d, 2H, ^4J = 1.5 Hz, H_l), 0.09 (s, 9H, H_m). **$^{13}C\{^1H\}$ NMR (100.64 MHz, $CDCl_3$)**: δ (ppm) = 158.04 (C_k), 128.88 (C_j), 128.53 (C_g), 128.33 (C_e), 128.11 (C_i), 126.01 (C_h), 125.67 (C_f), 83.24 (C_d), 69.41 (C_a), 69.37 (C_b), 67.16 (C_c), 54.74 (C_k), 1.16 (C_l). **IR (ATR, cm^{-1})** ν = 1628 (C=N), 1598 (C=C). **Elemental Analysis** for $C_{23}H_{27}FeN$: Found C, 68.73; H, 6.71; N, 2.39 %; Calculated C, 68.82; H, 6.78; N, 3.49 %. **EI-MS**: m/z 401 ($[M]^+$, 100%).

2.6.5 Synthesis of Polynuclear Ferrocenyl-imino Complexes

2.6.5.1 (*E*,*E*)-Tris(2-aminoethyl)-4-vinylferrocenylbenzaldimine (2.7)

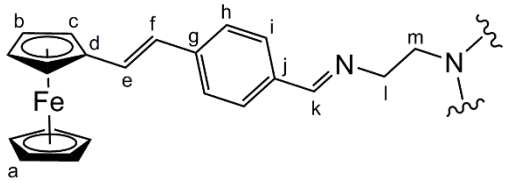

Tris-(2-aminoethyl)-amine (0.0120 g, 0.0843 mmol) dissolved in 10 mL of methanol was added dropwise to a solution of **2.3** (0.0800 g, 0.253 mmol) in 40 mL of methanol and the bright red suspension was stirred at 40 °C for 22 hours. The desired product **2.7** formed as an orange precipitate, which was

collected by suction filtration and washed with petroleum ether. Yield: 0.0813 g, 92.6 %. Mp: 115 – 116 °C. **^{1}H NMR (400.22 MHz, $CDCl_3$)**: δ (ppm) = 8.07 (s, 3H, H_k), 7.48 (d, 6H, ^{3}J = 8.3 Hz, H_i), 7.40 (d, 6H, ^{3}J = 8.4 Hz, H_h), 6.95 (d, 3H, ^{3}J = 16.1 Hz, H_e), 6.72 (d, 3H, ^{3}J = 16.1 Hz, H_f) 4.48 (t, 6H, ^{3}J = 1.7 Hz, H_c), 4.31 (t, 6H, ^{3}J = 1.7 Hz, H_b), 4.15 (s, 15H, H_a), 3.69 (t, 6H, ^{3}J = 6.2 Hz, H_l), 2.95 (t, 6H, ^{3}J = 6.1 Hz, H_k). **^{13}C{^{1}H} NMR (100.64 MHz, $CDCl_3$)**: δ (ppm) = 161.74 (C_k), 140.21 (C_j), 134.87 (C_g), 128.67 (C_e), 128.58 (C_i), 126.00 (C_h), 125.60 (C_f), 83.13 (C_d), 69.44 (C_a and C_b), 67.22 (C_c), 60.46 (C_l), 55.98 (C_m). **IR (ATR, cm^{-1})** ν = 1631 (C=N), 1598 (C=C). **Elemental Analysis** for $C_{63}H_{60}Fe_3N_4$: Found C, 71.89; H, 5.83; N, 4.58 %; Calculated C, 72.71; H, 5.81; N, 5.38 %. **HR-ESI-MS**: *m*/*z* 1041.2966 ($[M+H]^+$, 54 %), *m*/*z* 521.1527 ($[M+2H]^{2+}$, 100 %), *m*/*z* 347.7709 ($[M+3H]^{3+}$, 64 %).

2.6.5.2 (*E*,*E*)-1-DAB-4-vinylferrocenylbenzaldimine (2.8)

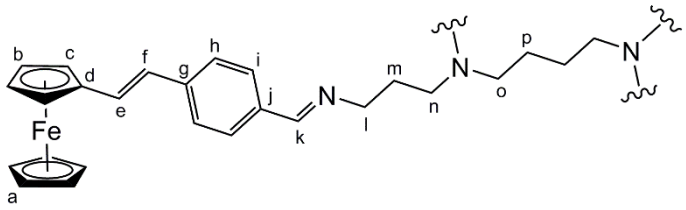

DAB-G1-$(NH_2)_4$ (0.0205 g, 0.0632 mmol) dissolved in 10 mL of methanol was added dropwise to a solution of **2.3** (0.0799 g, 0.253 mmol) in 40 mL of methanol and the bright red suspension was stirred at 40 °C for 36 hours. The desired product **2.8** formed as an orange precipitate, which was collected by suction filtration and washed with petroleum ether (40 – 60 °C). Yield: 0.0847 g, 88.8 %. Mp: 109 – 111 °C. **^{1}H NMR (400.22 MHz, $CDCl_3$)**: δ (ppm) = 8.24 (s, 4H, H_k), 7.66 (d, 8H, ^{3}J = 8.3 Hz, H_i), 7.43 (d, 8H, ^{3}J = 8.4 Hz, H_h), 6.93 (d, 4H, ^{3}J = 16.1 Hz, H_e), 6.69 (d, 4H, ^{3}J = 16.1 Hz, H_f) 4.46 (t, 8H, ^{3}J = 1.7 Hz, H_c), 4.30 (t, 8H, ^{3}J = 1.7 Hz, H_b), 4.14 (s, 20H, H_a), 3.63 (t, 8H, ^{3}J = 7.0 Hz, H_l), 2.52 (t, 8H, ^{3}J = 7.0 Hz, H_n), 2.43 (m, 4H, H_o), 1.85 (m, 8H, H_m), 1.45 (m, 4H, H_p). **^{13}C{^{1}H} NMR (100.64 MHz, $CDCl_3$)**: δ (ppm) = 160.74 (C_k), 140.08 (C_j), 134.77 (C_g), 128.47 (C_e and C_i), 126.06 (C_h), 125.47 (C_f), 83.02 (C_d), 69.27 (C_a and C_b), 67.06 (C_c), 59.81 (C_n), 54.14 (C_l), 51.74 (C_o), 28.46 (C_m), 25.28 (C_p). **IR (ATR, cm^{-1})** ν = 1631 (C=N), 1600 (C=C). **Elemental Analysis** for $C_{92}H_{96}Fe_4N_6 \cdot H_2O$: Found C, 72.45; H, 6.61; N, 4.75 %; Calculated C, 72.36; H, 6.47; N, 5.50 %. **HR-ESI-MS**: *m*/*z* 399.2807 ($[M+2CH_3CN+4H]^{4+}$, 18 %).

2.6.5.3 (*E*,*E*)-1-DAB-4-vinylferrocenylbenzaldimine (2.9)

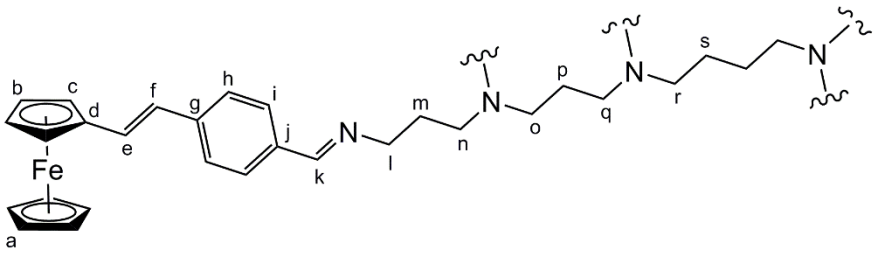

DAB-G2-$(NH_2)_8$ (0.0205 g, 0.0632 mmol) dissolved in 10 mL of methanol was added dropwise to a solution of **2.3** (0.0799 g, 0.253 mmol) in 40 mL of methanol and the bright red suspension was stirred at 40 °C for 36 hours. The solvent was removed and the resulting orange residue dissolved in a minimum amount of DCM. The dark red solution was added dropwise to a large excess of petroleum ether (40 – 60 °C). The desired product **2.9** formed as an orange precipitate, which was collected by suction filtration and dried under vacuum. Yield: 0.0594 g, 47.6 %. Mp: 78 – 80 °C. **^{1}H NMR (400.22 MHz, $CDCl_3$):** δ (ppm) = 8.22 (s, 8H, H_k), 7.64 (d, 16H, ^3J = 8.3 Hz, H_i), 7.41 (d, 16H, ^3J = 8.4 Hz, H_h), 6.91 (d, 8H, ^3J = 16.1 Hz, H_e), 6.68 (d, 8H, ^3J = 16.1 Hz, H_f) 4.45 (t, 16H, ^3J = 1.7 Hz, H_c), 4.29 (t, 16H, ^3J = 1.8 Hz, H_b), 4.13 (s, 40H, H_a), 3.61 (t, 16H, ^3J = 6.6 Hz, H_l), 2.52 (br m, 16H, H_n), 2.43 (br m, 20H, H_o and H_q and H_r), 1.84 (br m, 16H, H_m), 1.68 (m, 16H, H_p), 1.42 (br m, 4H, H_s). **^{13}C{^{1}H} NMR (100.64 MHz, $CDCl_3$)**: δ (ppm) = 160.83 (C_k), 140.19 (C_j), 134.92 (C_g), 128.63 (C_e and C_i), 126.05 (C_h), 125.63 (C_f), 83.17 (C_c), 69.42 (C_a and C_b), 67.21 (C_c), 59.99 (C_m), 54.48, 52.53 (C_k), 51.92 ($C_{l/n}$), 41.00, 28.63 ($C_{o/p}$), 25.36, 24.90. **IR (ATR, cm^{-1})** ν = 1631 (C=N), 1600 (C=C). **Elemental Analysis** for $C_{192}H_{208}Fe_8N_{14}\cdot 2.5H_2O$: Found C, 71.81; H, 6.79; N, 5.80 %; Calculated C, 71.98; H, 6.70; N, 6.12 %. **HR-ESI-MS**: *m*/*z* 1061.3795 ($[M+2H+Na]^{3+}$, 35 %).

2.6.6 Synthesis of Mononuclear Ferrocenyl-amino Complexes

2.6.6.1 (*E*)-1-propyl-4-vinylferrocenylbenzaldamine (2.10)

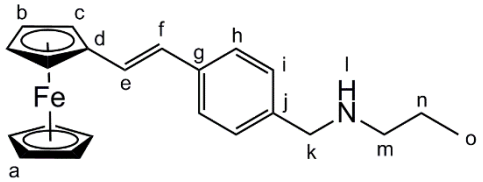

n-Propylamine (0.187 g, 3.16 mmol) dissolved in 10 mL of methanol was added dropwise to a solution of **2.3** (0.101 g, 0.319 mmol) in 30 mL of methanol. The red suspension was stirred at 40 °C for 24 hours. The solvent of the resulting dark red suspension was reduced to dryness and the residue dissolved in 25 mL of dichloromethane. Sodium borohydride (0.0510 g, 1.32 mmol) was then added under N_2 at 0 °C, followed by 5 mL of methanol. The cloudy red solution was warmed to room temperature and

stirred for 5 hours, after which the solution became clear and bright orange in colour. The solution was then quenched with 15 mL of water at 0 °C, the solvent (DCM and MeOH) reduced and the resulting solution was washed using a DCM/water extraction. The organic (DCM) fractions were collected and the solvent reduced to afford the desired product **2.10** as a bright red-orange powder, which was dried under vacuum. Yield: 0.103 g, 99.4 %. Mp: 89.5 – 92.1 °C. **^{1}H NMR (400.22 MHz, $CDCl_3$)**: δ (ppm) = 7.40 (d, 2H, ^{3}J = 8.1 Hz, H_i), 7.30 (d, 2H, ^{3}J = 8.3 Hz, H_h), 6.86 (m, 1H, H_e), 6.68 (m, 1H, H_f), 4.46 (t, 2H, ^{3}J = 1.8 Hz, H_c), 4.28 (t, 2H, ^{3}J = 1.8 Hz, H_b), 4.13 (s, 5H, H_a), 3.79 (s, 2H, H_k), 2.62 (t, 2H, ^{3}J = 7.2 Hz, H_m), 1.57 (m, 2H, H_n), 0.93 (t, 3H, ^{3}J = 7.3 Hz, H_o). **^{13}C{^{1}H} NMR (100.64 MHz, $CDCl_3$)**: δ (ppm) = 138.70 (C_j), 136.92 (C_g), 128.75 (C_i), 126.77 (C_e), 125.96 (C_f), 125.92 (C_h), 83.55 (C_d), 69.33 (C_a), 69.12 (C_b), 66.97 (C_c), 53.70 (C_k), 51.22 (C_m), 23.10 (C_n), 11.89 (C_o). **IR (ATR, cm^{-1})** ν = 1611 (C=C), 3298, 1631 (N-H). **EI-MS**: m/z 359 ([M]$^{+}$, 100%). **Elemental Analysis** for $C_{22}H_{25}FeN{\cdot}H_2O$: Found C, 70.31; H, 7.73; N, 2.86 %; Calculated C, 70.03; H, 7.21; N, 3.71 %. **HPLC**: > 95 % purity, t_r = 4.10 min.

2.6.6.2 (*E*)-1-(2,2-dimethyl-1-propyl)-4-vinylferrocenylbenzaldamine (2.11)

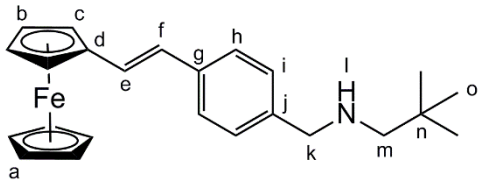

2,2-Dimethyl-1-propanamine (0.112 g, 1.28 mmol) was added dropwise to a solution of **2.3** (0.0800 g, 0.253 mmol) in 30 mL of methanol. The red suspension was stirred under N_2 at 40 °C for 24 hours. The solvent of the resulting dark red suspension was removed and the residue dissolved in 25 mL of dichloromethane. Sodium borohydride (0.0383 g, 1.01 mmol) was then added under N_2 at 0 °C, followed by 5 mL of methanol. The cloudy red solution was warmed to room temperature and stirred for 5 hours, after which the solution became clear and bright orange in colour. The solution was then quenched with 15 mL of water at 0 °C, the solvent (DCM and MeOH) reduced and the resulting solution was washed using a DCM/water extraction. The organic (DCM) fractions were collected and the solvent reduced to afford the desired product **2.11** as a bright red-orange powder, which was dried under vacuum. Yield: 0.115 g, 94.2 %. M.p: 95.9 – 98.0 °C. **^{1}H NMR (400.22 MHz, $CDCl_3$)**: δ (ppm) = 7.40 (d, 2H, ^{3}J = 8.1 Hz, H_i), 7.29 (d, 2H, ^{3}J = 8.3 Hz, H_h), 6.86 (d, 1H, ^{3}J = 16.1 Hz, H_e), 6.70 (d, 1H, ^{3}J = 16.2 Hz, H_f), 4.46 (t, 2H, ^{3}J = 1.8 Hz, H_c), 4.28 (t, 2H, ^{3}J = 1.8 Hz, H_b), 4.14 (s, 5H, H_a), 3.80 (s, 2H, H_k), 2.37 (s, 1H, H_m), 0.93 (s, 9H, H_o). **^{13}C{^{1}H} NMR (100.64 MHz, $CDCl_3$)**: δ (ppm) = 139.84 (C_j), 136.68 (C_g), 128.44 (C_i), 126.54 (C_e), 126.10 (C_f), 125.88 (C_h), 83.68 (C_c), 69.33 (C_a), 69.08 (C_b), 66.97 (C_c) 61.79 (C_k), 54.61 (C_m), 31.67 (C_n), 27.95 (C_o). **IR (ATR, cm^{-1})** ν = 1607 (C=C), 3279, 1633 (N-

H). **EI-MS**: m/z 387 ([M]$^+$, 100%). **Elemental Analysis** for $C_{24}H_{29}FeN{\cdot}0.5H_2O$: Found C, 72.46; H, 7.62; N, 3.07 %; Calculated C, 72.73; H, 7.63; N, 3.53 %.

2.6.6.3 (*E*)-1-(trimethylsilyl-methyl)-4-vinylferrocenylbenzaldamine (2.12)

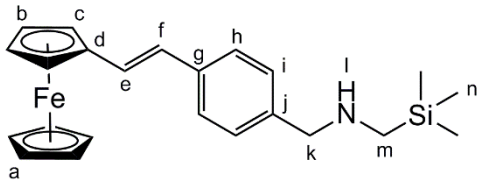

Trimethylsilane-1-methylamine (0.131 g, 1.27 mmol) was added dropwise to a solution of **2.3** (0.0800 g, 0.253 mmol) in 30 mL of methanol. The red suspension was stirred under at 40 °C for 24 hours. The solvent of the resulting dark red suspension was removed and the residue dissolved in 25 mL of dichloromethane. Sodium borohydride (0.0400 g, 1.06 mmol) was then added under N_2 at 0 °C, followed by 5 mL of methanol. The cloudy red solution was warmed to room temperature and stirred for 5 hours, after which the solution became clear and bright orange in colour. The solution was then quenched with 15 mL of water at 0 °C, the solvent (DCM and MeOH) reduced and the resulting solution was washed using a DCM/water extraction. The organic (DCM) fractions were collected and the solvent reduced to afford the desired product **2.12** as a bright red-orange powder, which was dried under vacuum. Yield: 0.101 g, 79.4 %. M.p: 63.6 – 66.2 °C. **^{1}H NMR (400.22 MHz, $CDCl_3$)**: δ (ppm) = 7.40 (d, 2H, ^3J = 8.1 Hz, H_i), 7.30 (d, 2H, ^3J = 8.3 Hz, H_h), 6.86 (d, 1H, ^3J = 16.1 Hz, H_e), 6.69 (d, 1H, ^3J = 16.1 Hz, H_f), 4.46 (t, 2H, ^3J = 1.8 Hz, H_c), 4.28 (t, 2H, ^3J = 1.8 Hz, H_b), 4.13 (s, 5H, H_a), 3.81 (s, 2H, H_k), 2.08 (s, 2H, H_m), 0.07 (s, 9H, H_n). **^{13}C{^{1}H} NMR (100.64 MHz, $CDCl_3$)**: δ (ppm) = 138.82 (C_j), 136.96 (C_g), 128.72 (C_i), 126.80 (C_e), 126.08 (C_f), 125.99 (C_h), 83.58 (C_d), 69.34 (C_a), 69.12 (C_b), 66.99 (C_c), 52.89 (C_k), 29.83 (C_m), 1.17 (C_n). **IR (ATR, cm^{-1})** ν = 1607 (C=C), 3283, 1631 (N-H). **EI-MS**: m/z 403 ([M]$^+$, 100%). **Elemental Analysis** for $C_{23}H_{29}FeNSi{\cdot}0.25CH_2Cl_2$: Found C, 65.88; H, 6.71; N, 1.95 %; Calculated C, 65.76; H, 7.00; N, 3.30 %.

2.6.7 Synthesis of Polynuclear Ferrocenyl-amino Complexes

2.6.7.1 (*E*)-1-Tris(2-aminoethyl)-4-vinylferrocenylbenzaldamine (2.13)

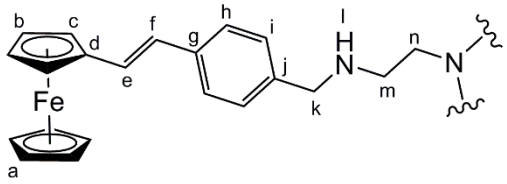

Tris-(2-aminoethyl)-amine (0.0120 g, 0.0843 mmol) dissolved in 10 mL of methanol was added dropwise to a solution of **2.3** (0.0801 g, 0.253 mmol) in 40 mL of methanol. The bright red suspension was stirred at 40 °C for 24 hours. The solvent of the resulting red-orange suspension was removed and the residue dissolved in 25 mL of dichloromethane. Sodium borohydride (0.0504 g, 1.32 mmol) was then added under N_2 at 0 °C, followed by 5 mL of methanol. The cloudy red solution was warmed to room temperature and stirred for overnight, after which the solution became clear and bright red in colour. The solution was then quenched with 15 mL of water at 0 °C, the solvent (DCM and MeOH) reduced and the resulting solution was washed using a DCM/water extraction. The organic (DCM) fractions were collected and the solvent reduced to afford the desired product **2.13** as a bright red-orange solid. This solid was washed with petroleum ether (40 – 60 °C) to afford an orange precipitate, the desired compound **2.13**, which was collected by suction filtration. Yield: 0.104 g, 78.7 %. Mp: 65 – 66 °C. **^{1}H NMR (400.22 MHz, $CDCl_3$)**: δ (ppm) = 7.35 (d, 2H, ^3J = 8.1 Hz, H_i), 7.23 (d, 2H, ^3J = 7.1 Hz, H_h), 6.84 (d, 1H, ^3J = 16.2 Hz, H_e), 6.68 (d, 1H, ^3J = 16.2 Hz, H_f), 4.44 (t, 2H, ^3J = 1.8 Hz, H_c), 4.27 (t, 2H, ^3J = 1.8 Hz, H_b), 4.12 (s, 5H, H_a), 3.74 (s, 2H, H_k), 2.69 (t, 6H, ^3J = 5.8 Hz, H_m), 2.61 (t, 6H, ^3J = 5.6 Hz, H_n). **^{13}C{^{1}H} NMR (100.64 MHz, $CDCl_3$)**: 136.94 (C_j), 128.75 (C_g), 128.71 (C_i), 126.85 (C_e), 126.02 (C_h), 125.95 (C_f), 83.55 (C_d), 69.35 (C_a), 69.13 (C_b), 67.03 (C_c), 54.41 (C_m), 53.71 (C_k), 47.16 (C_n). **IR (ATR, cm^{-1})** ν = 1609 (C=C), 3283, 1631 (N-H). **Elemental Analysis** for $C_{63}H_{66}Fe_3N_4{\cdot}0.25H_2O$: Found C, 72.29; H, 6.36; N, 5.35; Calculated C, 71.98; H, 6.38; N, 5.33%. **HR-ESI-MS**: *m*/*z* 1079.3688 ($[M+CH_3OH+H]^+$, 10 %).

2.6.7.2 (*E*)-1-DAB-4-vinylferrocenylbenzaldamine (2.14)

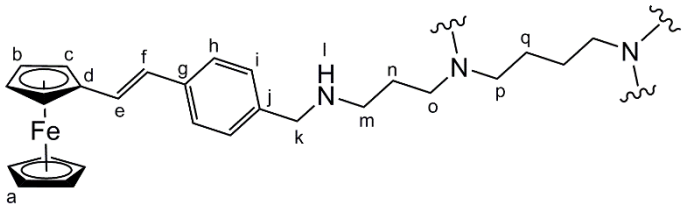

DAB-G1-$(NH_2)_4$ (0.0205 g, 0.0632 mmol) dissolved in 10 mL of methanol was added dropwise to a solution of **2.3** (0.0801 g, 0.253 mmol) in 30 mL of methanol and the bright red suspension was stirred at 40 °C for 24 hours. The solvent of the resulting orange suspension was removed and the residue

dissolved in 25 mL of dichloromethane. Sodium borohydride (0.0503 g, 1.32 mmol) was then added under N_2 at 0 °C, followed by 5 mL of methanol. The cloudy red solution was warmed to room temperature and stirred overnight, after which the solution became clear and bright red in colour. The solution was then quenched with 15 mL of water at 0 °C, the solvent (DCM and MeOH) reduced and the resulting solution was washed using a DCM/water extraction. The organic (DCM) fractions were collected and the solvent reduced to afford the desired product **2.14** as a bright red-orange sticky residue. This solid was redissolved in a minimum amount of DCM and added dropwise to a reservoir of hexane. An orange precipitate, the desired compound **2.14**, formed, which was collected by suction filtration. Yield: 0.0530 g, 55.5 %. Mp: 68 – 71 °C **^{1}H NMR (400.22 MHz, $CDCl_3$)**: δ (ppm) = 7.38 (d, 8H, ^3J = 8.0 Hz, H_i), 7.26 (d, 8H, ^3J = 8.3 Hz, H_h), 6.84 (d, 4H, ^3J = 16.1 Hz, H_e), 6.68 (d, 4H, ^3J = 16.1 Hz, H_f), 4.44 (t, 8H, ^3J = 1.8 Hz, H_c), 4.27 (t, 8H, ^3J = 1.8 Hz, H_b), 4.12 (s, 20H, H_a), 3.74 (s, 8H, H_k), 2.64 (m, 8H, H_m), 2.45-2.39 (overlapping m, 12H, H_o and H_p), 1.65 (br m, 8H, H_n), 1.38 (br m, 4H, H_q). **^{13}C{^{1}H} NMR (100.64 MHz, $CDCl_3$)**: δ (ppm) = 139.14 (C_j), 136.84 (C_g), 128.70 (C_i), 128.65 (C_e), 126.72 (C_f), 125.97 (C_h), 83.62 (C_d), 69.35 (C_a), 69.12 (C_b), 67.01 (C_c), 54.23 (C_p) , 53.99 (C_k), 52.60 (C_o), 48.25 (C_m), 27.56 (C_n), 25.18 (C_q). **IR (ATR, cm^{-1})** ν = 1609 (C=C), 3302, 1633 (N-H). **Elemental Analysis** for $C_{92}H_{104}Fe_4N_6{\cdot}4H_2O$: Found C, 69.05; H, 6.90; N, 4.89 %; Calculated C, 69.63; H, 7.10; N, 5.29 %. **HR-ESI-MS**: *m*/*z* 759.2933 ($[M+2H]^{2+}$, 42 %).

2.6.7.3 (*E*)-1-DAB-4-vinylferrocenylbenzaldamine (2.15)

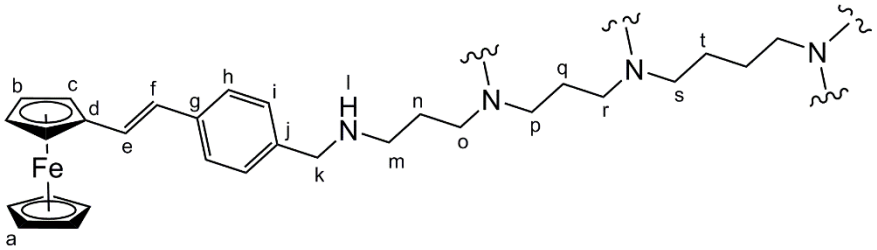

DAB-G2-$(NH_2)_8$ (0.0397 g, 0.0514 mmol) dissolved in 10 mL of methanol was added dropwise to a solution of **2.3** (0.130 g, 0.411 mmol) in 30 mL of methanol and the bright red suspension was stirred at 40 °C for 24 hours. The solvent of the resulting orange suspension was removed and the residue dissolved in 25 mL of dichloromethane. Sodium borohydride (0.0630 g, 1.67 mmol) was then added under N_2 at 0 °C, followed by 5 mL of methanol. The cloudy red solution was warmed to room temperature and stirred for overnight, after which the solution became clear and bright red in colour. The solution was then quenched with 15 mL of water at 0 °C, the solvent (DCM and MeOH) reduced and the resulting solution was washed using a DCM/water extraction. The organic (DCM) fractions were collected and the solvent reduced to afford the desired product **2.15** as a bright red-orange sticky residue. This solid was redissolved in a minimum amount of DCM and added dropwise to a reservoir of hexane. An orange precipitate, the desired compound **2.15**, formed, which was collected by suction

filtration. Yield: 0.0747 g, 45.8 %. Yield: 0.0826 g, 50.6 %. Mp: 92 – 94 °C. **^{1}H NMR (400.22 MHz, $CDCl_3$)**: δ (ppm) = 7.37 (d, 16H, ^3J = 6.8 Hz, H_i), 7.25 (d, 16H, ^3J = 6.8 Hz, H_h), 6.84 (d, 8H, ^3J = 16.0 Hz, H_e), 6.68 (d, 8H, ^3J = 16.0 Hz, H_f), 4.44 (t, 16H, ^3J = 1.8 Hz, H_c), 4.27 (t, 16H, ^3J = 1.8 Hz, H_b), 4.12 (s, 40H, H_a), 3.73 (s, 16H, H_k), 2.63 (m, 16H, H_m), 2.46-2.41 (overlapping m, 36H, H_o and H_p and H_r and H_s), 1.65-1.57 (br m, 24H, H_n and H_q), 1.41 (m, 4H, H_t). **^{13}C{^{1}H} NMR (100.64 MHz, $CDCl_3$)**: δ (ppm) = 136.83 (C_j), 128.86 (C_g), 128.65 (C_i), 126.73 (C_e), 126.09 (C_f), 125.98 (C_h), 83.60 (C_d), 69.35 (C_a), 69.13 (C_b), 67.01 (C_c), 53.97 (C_o), 53.91 (C_k), 52.51 (C_p), 52.42 (C_r), 48.20 (C_m), 33.98 (C_s), 27.49 (C_n), 25.48 (C_t), 24.54 (C_q). **IR (ATR, cm^{-1})** ν = 1609 (C=C), 3294, 1633 (N-H). **Elemental Analysis** for $C_{192}H_{224}Fe_8N_{14}{\cdot}5CH_2Cl_2$: Found C, 65.05; H, 6.83; N, 4.55 %; Calculated C, 65.74; H, 6.55; N, 5.45 %. **HR-ESI-MS**: *m*/*z* 318.0697 ($[M+10H]^{10+}$, 28 %).

2.7 References

1. R. Shepherd and R. Wilkinson, *J. Med. Chem.,* 1962, **5**, 823-835.
2. R. Shepherd, C. Baughn, M. Cantrall, B. Goodstein, J. Thomas and R. Wilkinson, *Ann. N. Y. Acad. Sci.,* 1966, **135**, 686-710.
3. R. E. Lee, M. Protopopova, E. Crooks, R. A. Slayden, M. Terrot and C. E. Barry, *J. Comb. Chem.,* 2003, **5**, 172-187.
4. E. Bogatcheva, C. Hanrahan, B. Nikonenko, R. Samala, P. Chen, J. Gearhart, F. Barbosa, L. Einck, C. A. Nacy and M. Protopopova, *J. Med. Chem.,* 2006, **49**, 3045-3048.
5. R. Tripathi, N. Saxena, V. Tiwari, S. Verma, V. Chaturvedi, Y. Manju, A. Srivastva, A. Gaikwad and S. Sinha, *Bioorg. Med. Chem.,* 2006, **14**, 8186-8196.
6. V. Faugeroux, Y. Génisson, Y. Salma, P. Constant and M. Baltas, *Bioorg. Med. Chem.,* 2007, **15**, 5866-5876.
7. R. Yendapally and R. E. Lee, *Bioorg. Med. Chem. Lett.,* 2008, **18**, 1607-1611.
8. D. Razafimahefa, D. A. Ralambomanana, L. Hammouche, L. Pélinski, S. Lauvagie, C. Bebear, J. Brocard and J. Maugein, *Bioorg. Med. Chem. Lett.,* 2005, **15**, 2301-2303.
9. D. A. Ralambomanana, D. Razafimahefa-Ramilison, A. C. Rakotohova, J. Maugein and L. Pelinski, *Bioorg. Med. Chem.,* 2008, **16**, 9546-9553.
10. S. Müller, G. H. Coombs and R. D. Walter, *Trends Parasitol.,* 2001, **17**, 242-249.
11. C. Bacchi and N. Yarlett, *Mini Rev. Med. Chem.,* 2002, **2**, 553-563.
12. O. Heby, S. C. Roberts and B. Ullman, *Biochem. Soc. Trans.,* 2003, **31**, 415-419.
13. H. Wallace, A. Fraser and A. Hughes, *Biochem. J.,* 2003, **376**, 1-14.
14. Z. Tian, S. Xie, Z. Mei, J. Zhao, W. Gao and C. Wang, *Org. Biomol. Chem.,* 2009, **7**, 4651-4660.

15. I. B. Müller, R. D. Gupta, K. Lüersen, C. Wrenger and R. D. Walter, *Mol. Biochem. Parasitol.,* 2008, **160**, 1-7.
16. R. Das Gupta, T. Krause-Ihle, B. Bergmann, I. B. Muller, A. R. Khomutov, S. Muller, R. D. Walter and K. Luersen, *Antimicrob. Agents Chemother.,* 2005, **49**, 2857-2864.
17. M. L. Edwards, D. Stemerick, A. Bitonti, J. Dumont, P. McCann, P. Bey and A. Sjoerdsma, *J. Med. Chem.,* 1991, **34**, 569-574.
18. M. Liu and J. M. Fréchet, *Pharm. Sci. Technol. Today,* 1999, **2**, 393-401.
19. A. K. Patri, I. J. Majoros and J. R. Baker, *Curr. Opin. Chem. Biol.,* 2002, **6**, 466-471.
20. E. R. Gillies and J. M. Frechet, *Drug Discov. Today,* 2005, **10**, 35-43.
21. A. D'Emanuele and D. Attwood, *Adv. Drug Deliv. Rev.,* 2005, **57**, 2147-2162.
22. A. K. Patri, J. F. Kukowska-Latallo and J. R. Baker, *Adv. Drug Deliv. Rev.,* 2005, **57**, 2203-2214.
23. M. Gallei, R. Klein and M. Rehahn, *Macromolecules,* 2010, **43**, 1844-1854.
24. M. I. Reyes Valderrama, R. A. Vasquez García, T. Klimova, E. Klimova, L. Ortiz-Frade and M. Martinez García, *Inorg. Chim. Acta,* 2008, **361**, 1597-1605.
25. B. E. Maryanoff and A. B. Reitz, *Chem. Rev.,* 1989, **89**, 863-927.
26. J. P. Knowles and A. Whiting, *Org. Biomol. Chem.,* 2007, **5**, 31-44.
27. H. J. Bestmann, *Chem. Ber.,* 1962, **95**, 58-63.

Chapter 3

Synthesis and characterisation of mono- and polynuclear ferrocenylthiosemicarbazone complexes

3.1 Introduction

As previously discussed, the organic scaffolds of drug candidates can be altered or derivatised to incorporate biologically active motifs to enhance permeability and retention within biological targets and thus augment biological activity. This derivatisation may also improve the chemical and physical properties of the compound. One such biologically promising alteration is the use of thiosemicarbazones, a class of thioureas which are structurally similar to semicarbazones, all shown in Fig. 3.1. Thiosemicarbazones display a broad spectrum of biological activity including antifungal, antitumoral, antiviral and antimicrobial activity.[1-8] This pharmacological versatility coupled with the ease of chemical derivatisation of this group, has led to the widespread use of thiosemicarbazones and their metal complexes in drug development.[9]

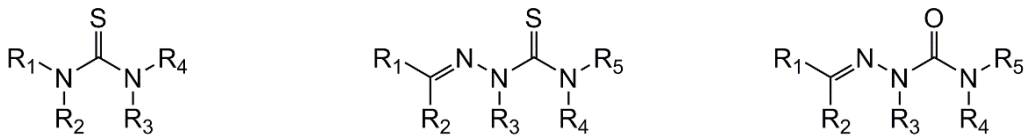

Fig. 3.1: The general structure of a thiourea (**a**), thiosemicarbazone (**b**) and semicarbazone (**c**).

Thiacetazone, a thiosemicarbazone-based drug shown in Fig. 3.2, was one of the first commercially available for the treatment of tuberculosis.[10-12] Used in combination with isoniazid, thiacetazone has a mechanism of action similar to that of ethambutol, by which it inhibits cyclopropanation of cell wall mycolic acids and thus inhibits cell wall synthesis of *Mycobacterium tuberculosis*.[10-14] The use of this drug is declining due to adverse skin reactions and toxicity,[10] however, thiosemicarbazone compounds continue to be explored in antimycobacterial research.[14, 15]

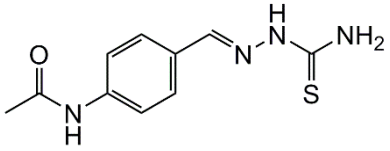

Fig. 3.2: Thiosemicarbazone-based anti-TB drug, thiacetazone.

Transition metal-containing complexes of thiosemicarbazones have also gained great interest, showing activity against various microbes, including *Mycobacterium tuberculosis*.[16-22] Klahn and co-workers[23] prepared a series of cyrhetrene- and ferrocene-containing palladium(II) and platinum(II) complexes of thiosemicarbazones, an example of which is shown in Fig. 3.3.[23] These heterobimetallic complexes were evaluated for their *in vitro* activity against the mc^{2}7000 *M.tb* strain and displayed low to moderate micromolar MIC values.[23]

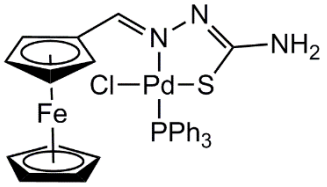

Fig. 3.3: A ferrocenylthiosemicarbazone-containing palladium(II) complex.

Among their biological applications, thiosemicarbazones have been widely used in antimalarial research. An advantage of utilizing thiosemicarbazones against protozoans such as plasmodia is their ability to act on targets other than β-haematin, which may result in overcoming drug resistance. Thiosemicarbazones have been shown to display antiplasmodial activity through inhibition of cysteine proteases, enzymes essential for parasite survival.[6] A great body of research has been done on the application of mono- and polynuclear transition metal-containing thiosemicarbazone complexes in antiplasmodial studies, with some of the most promising results achieved with the incorporation of ferrocene.[20, 24-27] In addition to its antimycobacterial activity, the complex shown in Fig. 3.3 was also among a series of ferrocenylthiosemicarbazone palladium(II) complexes reported to exhibit good antiplasmodial activity against both the chloroquine-sensitive (CQS) NF54 and chloroquine-resistant (CQR) Dd2 strain.[28]

Perhaps most significant to this study, Khanye *et al.* conjugated ferrocenyl dithiocarbamate ligands to the periphery of a polypropyleneimine (PPI) dendrimer scaffold to afford tetranuclear ferrocenylthiosemicarbazone complexes, as shown in Fig. 3.4.[26] These complexes were evaluated for their *in vitro* activity against the chloroquine-resistant W2 strain, displaying good activity in the low micromolar range.[26] Stringer *et al.* prepared mono- and trinuclear analogues of these complexes, which displayed low micromolar IC_{50} values against the chloroquine-resistant Dd2 strain.[27]

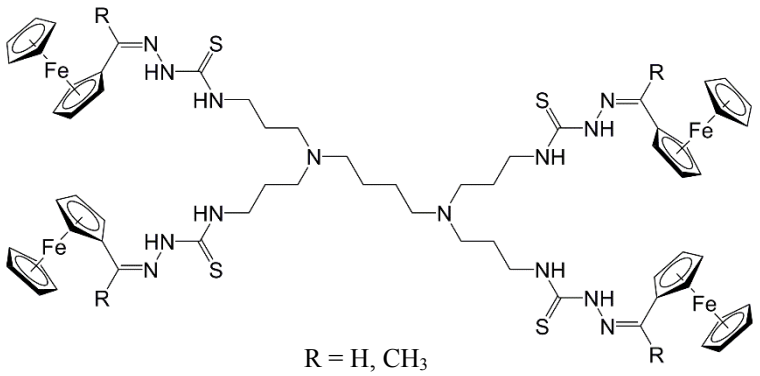

Fig. 3.4: A tetranuclear ferrocenylthiosemicarbazone complex.

The series of ferrocenyl-imino and amino complexes discussed in Chapter 2 contained ferrocene as a possible bioactive moiety, and amines as a drug delivery tool. As an extension to this study, a new series of compounds was prepared, conjugating the ferrocenyl-imino complexes with the pharmacologically active thiosemicarbazone moiety in order to improve the biological activity as well as the solubility. In this chapter, the synthesis and characterisation of these ferrocenylthiosemicarbazone complexes is described. The compounds were characterised using a range spectroscopic and analytical techniques.

3.2 Preparation of the dithiocarbamate precursors (3.1 – 3.2)

3.1.1 Synthesis

Methyl hydrazinecarbodithioate **3.1** was prepared according to a method described by Klayman *et al.,*[3] by the reaction of hydrazine hydrate with carbon disulfide in the presence of potassium hydroxide in a solution of isopropanol and water, followed by the addition of iodomethane. All reagents were added at 0 °C.

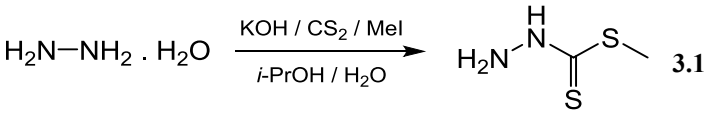

Scheme 3.1: Preparation of methyl hydrazinecarbodithioate **3.1**.

Compound **3.1** was isolated as a white crystalline solid in 12 % yield, displaying solubility in a range of alcoholic solvents, water and partial solubility in organic solvents such as dichloromethane and chloroform. The mechanism of this reaction involves the initial formation of a hydrazinecarbodithioate salt, followed by methylation of this salt with iodomethane to produce the dithiocarbamate **3.1**.

The ferrocenyl dithiocarbamate **3.2** was prepared via a Schiff-base condensation reaction of **2.3** with **3.1**. The reagents were refluxed in isopropanol overnight and **3.2** was obtained in 89 % yield as an orange powder, displaying low solubility in polar organic solvents (DCM, chloroform, ethyl acetate) and partial solubility in alcoholic solvents such as ethanol.

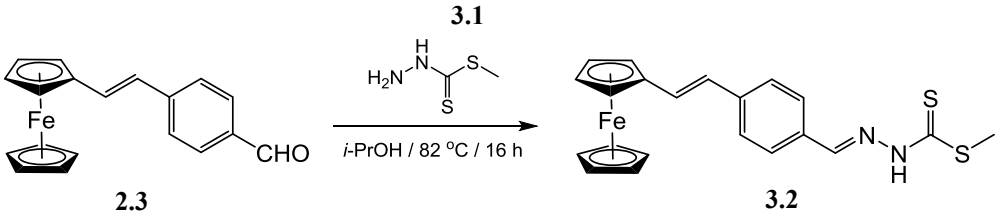

Scheme 3.2: Preparation of ferrocenyl dithiocarbamate **3.2**.

3.1.2 Characterisation

^{1}H Nuclear Magnetic Resonance Spectroscopy

The ^{1}H NMR spectrum of **3.1** (Fig. 3.5) displays a broad singlet at 10.77 ppm, corresponding to the hydrazinic proton. The two terminal amine protons give rise to a singlet at 5.06 ppm and the methyl protons are observed as a sharp singlet at 2.39 ppm. The highly deshielded nature of the methyl signal can be attributed to the electron-withdrawing nature of the adjacent sulfur atom. The integration is consistent with the proposed structure.

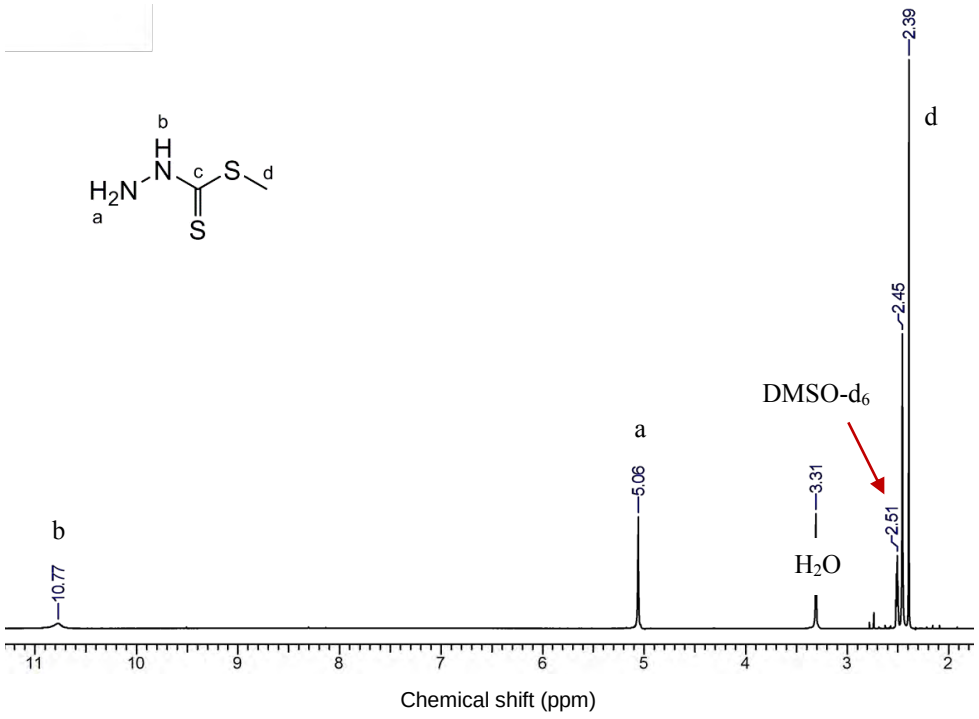

Fig. 3.5: ^{1}H NMR spectrum of **3.1** in DMSO-d_6.

The ^{1}H NMR spectrum of ferrocenyl dithiocarbamate **3.2**, shown in Fig. 3.6, confirms imine bond formation with the presence of a sharp singlet corresponding to the imine proton at 8.23 ppm. A number of signals are retained in this spectrum compared to the spectrum of the aldehyde precursor **2.2**. There are doublets at 7.66 and 7.59 ppm, respectively, for the two pairs of chemically equivalent protons of the 1,4-disubstituted aromatic ring. Each of these aromatic signals have a coupling constant of $J \sim 8$ Hz, corresponding to fixed *cis* configuration of the protons in the ring (see Chapter 2, Fig 2.5). The two alkenyl protons are each observed as a doublet (at 7.12 and 6.82 ppm respectively), with vicinal coupling constants of $J \sim 16$ Hz as the double bond has a *trans* configuration.

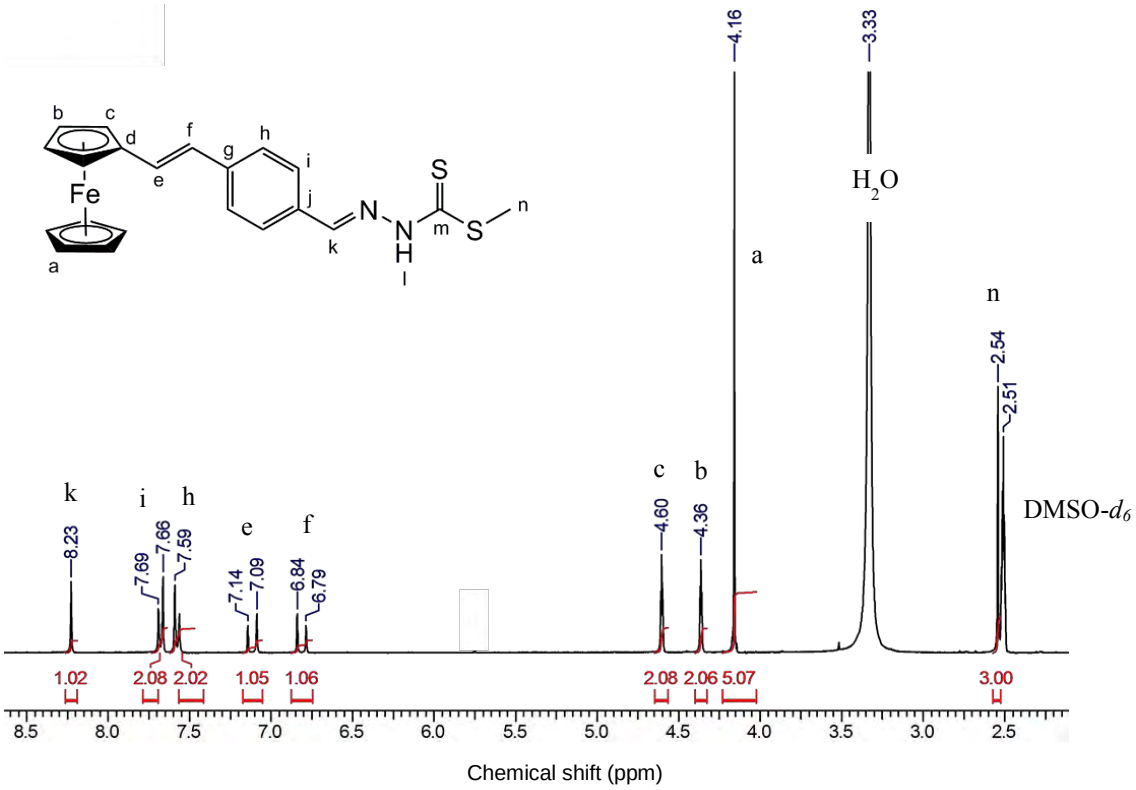

Fig. 3.6: ^{1}H NMR spectrum of **3.2** in DMSO-d_6.

The ^{1}H NMR spectrum displays three peaks for the ferrocenyl protons; a triplet for each of the two chemically equivalent pairs of protons of the substituted Cp ring, as well as a singlet for the five protons of the unsubstituted Cp ring. Furthermore, a sharp singlet at 2.54 ppm, which integrates for three protons, corresponds to the methyl protons of the thioester moiety of **3.2**.

$^{13}C\{^{1}H\}$ Nuclear Magnetic Resonance Spectroscopy

The $^{13}C\{^{1}H\}$ NMR spectrum of **3.2** displays the expected number of carbon signals, further confirming its chemical structure. The most deshielded peak at 198.43 ppm is attributed to the thiocarbonyl carbon atom and a peak at 146.74 corresponds to the carbon of the new imine bond, giving evidence of Schiff-

base condensation. The spectrum also displays a peak for each alkenyl carbon atom at 129.78 and 125.39 ppm respectively. The six aromatic carbon atoms give rise to four signals in the spectrum; two quaternary carbon atom signals (140.60 and 126.61 ppm) and two tertiary carbon atom signals (128.36 and 126.61 ppm), one for each pair of chemically equivalent carbon atoms. The ferrocenyl carbon atoms are observed as four signals; a signal at 83.22 for the quaternary carbon, peaks at 69.73 and 67.55 ppm for the carbon atoms of the substituted Cp ring and another at 69.56 ppm for the carbon atoms of the unsubstituted Cp ring. The carbon atom of the methyl group gives rise to a peak at 17.24 ppm.

Infrared Spectroscopy

Further evidence supporting the synthesis of precursors **3.1** and **3.2** is provided by infrared (IR) spectral data as shown in Fig. 3.7. The IR spectrum of **3.1** displays four absorption bands of interest. The two amine groups give rise to ν(N-H) stretching bands at 3262 and 3153 cm^{-1}, and a ν(N-H) bend at 1596 cm^{-1}. Further to this, ν(C=S) and ν(C-S) absorption bands are observed at 940 cm^{-1} and 703 cm^{-1} for the thiocarbonyl and thiol groups, respectively.

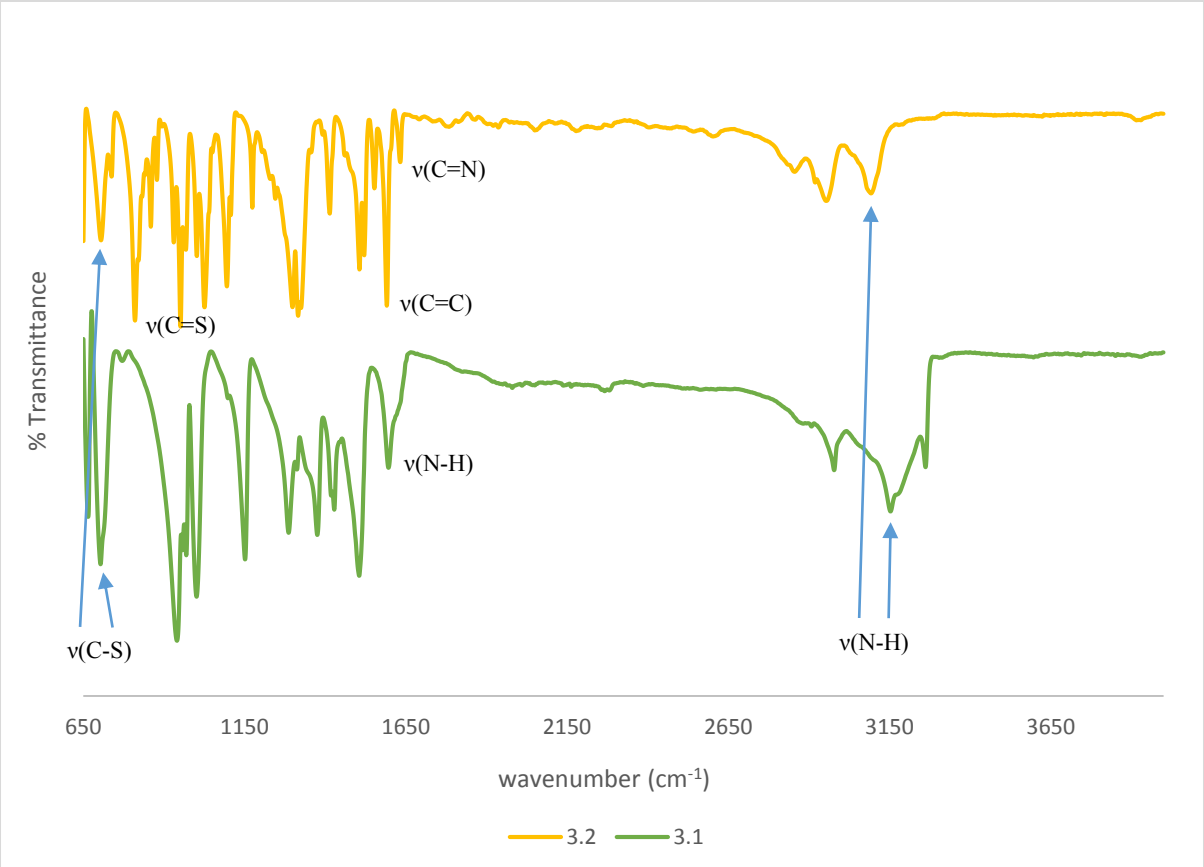

Fig. 3.7: The infrared spectra of **3.1** (bottom) and **3.2** (top).

Some of the absorption bands seen in the IR spectrum of **3.1** are retained in that of **3.2.** The thiol ν(C-S) absorption band is observed at 704 cm^{-1} and the thiocarbonyl ν(C=S) at 810 cm^{-1}, shifted to a lower wavenumber. The amine ν(N-H) stretching band is observed at 3093 cm^{-1}. Evidence of Schiff-base condensation is shown by the presence of an imine ν(C=N) absorption band at 1632 cm^{-1}. The alkenyl group gives rise to a ν(C=C) stretch at 1591 cm^{-1}.

Mass Spectrometry

The Electron-Impact mass spectrum of **3.2** further confirms the compound structure, with the base peak corresponding to the molecular ion $[M]^+$ at 420.0341 *m/z*.

3.2 Preparation of Mono- and Polynuclear Ferrocenylthiosemicarbazone complexes (3.3 – 3.6)

3.2.1 Synthesis

The ferrocenyl dithiocarbamate **3.2** was then used in the synthesis of new mono- and polynuclear ferrocenylthiosemicarbazone complexes (**3.3** – **3.6**). This was achieved by nucleophilic substitution reactions of **3.2** with the appropriate amine in dry ethanol under refluxing conditions. The preparation of **3.3** is shown in Scheme 3.3.

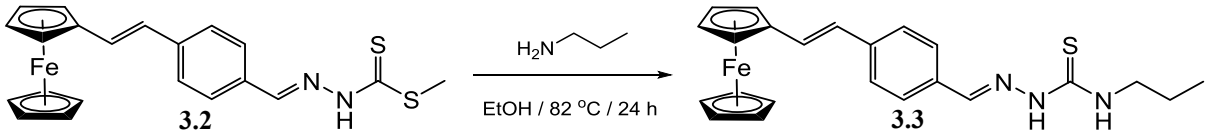

Scheme 3.3: Synthesis of mononuclear ferrocenylthiosemicarbazone complex **3.3**.

Interestingly, the mononuclear complex **3.3** was isolated in two different forms. The delocalisation of the electron lone pairs of the nitrogen gives rise to thione-thiol tautomerism, as shown in Fig. 3.8. The process of tautomerisation results in a shift in the double bond from the thiocarbonyl to the imine and a proton transfer from the nitrogen to the sulphur. This can occur in two ways, either delocalisation of lone pair electrons from the hydrazinic nitrogen or from the terminal amine group. However, in this case the latter has occurred, resulting in the formation of **3.3b**. Evidence of this thione-thiol tautomerism is seen in the ^1H NMR and infrared spectroscopy, discussed later. Thione-thiol tautomerism, similar to keto-enol or lactam-lactim tautomerism, has been observed in the literature and is a common phenomenon seen in thiosemicarbazones.[29-33]

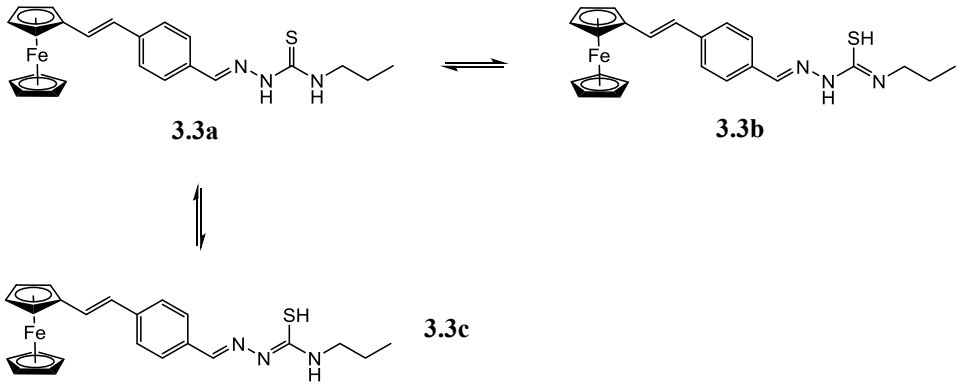

Fig. 3.8: Thione-thiol tautomerism possible for complex **3.3**.

Compound **3.3a** was obtained as a red-orange powder, while **3.3b** was isolated as a dark red-purple powder, both displaying solubility in polar organic solvents such as DCM, chloroform and ethyl acetate, as well as solubility in alcoholic solvents.

In a similar procedure to that shown in Scheme 3.3, the polynuclear ferrocenylthiosemicarbzone complexes **3.4** – **3.6** were prepared by nucleophilic substitution reactions of **3.2** with tris(2-aminoethyl)amine or the DAB dendrimer scaffolds (generation 1 and 2) in dry ethanol under refluxing conditions, as shown in Scheme. 3.4. These reactions were conducted for long periods due to the poor solubility of the ferrocenyl dithiocarbamate **3.2** in ethanol. The trinuclear complex **3.4** was isolated as a dark red powder, displaying similar solubility to that of **3.3a** and **3.3b**. Compounds **3.5** and **3.6**, the first and second generation dendritic complexes respectively, were obtained as dark orange-brown powders, displaying solubility in polar organic solvents such as DCM, chloroform as well as DMSO. The polynuclear complexes were isolated in low yields (36 – 43 %). Significantly, these polynuclear complexes displayed enhanced solubility in solvents such as DMSO, compared to the non-thiosemicarbazone polynuclear complexes described in Chapter 2.

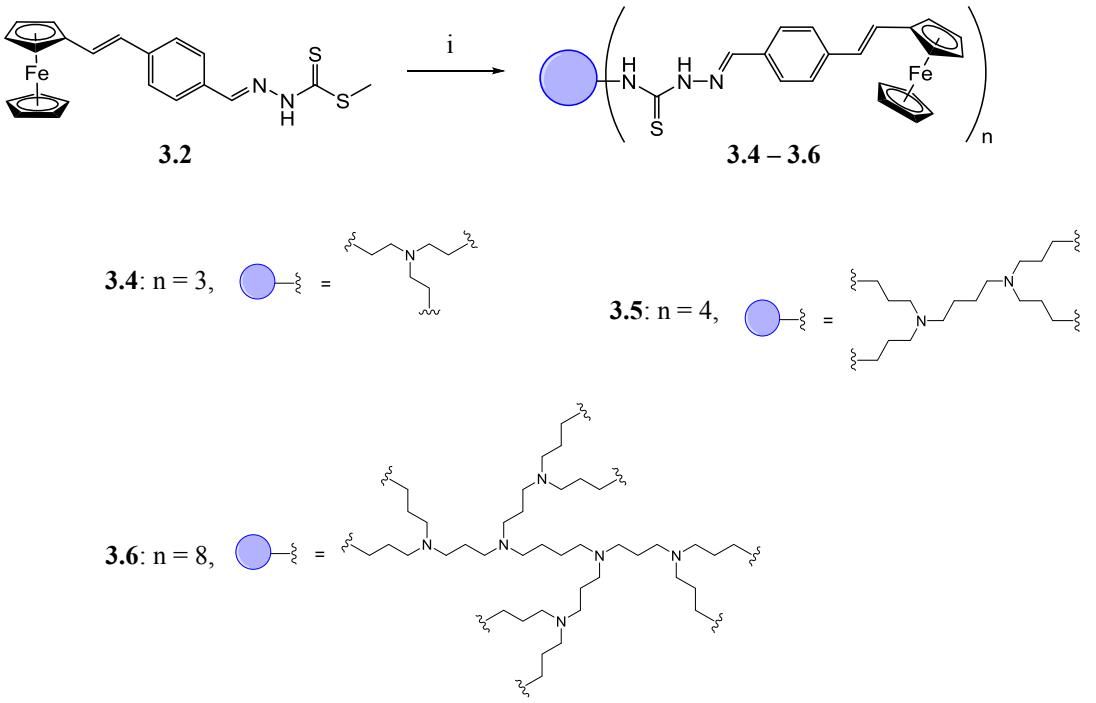

Scheme 3.4: Preparation of polynuclear ferrocenylthiosemicarbazone complexes **3.4** – **3.6**. i) tris(2-aminoethyl)-amine or DAB-Am-4 or DAB-Am-8 / EtOH / 82 °C / 3 days.

The nucleophilic substitution reaction involves the nucleophilic addition of an amine to the thiocarbonyl group, followed by the elimination of the -SCH_3 to give the thiosemicarbazone product. The mechanism of a general nucleophilic substitution reaction is shown in Fig. 3.9.

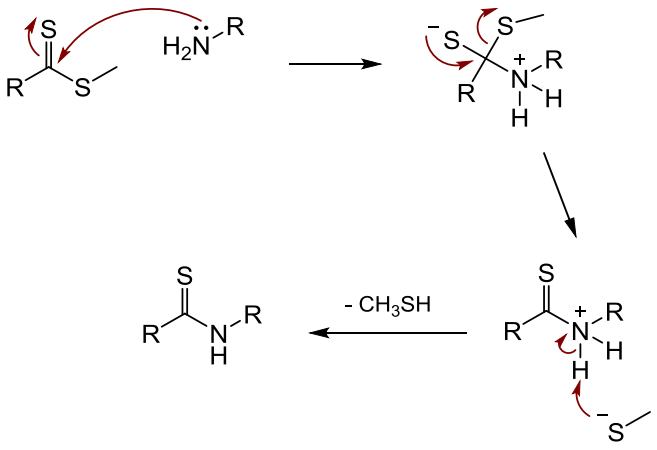

Fig. 3.9: Mechanism of a general nucleophilic substitution reaction.

3.2.2 Characterisation

^{1}H Nuclear Magnetic Resonance Spectroscopy

The ^{1}H NMR spectra of the ferrocenylthiosemicarbazone complexes **3.3a**, **3.3b** and **3.4** – **3.6**, recorded in DMSO-d_6, all retained several signals seen in the spectrum of the dithiocarbamate precursor **3.2**, with similar coupling constants and no significant change in chemical shifts and multiplicities. The two signals for the four aromatic protons are seen in the range 7.73 – 7.49 ppm, while that of the two alkenyl protons is observed between 7.08 and 6.76 ppm. Additionally, the spectra display the three peaks corresponding to the ferrocenyl protons between 4.59 and 4.13 ppm.

Significantly, in the ^{1}H NMR spectra of **3.3a** and **3.4** – **3.6**, the sharp singlet corresponding to the imine proton shows a shift upfield from 8.23 ppm in the spectrum of **3.2** to between 8.07 – 8.04 ppm. This is expected and can be attributed to the more electron-donating nature of the new amine group compared to the –SCH_3 group, which it displaces. Further evidence of displacement is shown by the presence of a broad signal for the new amine proton in the range 8.55 – 8.44 ppm. In the spectra of **3.3a** (Fig. 3.10) and **3.5** (Fig. 3.12), the hydrazinic proton is observed as broad singlet at 11.36 and 11.37 ppm, respectively. The ^{1}H NMR spectrum (Fig. 3.11) of **3.3b** provides evidence that the thiol tautomer is present in solution. A sharp singlet corresponding to the imine proton is present at 8.31 ppm, shifted significantly downfield compared to that of the thione tautomer **3.3a**. This may be a result of the accumulative electron-withdrawing effects of the imine (C=N) and thiol (SH) groups, which are not present in **3.3a**.

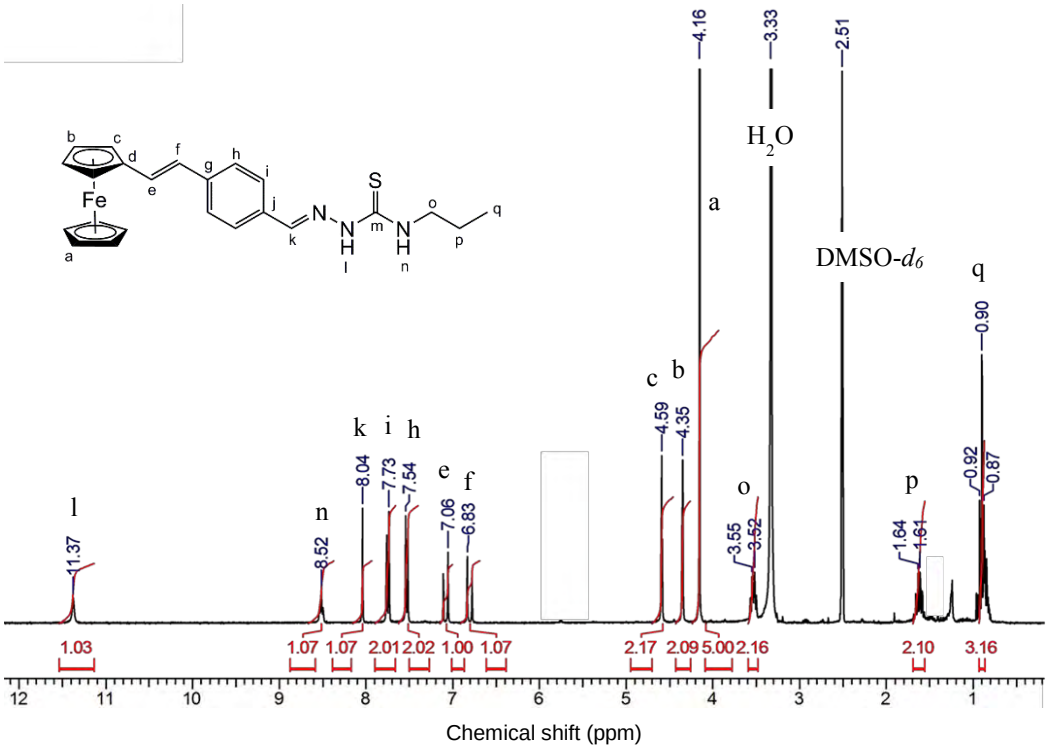

Fig. 3.10: ^{1}H NMR spectrum of **3.3a** in DMSO-d_6.

Furthermore, the ^{1}H NMR spectra of **3.3a** (Fig. 3.10) and **3.3b** display three peaks for the protons of the propyl chain. The methylene protons adjacent to the amine nitrogen are displayed as a deshielded quartet at 3.54 ppm and the methylene protons adjacent to the terminal methyl group give rise to a multiplet at 1.63 ppm. The methyl protons are observed as a triplet around 0.90 ppm.

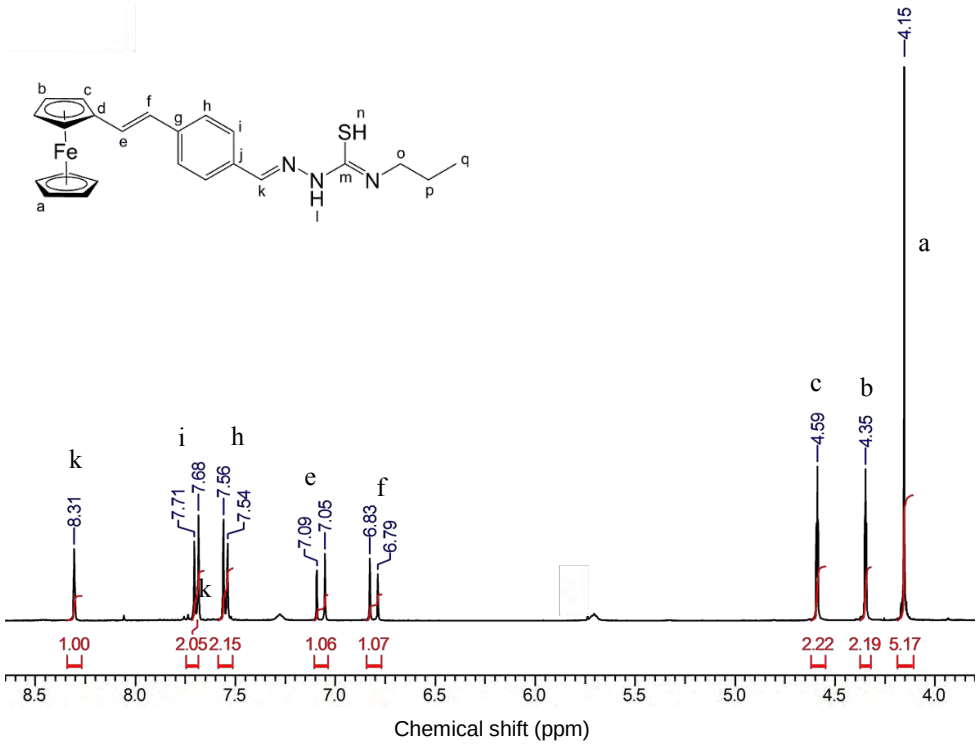

Fig. 3.11: Section of the ^{1}H NMR spectrum of **3.3b** in DMSO-d_6.

In the spectrum of the trinuclear complex **3.4**, there are multiplets at 3.75 and 2.87 ppm, respectively, corresponding to the methylene protons of the aliphatic branches. The spectrum of **3.5** displays five signals for the protons of the aliphatic dendritic core and branches. Peaks at 3.65, 2.45 and 1.75 ppm are assigned to the protons of the four branches, while those at 1.37 and 2.30 ppm are assigned to protons of the diaminobutane (DAB) core, as shown in Fig. 3.12.

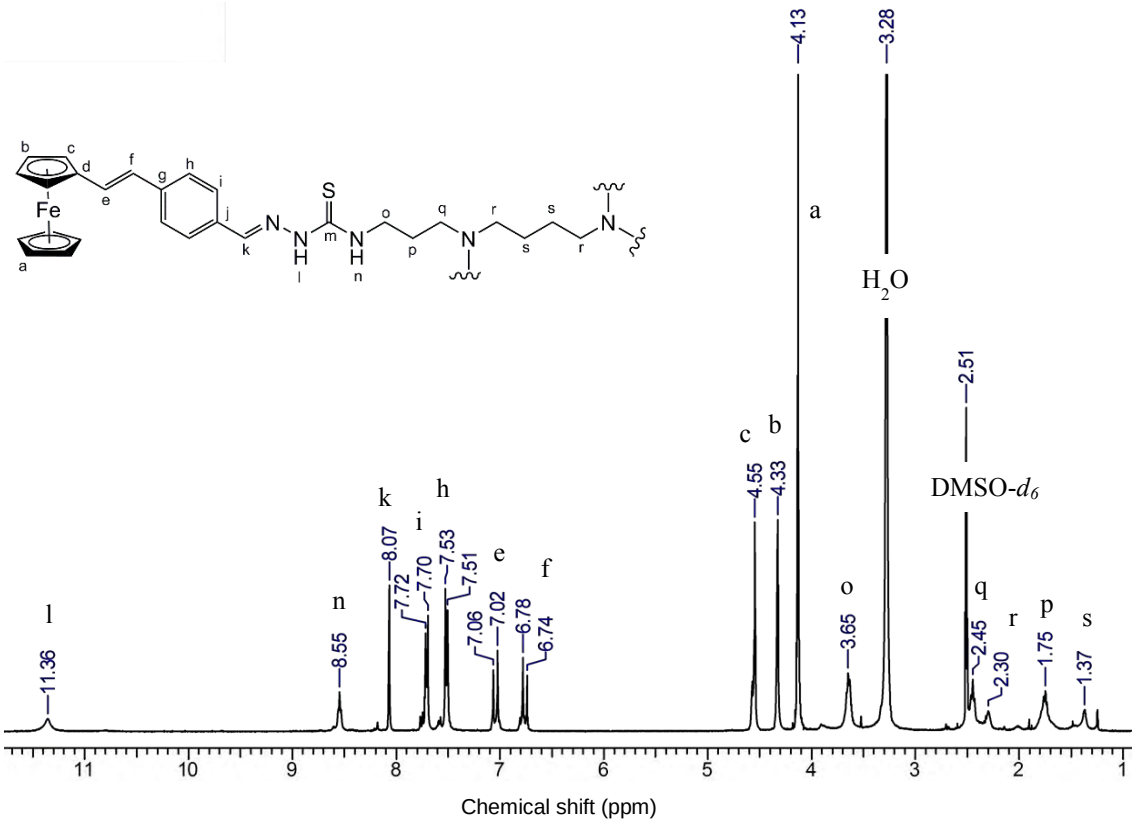

Fig. 3.12: ^{1}H NMR spectrum of **3.5** in DMSO-d_6.

The ^{1}H NMR spectrum of **3.6** displays significant broadening of peaks, which can be attributed to several protons averaging over the same chemical shift on the NMR timescale, as a result of the increased nuclearity of the complex. The eighty protons of the dendritic core and branches give rise to broad multiplets in the region 3.65 – 1.48 ppm, as assigned in Fig. 3.13.

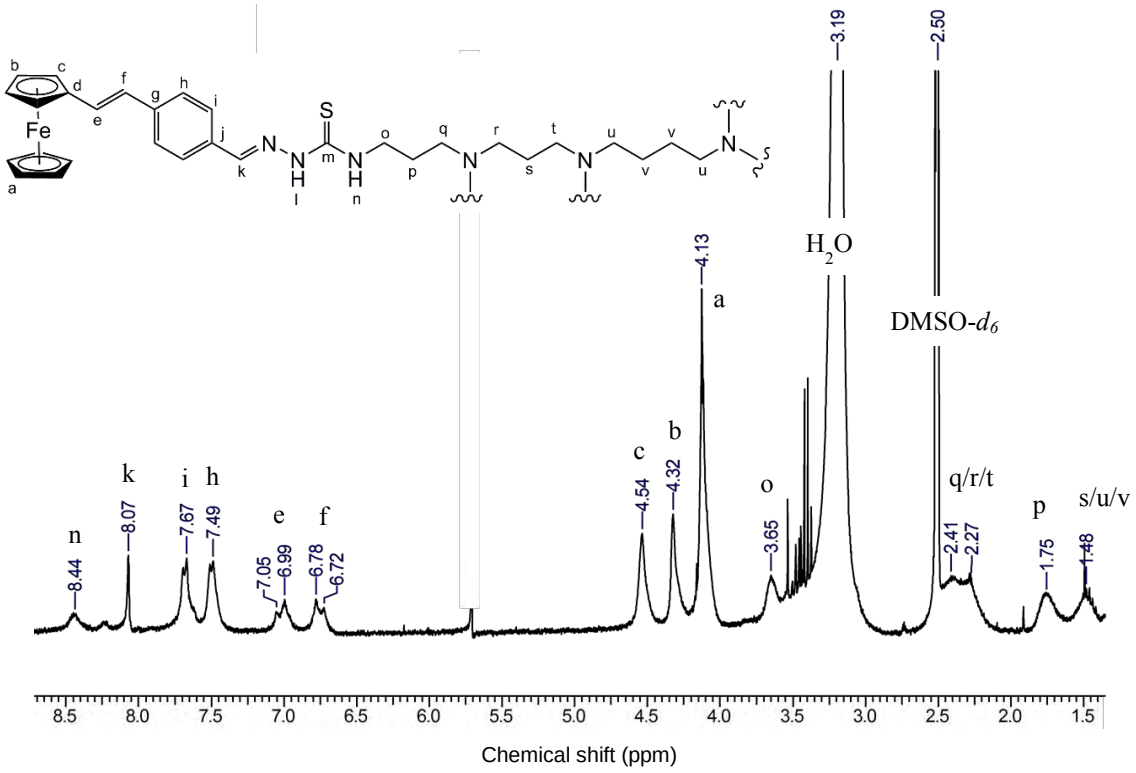

Fig. 3.13: ^{1}H NMR spectrum of **3.6** in DMSO-d_6.

$^{13}C\{^{1}H\}$ Nuclear Magnetic Resonance Spectroscopy

The $^{13}C\{^{1}H\}$ NMR spectra of **3.3** – **3.6** display all the expected signals. The aromatic ring gives rise to two quaternary carbon atom peaks in the region 140.25 – 132.87 ppm, and two tertiary carbon atom peaks in the region 128.70 – 126.28 ppm. The two alkene carbon atom peaks are displayed around 129 and 126 ppm. The carbon atoms of the ferrocenyl Cp rings give rise to a quaternary carbon signal around 83.37 – 83.33 ppm and three more signals in the region 69.59 – 67.44 ppm. In the $^{13}C\{^{1}H\}$ NMR spectrum of **3.3b**, the peak corresponding to the imine carbon atom adjacent to the phenyl ring appears at 160.64 ppm, displaying a considerable shift downfield compared to that of **3.2**, which appears at 146.74 ppm. This trend is also seen in the ^{1}H NMR spectrum and is attributed to the presence of the imine and thiol group, which exert electron-withdrawing effects. The carbon atoms of the propyl chain give rise to signals at 62.86, 24.19 and 12.19 ppm.

In the $^{13}C\{^{1}H\}$ NMR spectra of **3.4** – **3.6**, there is a significant upfield shift in the signal for the thione carbon, from 198.43 ppm in the precursor **3.2** to around 177.34 – 177.71 ppm. This can be attributed to and gives evidence of the presence of the new amino group, which has a more electron-donating effect than the –SCH_3 sulfur atom that it replaces. The peak for the imine carbon atom is observed in the range 142.46 – 142.86 ppm, also showing a slight upfield shift compared to that in **3.2**. This is also an effect of the electron-donating nature of the new amine group, however, the effect is less pronounced.

Furthermore, the carbon atoms of the three aliphatic branches of **3.4** are displayed as two signals (53.14 and 44.55 ppm). The aliphatic core and branches of **3.5** give rise to peaks at 54.25, 52.19, 43.37, 26.63 and 25.00 ppm. Similarly, the carbon atoms of the core and branches of **3.6** give rise to five signals in the region 52.41 – 24.60 ppm.

Infrared Spectroscopy

The solid state infrared spectra of **3.3** – **3.6** all display similar absorption bands. The IR spectra of **3.3a**, **3.3b** and **3.4** are shown in Fig. 3.14. Most significantly, the absence of the thiol ν(C-S) absorption band, which occurs around 703 cm^{-1} in the precursor **3.2**, gives evidence of displacement of the $–SCH_3$ group. A strong and sharp thiocarbonyl ν(C=S) stretch is also present at around 810 cm^{-1} for all complexes. This is significant for **3.3b**, as it suggests that the thione tautomer is present in the solid state.

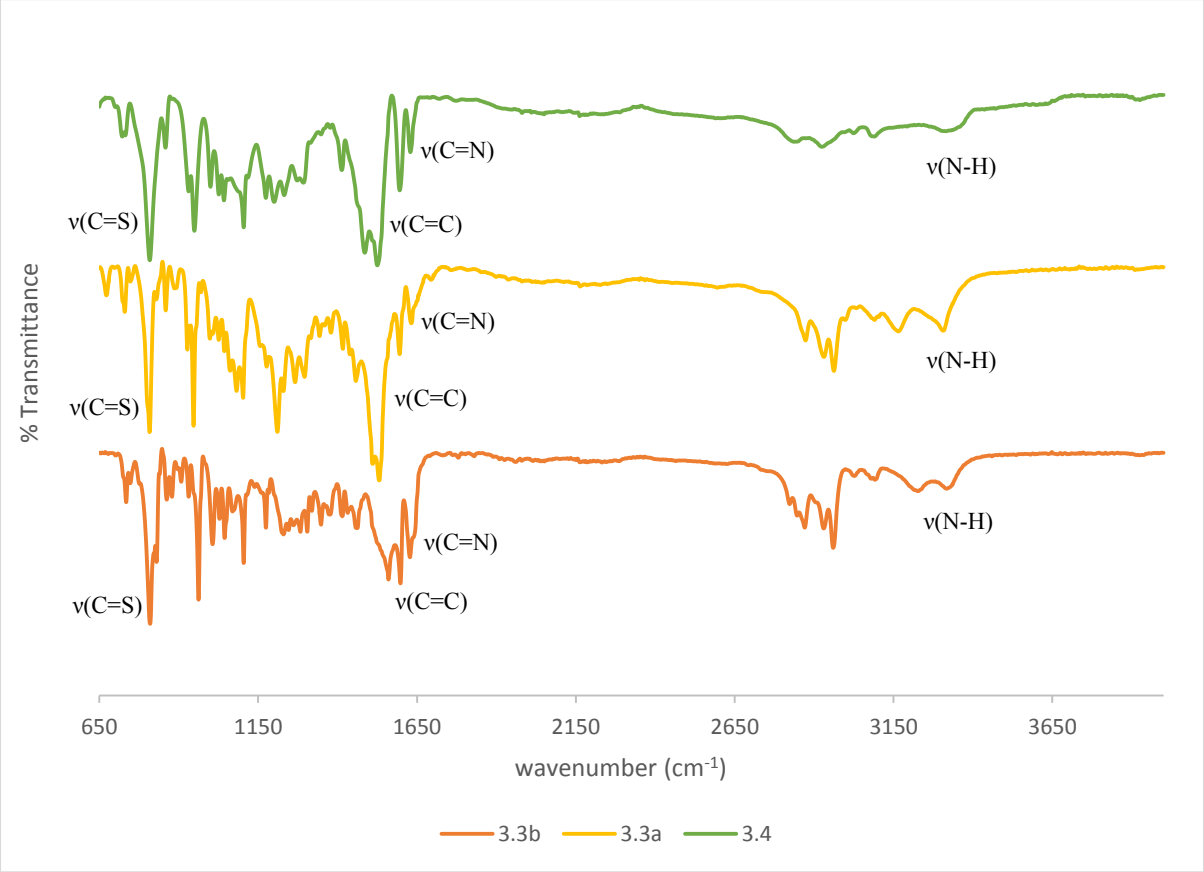

Fig. 3.14: The infrared spectrum of the polynuclear complexes **3.3a** (bottom), **3.3b** (middle) and **3.4** (top).

The amine moieties give rise to ν(N-H) stretching bands in the region 3313 – 3084 cm^{-1} and ν(N-H) bending vibrations between 1528 and 1524 cm^{-1}. The characteristic imine ν(C=N) band is retained in these spectra at similar wavenumbers (1630 – 1628 cm^{-1}) as compared to the ferrocenyl dithiocarbamate precursor **3.2** (at 1633 cm^{-1}). Furthermore, in each of the spectra the alkenyl group gives rise to an

absorption band around 1598 – 1595 cm^{-1}, shifted to slightly higher wavenumbers compared to **3.2**. A strong and sharp thiocarbonyl ν(C=S) stretch is also present at 810 cm^{-1}.

Mass Spectrometry

Mass spectral data of **3.3** – **3.6** further confirms the structures of these compounds. The EI mass spectrum of **3.3b** displays a peak corresponding to the molecular ion $[M]^+$ at *m/z* 431.0909. The ESI mass spectrum of **3.4** shows a base peak corresponding to $[M+H]^+$ (*m/z* 1263.2756), while the spectrum of **3.5** displays a base peak at *m/z* 903.2354 for $[M+2H]^{2+}$. In the mass spectrum of **3.6**, a peak corresponding to $[M+7H]^{7+}$ is observed at *m/z* 536.1647.

3.3 Summary

A new ferrocenyl dithiocarbamate (**3.2**) ligand and four new mono- and polynuclear ferrocenylthiosemicarbazone complexes (**3.3** – **3.6**) were prepared via Schiff-base condensation and nucleophilic substitution reactions, respectively. All compounds were characterised using various spectroscopic and analytical techniques. The dithiocarbamate **3.2** and polynuclear complexes **3.4** – **3.6** were found to be stable in air and in solution, as well as at elevated temperatures. The mononuclear complex was found to undergo thione-thiol tautomerism and was isolated in both forms. The thiol form was isolated as the major product. All complexes displayed similar solubility in solvents such as DCM, chloroform and DMSO. However, the mononuclear complexes (**3.3a** and **3.3b**) and the trinuclear complex (**3.4**) were soluble in alcoholic solvents such as ethanol, while the higher generation complexes (**3.5** and **3.6**) were insoluble.

3.4 Experimental

3.4.1 Materials

n-Propylamine, tris(2-aminoethyl)-amine, DAB-Am-4, hydrazine hydrate, carbon disulfide and iodomethane were purchased from Sigma Aldrich. DAB-Am-8 was purchased from SymoChem. Solvents were purchased from Kimix and Merck and ethanol was dried over molecular sieves. Methyl hydrazinecarbodithioate (**3.1**)[3] was prepared using a literature procedure.

3.4.2 Spectroscopic and Analytical Techniques

Infrared (IR) absorptions were measured on a Perkin-Elmer Spectrum 100 FT-IR Spectrometer as KBr pellets or using Attenuated Total Reflectance (ATR). Nuclear Magnetic Resonance (NMR) Spectra were recorded on a Varian Unity XR400 MHz (^{1}H at 399.95 MHz, ^{13}C at 100.58 MHz), Varian Mercury XR300 MHz (^{1}H at 300.08 MHz, ^{13}C at 75.46 MHz) or a Bruker Biospin GmbH (^{1}H at 400.22 MHz, ^{13}C at 100.64 MHz) spectrometer at 30 °C. Chemical shifts are reported using tetramethylsilane (TMS) as the internal standard. Elemental analysis for C, H and N were carried out using a Thermo Flash 1112 Series CHNS-O Analyser. Mass spectrometry determinations were carried out using Electron Impact (EI) on a JEOL GC Matell instrument or High Resolution Electrospray Ionisation (HR-ESI) on a Waters API Quattro Micro triple quadrupole mass spectrometer with data recorded using both the positive. Melting points were determined using a Reichert-Jung Thermovar or a Büchi Melting Point Apparatus B-540.

3.4.3 Synthesis of dithiocarbamate precursors

3.4.3.1 Methyl hydrazinecarbodithioate (3.1)[3]

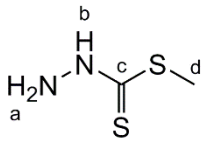

Hydrazine hydrate (6.64 mL) was added to a cooled solution of potassium hydroxide (5.99 g, 0.107 mmol) in water (25 mL) and isopropanol (25 mL). Ice-cooled carbon disulfide (6.44 mL) was added dropwise with stirring, giving rise to a yellow/orange solution. The mixture was stirred for a further 2.5 hours at room temperature, after which ice-cooled iodomethane (6.64 mL) was added dropwise over a 1 hour period and the mixture stirred for a further 1.5 hours at room temperature. The clear solution was cooled in an ice bath, resulting in the formation of a white precipitate, which was collected by suction filtration and washed with cold water. The resulting crude white powder, was recrystallized from DCM and collected by suction filtration as a white crystalline solid, the desired product **3.1**, which was then dried *in vacuo*. Yield: 1.61 g, 12.3 %. **^{1}H NMR (300.08 MHz, DSMO-*d*$_6$)**: δ (ppm) = 10.77

(br s, 1H, H_b), 5.06 (s, 2H, H_a), 2.39 (s, 3H, H_d). **IR (KBr, cm^{-1})** ν = 3262 (N-H), 3153 (N-H), 1505 (N-H), 703 (C-S).

3.4.3.2 Ferrocenyl dithiocarbamate (3.2)

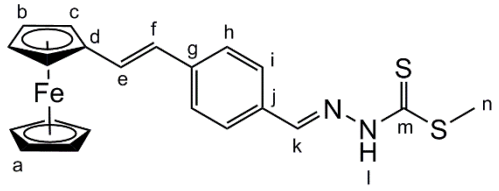

Compound **3.1** (0.325 g, 2.37 mmol) was added to a stirring solution of **2.3** (0.502 g, 1.58 mmol) in isopropanol (50 mL) and the red solution was refluxed for 16 hours, after which an orange precipitate had formed. The precipitate was collected by suction filtration and washed with 5 mL of isopropanol. The orange precipitate was then dissolved in a minimum amount of DCM and an excess of *n*-pentane was added to precipitate the desired product **3.2** as an orange solid. The product was collected by suction filtration and washed with *n*-pentane. Yield: 0.587 g, 88.5 %. M.p: 184 – 186 °C. **^{1}H NMR (400.22 MHz, DMSO-*d*$_6$)**: δ (ppm) = 8.23 (s, 1H, H_k), 7.68 (d, 2H, ^3J = 8.4 Hz, H_i), 7.59 (d, 2H, ^3J = 8.3 Hz, H_h), 7.12 (d, 1H, ^3J = 16.1 Hz, H_e), 6.82 (d, 1H, ^3J = 16.1 Hz, H_f), 4.60 (t, 2H, ^3J = 1.8 Hz, H_c), 4.36 (t, 2H, ^3J = 1.8 Hz, H_b), 4.16 (s, 5H, H_a), 2.54 (s, 3H, H_n). **^{13}C{^{1}H} NMR (100.64 MHz, DMSO-*d*$_6$)**: δ (ppm) = 198.43 (C_m), 146.74 (C_k), 140.60 (C_j), 132.06 (C_g), 129.78 (C_e), 128.36 (C_i), 126.61 (C_h), 125.39 (C_f), 83.22 (C_d), 69.73 (C_c), 69.56 (C_a), 67.55 (C_b), 17.24 (C_n). **IR (KBr, cm^{-1})** ν = 3093 (N-H), 1633 (C=N), 1591 (C=C), 1521 (N-H), 810 (C=S), 704 (C-S), 1108 (ferrocene). **Elemental Analysis** for $C_{21}H_{20}FeN_2S_2$: Found C, 59.47; H, 4.73; N, 5.97; S, 11.63 %; Calculated C, 60.00; H, 4.86; N, 6.66; S, 15.25 %. **EI-MS**: m/z 420.0341 ([M]$^+$, 66.9 %).

3.4.4 Synthesis of Mono- and Polynuclear Ferrocenylthiosemicarbazone complexes

3.4.4.1 Mononuclear ferrocenylthiosemicarbazone complex (3.3a)

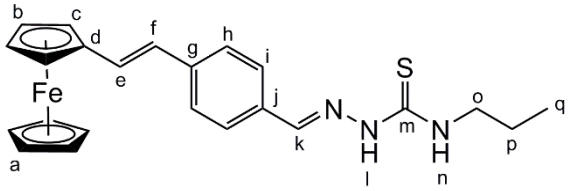

n-Propylamine (0.115 g, 1.93 mmol) was added to a stirring suspension of **3.2** (0.0812 g, 0.193 mmol) in 80 mL of dry ethanol and the bright red mixture was refluxed for 24 hours. The solvent of the resulting clear red solution was removed and the dark red residue dissolved in 20 mL of dichloromethane and 20 mL of water was added. The organic (DCM) layer was separated and the aqueous layer washed with

DCM (3 x 20 mL). The organic fractions were collected, dried over anhydrous sodium sulphate and filtered by gravity. The solvent was reduced to about 5 mL and petroleum ether (40 – 60 °C) added to precipitate the desired product **3.3a** as an orange powder. **^{1}H NMR (300.08 MHz, DMSO-*d*$_6$)**: δ (ppm) = 11.37 (br s, 1H, H_l), 8.52 (m, 1H, H_n), 8.04 (s, 1H, H_k), 7.73 (d, 2H, ^3J = 8.4 Hz, H_i), 7.54 (d, 2H, ^3J = 8.3 Hz, H_h), 7.06 (d, 1H, ^3J = 16.1 Hz, H_e), 6.83 (d, 1H, ^3J = 16.1 Hz, H_f), 4.35 (d, 2H, ^3J = 1.8 Hz, H_b), 4.59 (d, 2H, ^3J = 1.8 Hz, H_c), 4.16 (s, 5H, H_a), 3.54 (m, 2H, H_o), 1.63 (m, 2H, H_p), 0.90 (m, 3H, H_q). **IR (KBr, cm^{-1})** ν = 3313 (N-H), 3226 (N-H), 1628 (C=N), 1598 (C=C), 1524 (N-H), 810 (C=S), 1105 (ferrocene).

3.4.4.2 Mononuclear ferrocenylthiosemicarbazone complex (3.3b)

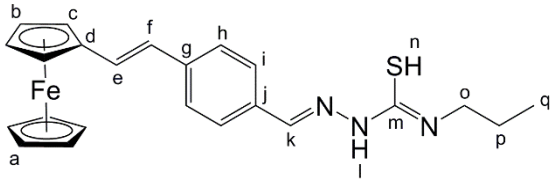

n-Propylamine (0.115 g, 1.93 mmol) was added to a stirring suspension of **3.2** (0.0812 g, 0.193 mmol) in 80 mL of dry ethanol and the bright red mixture was refluxed for 24 hours. The solvent of the resulting clear red solution was removed and the dark red residue dissolved in 20 mL of dichloromethane and 20 mL of water was added. The organic (DCM) layer was separated and the aqueous layer washed with DCM (3 x 20 mL). The organic fractions were collected, dried over anhydrous sodium sulphate and filtered by gravity. The solvent of the filtrate was removed to give the desired compound **3.3b** as a red-purple powder, which was dried *in vacuo*. Yield: 0.0616 g, 74.0 %. M.p: 117 – 119 °C. **^{1}H NMR (400.22 MHz, DMSO-*d*$_6$)**: δ (ppm) = 8.30 (s, 1H, H_k), 7.69 (d, 2H, ^3J = 8.4 Hz, H_i), 7.55 (d, 2H, ^3J = 8.3 Hz, H_h), 7.08 (d, 1H, ^3J = 16.1 Hz, H_e), 6.81 (d, 1H, ^3J = 16.1 Hz, H_f), 4.59 (d, 2H, ^3J = 1.8 Hz, H_c), 4.35 (d, 2H, ^3J = 1.8 Hz, H_b), 4.15 (s, 5H, H_a), 3.53 (m, 2H, H_o), 1.65 (m, 2H, H_p), 0.92 (m, 3H, H_q). **^{13}C{^{1}H} NMR (100.64 MHz, DMSO-*d*$_6$)**: δ (ppm) = 160.64 (C_k), 140.25 (C_j), 135.01 (C_g), 129.20 (C_e), 128.70 (C_i), 126.28 (C_h), 125.53 (C_f), 83.33 (C_d), 69.59 (C_c), 69.51 (C_a), 67.47 (C_b), 62.86 (C_o), 24.19 (C_p), 12.19 (C_q). **IR (KBr, cm^{-1})** ν = 3313 (N-H), 3226 (N-H), 1628 (C=N), 1598 (C=C), 1524 (N-H), 810 (C=S), 1105 (ferrocene). **Elemental Analysis** for $C_{23}H_{25}FeN_3S$: Found C, 67.59; H, 7.86; N, 6.65; S, 1.53 %; Calculated C, 64.04; H, 5.84; N, 9.74; S, 7.43 %. **EI-MS**: m/z 431.0909 ([M]$^+$, 94.6 %).

3.4.4.3 TRIS-ferrocenylthiosemicarbazone complex (3.4)

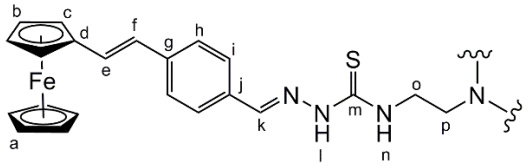

Tris(2-aminoethyl)-amine (0.0116 g, 0.0794 mmol) dissolved in 10 mL of dry ethanol was added to a stirring suspension of **3.2** (0.105 g, 0.238 mmol) in 100 mL of dry ethanol and the red mixture was refluxed for 3 days. The solvent of the resulting red solution was reduced while still warm, giving the desired compound **3.4** as a dark red precipitate, which was collected by suction filtration and washed with excess *n*-pentane. Yield: 0.0421 g, 42.0 %. M.p: 158 – 160 °C. **^{1}H NMR (400.22 MHz, DMSO-*d*$_6$)**: δ (ppm) = 11.51 (br s, 3H, H_l), 8.47 (t, 3H, ^3J = 5.3 Hz, H_n), 8.05 (br s, 3H, H_k), 7.72 (d, 6H, ^3J = 8.3 Hz, H_i), 7.52 (d, 6H, ^3J = 8.3 Hz, H_h), 7.04 (d, 3H, ^3J = 16.2 Hz, H_e), 6.77 (d, 3H, ^3J = 16.2 Hz, H_f), 4.55 (m, 6H, H_c), 4.34 (m, 6H, H_b), 4.13 (s, 15H, H_a), 3.75 (m, 6H, H_o), 2.88 (m, 6H, H_p). **^{13}C{^{1}H} NMR (100.64 MHz, DMSO-*d*$_6$)**: 177.44 (C_m), 142.47 (C_k), 139.59 (C_j), 132.87 (C_g), 128.98 (C_e), 128.05 (C_i), 126.42 (C_h), 125.55 (C_f), 83.34 (C_d), 69.63 (C_b), 69.54 (C_a), 67.44 (C_c), 53.14 (C_o), 42.55 (C_p). **IR (KBr, cm^{-1})** ν = 3311 (N-H), 3084 (N-H), 1628 (C=N), 1596 (C=C), 1525 (N-H), 809 (C=S), 1105 (ferrocene). **Elemental Analysis** for $C_{66}H_{66}Fe_3N_{10}S_3.H_2O$: Found C, 61.81; H, 5.80; N, 9.93; S, 4.24 %; Calculated C, 61.88; H, 5.35; N, 10.93; S, 7.51 %. **HR-ESI-MS**: *m*/*z* 1263.2756 ([M+H]$^+$, 100 %).

3.4.4.4 DAB-G1-ferrocenylthiosemicarbazone complex (3.5)

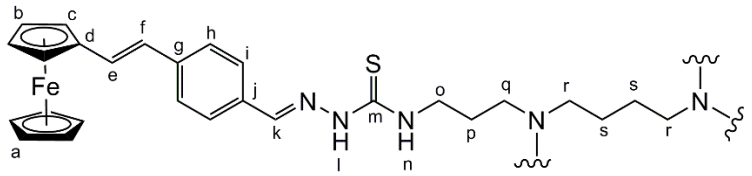

DAB-Am-4 (0.0188 g, 0.0595 mmol) dissolved in 10 mL of dry ethanol was added dropwise to a stirring suspension of **3.2** (0.102 g, 0.238 mmol) in 100 mL of dry ethanol and the red mixture was refluxed for 3 days. The resulting red solution was decanted off, leaving as a red/orange oily residue in the flask. The oily residue was washed with hot ethanol, dissolved in a minimum amount of DCM and an excess amount of *n*-pentane was added to precipitate the desired compound **3.5** as an orange powder, which was collected by suction filtration and dried *in vacuo*. Yield: 0.0463 g, 43.1 %. M.p: 165 – 167 °C. **^{1}H NMR (400.22 MHz, DMSO-*d*$_6$)**: δ (ppm) = 11.36 (br s, 4H, H_l), 8.55 (br s, 4H, H_n), 8.07 (br s, 4H, H_k), 7.71 (d, 8H, ^3J = 8.4 Hz, H_i), 7.52 (d, 8H, ^3J = 8.3 Hz, H_h), 7.04 (d, 4H, ^3J = 16.1 Hz, H_e), 6.76 (d, 4H, ^3J = 16.1 Hz, H_f), 4.55 (m, 8H, H_c), 4.33 (m, 8H, H_b), 4.13 (s, 20H, H_a), 3.65 (m, 8H, H_o), 2.45 (m,

8H, H_q), 2.30 (m, 4H, H_r), 1.75 (m, 8H, H_p), 1.37 (m, 4H, H_s). **$^{13}C\{^1H\}$ NMR (100.64 MHz, DMSO-*d*$_6$)**: δ (ppm) = 177.34 (C_m), 142.46 (C_k), 139.57 (C_j), 132.90 (C_g), 128.97 (C_e), 128.06 (C_i), 126.36 (C_h), 125.59 (C_f), 83.37 (C_d), 69.59 (C_c), 69.52 (C_a), 67.44 (C_b), 54.25 (C_o), 52.19 (C_r), 43.37 (C_q), 26.63 (C_p), 25.00 (C_s). **IR (KBr, cm^{-1})** ν = 3310 (N-H), 3087 (N-H), 1629 (C=N), 1595 (C=C), 1527 (N-H), 810 (C=S), 1105 (ferrocene). **Elemental Analysis** for $C_{96}H_{104}Fe_4N_{14}S_4.4H_2O$: Found C, 61.50; H, 6.30; N, 10.77; S, 5.49 %; Calculated C, 61.41; H, 6.01; N, 10.44; S, 6.83 % %. **HR-ESI-MS**: *m*/*z* 903.2354 ($[M+2H]^{2+}$, 100 %).

3.4.4.5 DAB-G2-ferrocenylthiosemicarbazone complex (3.6)

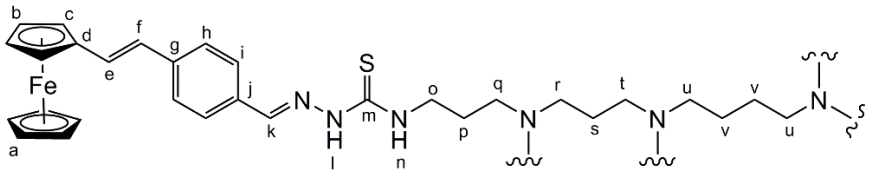

DAB-Am-8 (0.0231 g, 0.0298 mmol) dissolved in 10 mL of dry ethanol was added dropwise to a stirring suspension of **3.2** (0.110 g, 0.238 mmol) in 100 mL of dry ethanol and the red mixture was refluxed for 3 days. The resulting red solution was decanted off, leaving a red/orange oily residue in the flask. The oily residue was washed with hot ethanol, dissolved in a minimum amount of DCM and an excess amount of *n*-pentane was added to precipitate the desired compound **3.6** as an orange/brown powder, which was collected by suction filtration and dried *in vacuo*. Yield: 0.0404 g, 36.2 %. M.p: 168 – 170 °C. **^{1}H NMR (400.22 MHz, DMSO-*d*$_6$)**: δ (ppm) = 8.44 (br s, 8H, H_n), 8.07 (br s, 8H, H_k), 7.67 (d, 16H, ^3J = 8.4 Hz, H_i), 7.49 (d, 16H, ^3J = 8.3 Hz, H_h), 7.02 (d, 8H, ^3J = 16.1 Hz, H_e), 6.76 (d, 8H, ^3J = 16.1 Hz, H_f), 4.54 (m, 16H, H_c), 4.32 (m, 16H, H_b), 4.13 (br s, 40H, H_a), 3.65 (m, 16H, H_o), 2.27-2.41 (br m, 32H, $H_{q/r/t}$), 1.75 (br s, 16H, H_p), 1.48 (m, 16H, $H_{s/u/v}$). **$^{13}C\{^1H\}$ NMR (100.64 MHz, DMSO-*d*$_6$)**: 177.71 (C_m), 142.86 (C_k), 139.77 (C_j), 132.93 (C_g), 129.04 (C_e), 127.98 (C_i), 126.36 (C_h), 125.64 (C_f), 83.34 (C_d), 69.57 (C_c), 69.51 (C_a), 67.47 (C_b), 52.41 (C_o), 49.56 (C_q), 49.02 (C_r), 43.44 (C_u), 32.02 (C_t), 26.80 (C_p), 26.37 (C_s), 24.60 (C_v). **IR (KBr, cm^{-1})** ν = 3313 (N-H), 3194 (N-H), 1630 (C=N), 1597 (C=C), 1528 (N-H), 810 (C=S), 1105 (ferrocene). **Elemental Analysis** for $C_{200}H_{224}Fe_8N_{30}S_8.7H_2O$: Found C, 61.99; H, 6.94; N, 10.48; S, 4.04 %; Calculated C, 61.95; H, 6.19; N, 10.84; S, 6.62 %. **HR-ESI-MS**: *m*/*z* 536.1647 ($[M+7H]^{7+}$, 100 %).

3.5 References

1. H. G. Petering, H. H. Buskirk and G. E. Underwood, *Cancer Res.,* 1964, **24**, 367-372.
2. D. L. Klayman, J. F. Bartosevich, T. S. Griffin, C. J. Mason and J. P. Scovill, *J. Med. Chem.,* 1979, **22**, 855-862.
3. D. L. Klayman, J. P. Scovill, J. F. Bartosevich and C. J. Mason, *J. Med. Chem.,* 1979, **22**, 1367-1373.
4. D. L. Klayman, J. P. Scovill, J. F. Bartosevich and J. Bruce, *J. Med. Chem.,* 1983, **26**, 35-39.
5. D. Kovala-Demertzi, A. Domopoulou, M. A. Demertzis, G. Valle and A. Papageorgiou, *J. Inorg. Biochem.,* 1997, **68**, 147-155.
6. D. C. Greenbaum, Z. Mackey, E. Hansell, P. Doyle, J. Gut, C. R. Caffrey, J. Lehrman, P. J. Rosenthal, J. H. McKerrow and K. Chibale, *J. Med. Chem.,* 2004, **47**, 3212-3219.
7. W. Hu, W. Zhou, C. Xia and X. Wen, *Bioorg. Med. Chem. Lett.,* 2006, **16**, 2213-2218.
8. R. B. de Oliveira, E. M. de Souza-Fagundes, R. P. Soares, A. A. Andrade, A. U. Krettli and C. L. Zani, *Eur. J. Med. Chem.,* 2008, **43**, 1983-1988.
9. H. Beraldo and D. Gambino, *Mini Rev. Med. Chem.,* 2004, **4**, 31-39.
10. S. H. Belgorod, H. Alexander, C. E. Meidt and J. McGaley, *Chest,* 1951, **20**, 1-18.
11. W. Fox, *Chest,* 1979, **76**, 785-796.
12. E. D. Chan and M. D. Iseman, *Brit. Med. J,* 2002, **325**, 1282-1286.
13. Chopra and P. Brennan, *Tubercle Lung Dis.,* 1998, **78**, 89-98.
14. G. D. Coxon, D. Craig, R. M. Corrales, E. Vialla, L. Gannoun-Zaki and L. Kremer, *PloS one,* 2013, **8**, e53162.
15. G. Kanagaraj and G. Rao, *Polyhedron,* 1993, **12**, 383-387.
16. N. E. Morrison and F. M. Collins, *Int. J. of Lepr. Other Mycobact. Dis.,* 1981, **49**, 180-186.
17. F. M. Collins, D. L. Klayman and N. E. Morrison, *J. Gen. Microbiol.,* 1982, **128**, 1349-1356.
18. Maia, Pedro I da S, F. R. Pavan, C. Q. Leite, S. S. Lemos, G. F. de Sousa, A. A. Batista, O. R. Nascimento, J. Ellena, E. E. Castellano and E. Niquet, *Polyhedron,* 2009, **28**, 398-406.
19. F. R. Pavan, Maia, Pedro I da S, S. R. Leite, V. M. Deflon, A. A. Batista, D. N. Sato, S. G. Franzblau and C. Q. Leite, *Eur. J. Med. Chem.,* 2010, **45**, 1898-1905.
20. S. D. Khanye, B. Wan, S. G. Franzblau, J. Gut, P. J. Rosenthal, G. S. Smith and K. Chibale, *J. Organomet. Chem.,* 2011, **696**, 3392-3396.
21. S. A. Khan and M. Yusuf, *Eur. J. Med. Chem.,* 2009, **44**, 2270-2274.
22. C. Quintana, A. H. Klahn, V. Artigas, M. Fuentealba, C. Biot, I. Halloum, L. Kremer and R. Arancibia, *Inorg. Chem. Commun.,* 2015, **55**, 48-50.
23. R. Arancibia, C. Quintana, C. Biot, M. E. Medina, S. Carrère-Kremer, L. Kremer and A. H. Klahn, *Inorg. Chem. Commun.,* 2015, **55**, 139-142.

24. M. Adams, Y. Li, H. Khot, C. De Kock, P. J. Smith, K. Land, K. Chibale and G. S. Smith, *Dalton Trans.,* 2013, **42**, 4677-4685.
25. M. Adams, C. de Kock, P. J. Smith, K. M. Land, N. Liu, M. Hopper, A. Hsiao, A. R. Burgoyne, T. Stringer and M. Meyer, *Dalton Trans.,* 2015, **44**, 2456-2468.
26. S. D. Khanye, J. Gut, P. J. Rosenthal, K. Chibale and G. S. Smith, *J. Organomet. Chem.,* 2011, **696**, 3296-3300.
27. T. Stringer, D. Taylor, C. de Kock, H. Guzgay, A. Au, S. H. An, B. Sanchez, R. O'Connor, N. Patel and K. M. Land, *Eur. J. Med. Chem.,* 2013, **69**, 90-98.
28. M. Adams, C. De Kock, P. J. Smith, P. Malatji, A. T. Hutton, K. Chibale and G. S. Smith, *J. Organomet. Chem.,* 2013, **739**, 15-20.
29. T. S. Lobana, A. Sánchez, J. S. Casas, A. Castiñeiras, J. Sordo, M. S. García-Tasende and E. M. Vázquez-López, *Dalton Trans.,* 1997, 4289-4300.
30. T. S. Lobana, S. Khanna, R. J. Butcher, A. Hunter and M. Zeller, *Polyhedron,* 2006, **25**, 2755-2763.
31. T. S. Lobana, G. Bawa, R. J. Butcher, B. Liaw and C. W. Liu, *Polyhedron,* 2006, **25**, 2897-2903.
32. E. Akgemci, H. Bingol, T. Atalay and M. Ersoz, *Electrochim. Acta,* 2007, **53**, 673-679.
33. K. Alomar, A. Landreau, M. Kempf, M. A. Khan, M. Allain and G. Bouet, *J. Inorg. Biochem.,* 2010, **104**, 397-404.

Chapter 4

Antimycobacterial and antiplasmodial evaluation of mono- and polynuclear ferrocenyl-derived complexes

4.1 Introduction

Tuberculosis and malaria remain highly prevalent microbial diseases, affecting many parts of the world, particularly developing countries.[1] Although effective drug therapies are currently in use for both diseases,[2, 3] the emergence of drug resistance has led to the need for the development of new drugs. In addition, new drug design strategies have to be explored.

As mentioned in Chapter 1, the use of ferrocene in therapeutic compounds has proven a promising modification. Ferrocene has several properties which lends itself to application in biology.[4-6] Perhaps most significantly, ferrocene is highly lipophilic and thus can allow the compound to interact with lipid layers, such as the cell wall and cell membrane, aiding permeation.[4-6] This is particularly important for drugs targeting *Mycobacterium tuberculosis*, as the cell wall and membrane of the bacillus often needs to be permeated in order for antimycobacterial action to take place.[7, 8] Lipophilicity is also an important property in terms of *Plasmodium falciparum*, allowing the compound to gain access to the digestive vacuole of the parasite to prevent pathogenesis. The unique electrochemical properties of ferrocene may also allow for the generation of reactive oxygen species (ROS), which are known to have biological activity.[4-6] A prime example of a promising drug candidate is Ferroquine,[9] a chloroquine derivative incorporating ferrocene in its side chain, which reached phase IIb clinical trials for malaria.[10]

Conjugating the ferrocene moiety to organic scaffolds which would aid in drug delivery and potency, is also an important concept to consider. The use of polyamines, an abundant naturally occurring group of biomolecules,[11-13] may show promise in terms of selective uptake in diseases such as malaria,[14, 15] as described in Chapter 2. This can be by means of polyamine transporters (PATs). With this in mind, a series of ferrocenyl-derived imino and amino complexes, shown in Fig. 4.1, were evaluated as potential antimycobacterial and antiplasmodial agents. The imino and amino derivatives were both tested in order to determine the effect of the differing imino and amino moieties on the biological activity.

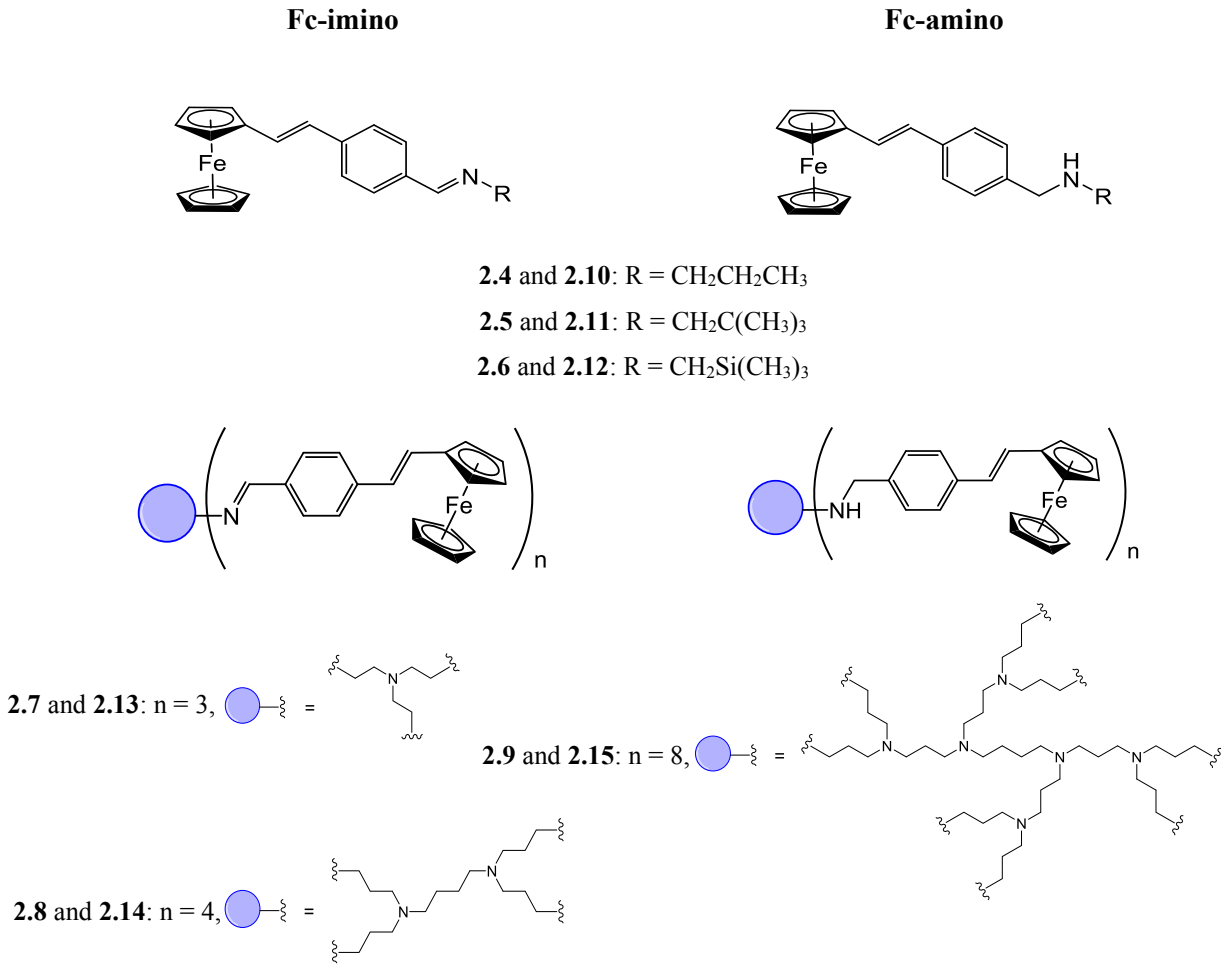

Fig. 4.1: Structures of the ferrocenyl-imine and ferrocenyl-amine complexes screened in antimycobacterial and antiplasmodial studies.

The complexes shown in Fig. 4.1 contain a ferrocenyl moiety, for its diverse biological activity, lipophilic nature and electrochemical properties. They also contain an alkene and benzyl moiety, further increasing the lipophilicity, but which may also be beneficial for binding within biological systems. However, these complexes do not contain any known pharmacophore that would impart specific biological activity. A pharmacophore that has widespread application in both antimycobacterial and antiplasmodial research is the thiosemicarbazone moiety. As mentioned in Chapter 3, one of the first known drugs in anti-TB treatment was thiosemicarbazone-based thiacetazone.[16-18] In antiplasmodial research, thiosemicarbazone-based drug candidates display a unique mechanism of action involving the inhibition of cysteine proteases.[19] Thus, a second series of ferrocenyl complexes incorporating the thiosemicarbazone moiety, as shown in Fig. 4.2, was also evaluated for its antimycobacterial and antiplasmodial activity, with the expectation that this derivatisation may result in enhanced biological activity compared to the imino and amino complexes.

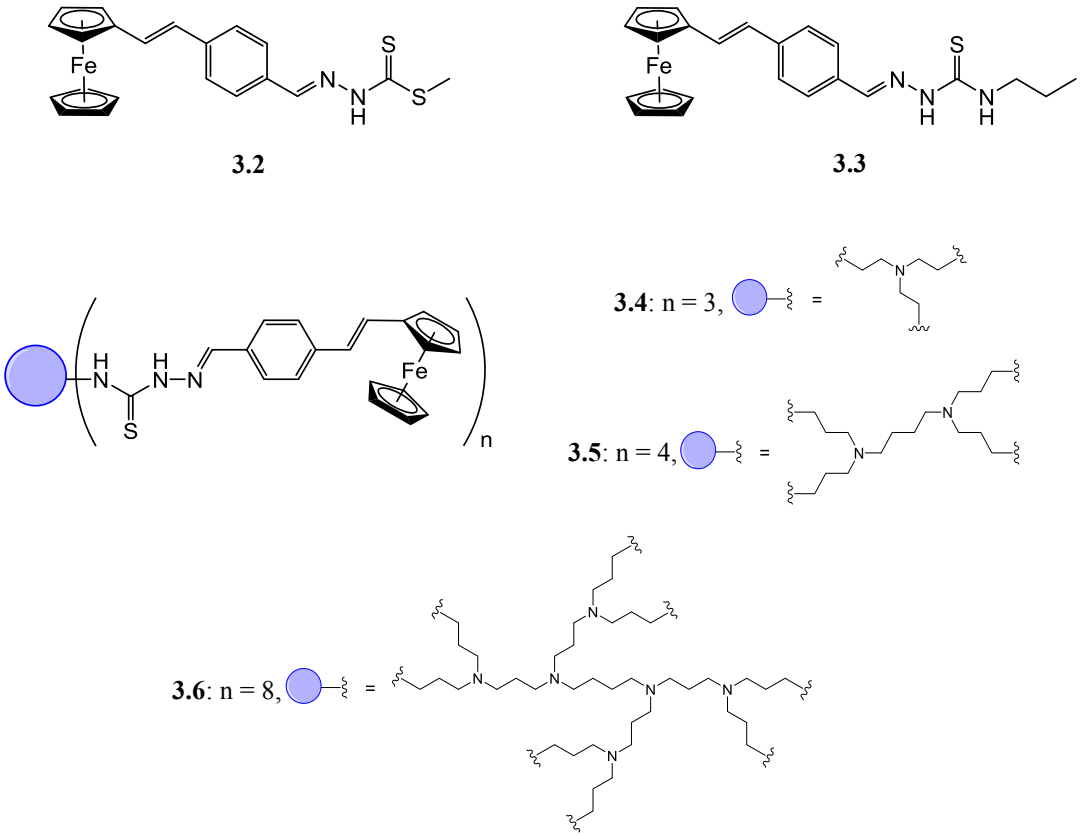

Fig. 4.2: Structures of the ferrocenylthiosemicarbazone complexes screened in antimycobacterial and antiplasmodial studies.

4.2 Preliminary Antimycobacterial Studies

Selected complexes, the mono- and trinuclear ferrocenyl-imino **2.4** – **2.7**, the ferrocenyl-amino **2.10** – **2.12** and all of the ferrocenylthiosemicarbazone complexes **3.3** – **3.6** were evaluated for their antimycobacterial activity against the H37Rv strain of *Mycobacterium tuberculosis*, by determination of their minimum inhibitory concentration (MIC) values. The MIC is the lowest concentration of an antimicrobial that will inhibit the visible growth of an organism. The MIC_{90} refers to the concentration that inhibits 90 % of the bacterial isolate growth. In this study, the current anti-TB drug rifampicin was used as a control, as well as ethambutol, which is some-what structurally similar to the compounds being tested.

4.2.1 Antimycobacterial evaluation of ferrocenyl-derived imino complexes (2.4 – 2.9)

The results of the antimycobacterial screening of the ferrocenyl-derived imino complexes are summarised in Table 4.1.

Table 4.1: MIC_{90} values obtained for the *in vitro* studies of the ferrocenyl-imino complexes **2.4** – **2.9**, as well as rifampicin (RIF) and ethambutol (EMB).

Compound	Nuclearity (n)	H37Rv MIC_{90}* (μM)
2.4	1	37.7
2.5	1	31.4
2.6	1	33.1
2.7	3	19.2
2.8	4	ND**
2.9	8	ND**
EMB	-	9.54
RIF	-	0.0249

*MIC_{90} is the concentration that inhibits 90 % of bacterial isolate growth.
**ND = Not determined due to low solubility in the test medium.

All compounds displayed moderate micromolar MIC values. Looking at the MIC_{90} values, the three mononuclear complexes **2.4** – **2.6** displayed similar values (31.4 – 37.7 μM), thus exhibiting similar activity. The incorporation of the lipophilic silicon moiety in **2.6** compared to the carbon analogue **2.5** does not have an effect on its activity. The trinuclear complex **2.7** exhibited the highest antimycobacterial activity with the lowest MIC_{90} value of 19.2 μM, which is 2-fold higher than that of the clinically used antimycobacterial drug ethambutol (MIC_{90} = 9.54 μM). The MIC values for the

polynuclear complexes **2.8** (n = 4) and **2.9** (n = 8) could not be determined as they were not soluble at the tested concentration.

4.2.2 Antimycobacterial evaluation of ferrocenyl-derived amino complexes (2.10 – 2.15)

In order to compare the effect of the imino group versus the amino group on the antimycobacterial activity, the corresponding ferrocenyl-amino derivatives were also screened against the H37Rv mycobacterial strain. The results of the *in vitro* assays of complexes **2.10** – **2.15** are summarised in Table 4.2.

Table 4.2: MIC_{90} values obtained for the *in vitro* studies of the ferrocenyl-amino complexes (**2.10** – **2.15**).

Compound	Nuclearity (n)	H37Rv MIC_{90}* (μM)
2.10	1	> 500
2.11	1	251
2.12	1	> 500
2.13	3	265
2.14	4	ND**
2.15	8	ND**
EMB	-	9.54
RIF	-	0.0249

*ND = Not determined due to low solubility in the test medium.
*MIC_{90} is the concentration that inhibits 90 % of bacterial isolate growth.

Overall, the ferrocenyl-amino complexes exhibited little to no antimycobacterial activity, displaying high micromolar MIC values (> 251 μM). In this series, the carbon analogue **2.11** displayed greater activity (MIC_{90} = 251 μM) than the silicon analogue **2.12**, which was not active (MIC_{90} > 500 μM). The mononuclear complex **2.11** and trinuclear complex **2.13** were the most active of the series, displaying similar MIC_{90} values (251 and 265 μM). Once again, the MIC values for the polynuclear complexes **2.14** (n = 4) and **2.15** (n = 8) could not be determined as they were not soluble at the tested concentration range.

4.2.3 Antimycobacterial evaluation of ferrocenylthiosemicarbazone complexes (3.3 – 3.6)

Complexes **3.3** – **3.6** contain the thiosemicarbazone moiety, which is the pharmacophore present in Thiacetazone, a known anti-TB drug. Incorporation of this moiety conferred increased solubility to these complexes compared to the ferrocenyl-imino and amino complexes. Thus, the mononuclear complex as well as all polynuclear complexes were soluble at the desired concentration range and could be tested. The results of the *in vitro* screening of ferrocenylthiosemicarbazones **3.3** – **3.6** as well as the ferrocenyl dithiocarbamate precursor **3.2** are summarised in Table 4.3.

Table 4.3: MIC_{90} values obtained for the *in vitro* studies of the ferrocenyl dithiocarbamate (**3.2**) ferrocenylthiosemicarbazone complexes (**3.3** – **3.6**)

Compound	Nuclearity (n)	H37Rv MIC_{90}* (µM)
3.2	1	> 125
3.3	1	47.0
3.4	3	70.1
3.5	4	> 125
3.6	8	41.7
EMB	-	9.54
RIF	-	0.0249

*MIC_{90} is the concentration that inhibits 90 % of bacterial isolate growth.

The ferrocenylthiosemicarbazones were found to exhibit moderate antimycobacterial activity. The ferrocenyl dithiocarbamate precursor **3.2** and the tetranuclear complex **3.5** displayed relatively low activity with MIC_{90} values above 125 µM. The trinuclear complex **3.4** exhibited slightly better activity (70.1 µM), however, the mononuclear **3.3** and octanuclear complex **3.6** showed the best antimycobacterial activity of the series, displaying MIC_{90} values of 47.0 and 41.7 µM, respectively.

4.2.4 Comparison of Antimycobacterial activity

A comparison of the antimycobacterial data of the ferrocenyl-imino, ferrocenyl-amino and ferrocenylthiosemicarbazone complexes revealed some trends in their activities. A graphical representation of the results obtained for the antimycobacterial assays is shown in Fig. 4.3 below.

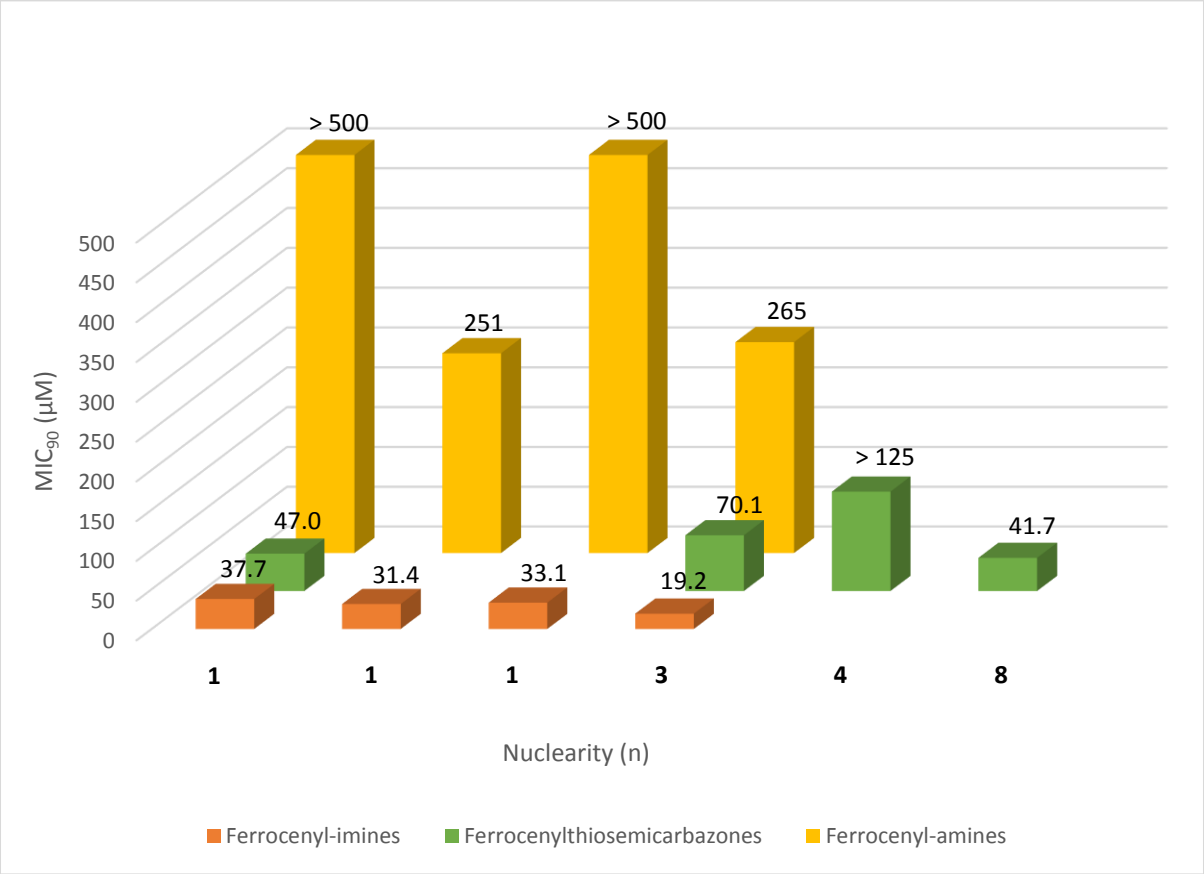

Fig. 4.3: Comparison of *in vitro* antimycobacterial activity of the ferrocenyl-imino (bottom), amino (top) and thiosemicarbazone (middle) complexes

Based on the relatively similar antimycobacterial activity of the mononuclear silicon derivative and its carbon analogue in the case of the ferrocenyl-imines and amines, the presence of the silicon in the side chain appears to have little influence on the antimycobacterial activity. Thus, the corresponding ferrocenylthiosemicarbazone silicon derivative and carbon analogue were not prepared and tested. Overall, the ferrocenyl-imines **2.4** – **2.7** exhibited the highest activity of the synthesised compounds, displaying MIC_{90} values similar to that of the ferrocenyl diamines reported by Pelinski and co-workers.[20] The presence of an amine moiety in **2.10** – **2.13**, which replaces the imine moiety, resulted in a decrease in activity in all cases.

The incorporation of the thiosemicarbazone moiety, a known pharmacophore, resulted in increased solubility and all complexes **3.3** – **3.6** could be tested. The ferrocenylthiosemicarbazone series displayed enhanced activity compared to the amino complexes. However, contrary to what was expected, this group did not result in enhanced antimycobacterial activity compared to the ferrocenyl-imino series. There appears to be no specific trends in activity with respect to the nuclearity of the complexes; the trinuclear complex **2.7** is most active in the imino series (and overall), the mononuclear complex **2.11** in the amino series and the octanuclear complex **3.6** in the thiosemicarbazone series. Although the activity of the ferrocenyl imino complexes was determined to be comparable to that of organometallic complexes in the literature, none of them are comparable to clinically used antimycobacterial drugs such as ethambutol and rifampicin.

4.3 Preliminary Antiplasmodial studies

The ferrocenyl-imino (**2.4** – **2.9**), ferrocenyl-amino (**2.10** – **2.15**) and thiosemicarbazone (**3.2** – **3.6**) complexes were evaluated for their ability to reduce parasitemia in the chloroquine-sensitive (CQS) NF54 strain of *Plasmodium falciparum* at the *in vitro* level. This was achieved by determination of their inhibitory concentration (IC_{50}) values, which is defined as the compounds concentration causing 50 % inhibition of parasitemia *in vitro*. Chloroquine, a quinoline-based antimalarial, and artesunate, an artemisinin-derived antimalarial, were used as controls in this biological study.

4.3.1 Antiplasmodial evaluation of ferrocenyl-derived imino complexes (2.4 – 2.9)

The IC_{50} values obtained for the antiplasmodial screening of the ferrocenyl-imines, as well as the nuclearity of the complexes are summarised in Table 4.4 below.

Table 4.4: IC_{50} values obtained for the *in vitro* antiplasmodial evaluation of the ferrocenyl-imino complexes **2.4** – **2.9** as well as ferroquine (FQ), chloroquine (CQ) and artesunate.

Compound	Nuclearity (n)	NF54 IC_{50}* (μM)
2.4	1	73.6 ± 12.3
2.5	1	76.3 ± 16.9
2.6	1	64.8 ± 11.5
2.7	3	51.1 ± 8.5
2.8	4	> 66
2.9	8	24.7 ± 4.8
FQ	1	0.0427 ± 0.00991
CQ	-	0.0303 ± 0.0160
Artesunate	-	0.0127 ± 0.00156

*IC_{50} is the compound concentration causing 50 % inhibition of parasitemia *in vitro*.

Complexes **2.4** – **2.9** all displayed moderate antiplasmodial activity, exhibiting IC_{50} values in the micromolar range. The mononuclear complexes **2.4** – **2.6** and the tetranuclear complex **2.8** were the least active of the series, displaying IC_{50} values above 64 μM. It is important to note that the mononuclear silicon derivative **2.6** showed better activity than its carbon analogue **2.5**, and the highest activity of the mononuclear complexes. The trinuclear complex **2.7** exhibited enhanced activity compared to the mononuclear complexes, with an IC_{50} value of 51.1 μM, while the octanuclear complex **2.9** exhibited the highest activity of the series, displaying an IC_{50} value of 24.7 μM. Thus, the polynuclear complexes exhibited slightly enhanced activity compared to the mononuclear derivatives.

4.3.2 Antiplasmodial evaluation of ferrocenyl-derived amino complexes (2.10 – 2.15)

The corresponding ferrocenyl-amino complexes were evaluated for their *in vitro* antiplasmodial activity against the CQS NF54 strain. The effect of the new amine moieties compared to the imine moieties can be elucidated by comparison of their IC_{50} values. The results of the antiplasmodial screening of **2.10** – **2.15** are summarised in Table 4.5.

Table 4.5: IC_{50} values obtained for the *in vitro* antiplasmodial evaluation of the ferrocenyl-amino (**2.10** – **2.15**) complexes as well as ferroquine (FQ), chloroquine (CQ) and artesunate.

Compound	Nuclearity (n)	NF54 IC_{50}* (μM)
2.10	1	4.87 ± 0.19
2.11	1	5.29 ± 0.46
2.12	1	2.88 ± 0.40
2.13	3	6.31 ± 0.65
2.14	4	7.18 ± 1.34
2.15	8	4.22 ± 0.87
FQ	1	0.0427 ± 0.00991
CQ	-	0.0303 ± 0.0160
Artesunate	-	0.0127 ± 0.00156

*IC_{50} is the compound concentration causing 50 % inhibition of parasitemia *in vitro*.

Complexes **2.10** – **2.15** all displayed good *in vitro* antiplasmodial activity, exhibiting IC_{50} values in the low micromolar range. The mononuclear complexes **2.10** and **2.11** showed comparable activity with IC_{50} values of 4.87 and 5.29 μM respectively. The silicon-containing derivative **2.12** displayed better activity compared to the carbon analogue **2.11**, as well as the highest activity in the series, with an IC_{50} value of 2.88 μM. The trinuclear and tetranuclear metallodendrimers **2.13** and **2.14** displayed comparable activity (6.31 and 7.18 μM, respectively), which is slightly decreased compared to the mononuclear complexes. This decreased activity may be a result of the poor solubility of the polynuclear complexes (**2.13** – **2.15**) in dimethylsulfoxide (DMSO), the solvent used to make the stock solutions. However, the octanuclear metallodendrimer **2.15** exhibited the highest activity of the polynuclear complexes, displaying an IC_{50} value of 4.22 μM.

4.3.3 Antiplasmodial evaluation of ferrocenylthiosemicarbazone complexes (3.3 – 3.6)

The thiosemicarbazone moiety is of great interest in antimalarial research due to its inherent biological activity and ability to inhibit plasmodial cysteine proteases. Complexes **3.3** – **3.6** contain this biologically favourable moiety and were evaluated for their antiplasmodial activity in order to determine its effect on activity when incorporated into scaffolds of this type. The results for the ferrocenyl dithiocarbamate **3.2** and the ferrocenylthiosemicarbazone complexes **3.3** – **3.6** are summarised in Table 4.6.

Table 4.6: IC_{50} values obtained for the *in vitro* antiplasmodial evaluation of the ferrocenylthiosemicarbazone complexes (**3.3** – **3.6**).

Compound	Nuclearity (n)	NF54 IC_{50}* (μM)
3.2	1	34.16 ± 2.22
3.3	1	18.06 ± 2.24
3.4	3	18.74 ± 3.99
3.5	4	67.64 ± 11.49
3.6	8	32.79 ± 0.23
FQ	1	0.0427 ± 0.00991
CQ	-	0.0303 ± 0.0160
Artesunate	-	0.0127 ± 0.00156

*IC_{50} is the compound concentration causing 50 % inhibition of parasitemia *in vitro*.

The ferrocenyl dithiocarbamate **3.2** and the ferrocenylthiosemicarbazone complexes **3.3** – **3.6** all displayed moderate *in vitro* antiplasmodial activity. The dithiocarbamate ligand **3.2** exhibited moderate activity, displaying an IC_{50} value of 34.2 μM. The higher generation (n = 4, 8) polynucelar complexes (**3.5** and **3.6**) were also found to be moderately active, the octanuclear complex **3.6** (IC_{50} = 32.8 μM) displaying two-fold greater activity than the tetranuclear complex **3.5** (IC_{50} = 67.6 μM). The mononuclear complex **3.3** and trinuclear complex **3.4** exhibited the highest activity in the series, displaying comparable IC_{50} values of 18.1 and 18.7 μM, respectively. The enhanced antiplasmodial activity of the mono- and trinuclear complexes suggests that the lower nuclearity complexes are the more promising candidates.

4.3.4 Comparison of Antiplasmodial activity

The data obtained from the *in vitro* antiplasmodial studies of the ferrocenyl-imino, ferrocenyl-amino and ferrocenylthiosemicarbazones was collated and compared, revealing some meaningful observations and trends in their activities. This comparison is graphically represented in Fig. 4.4 below.

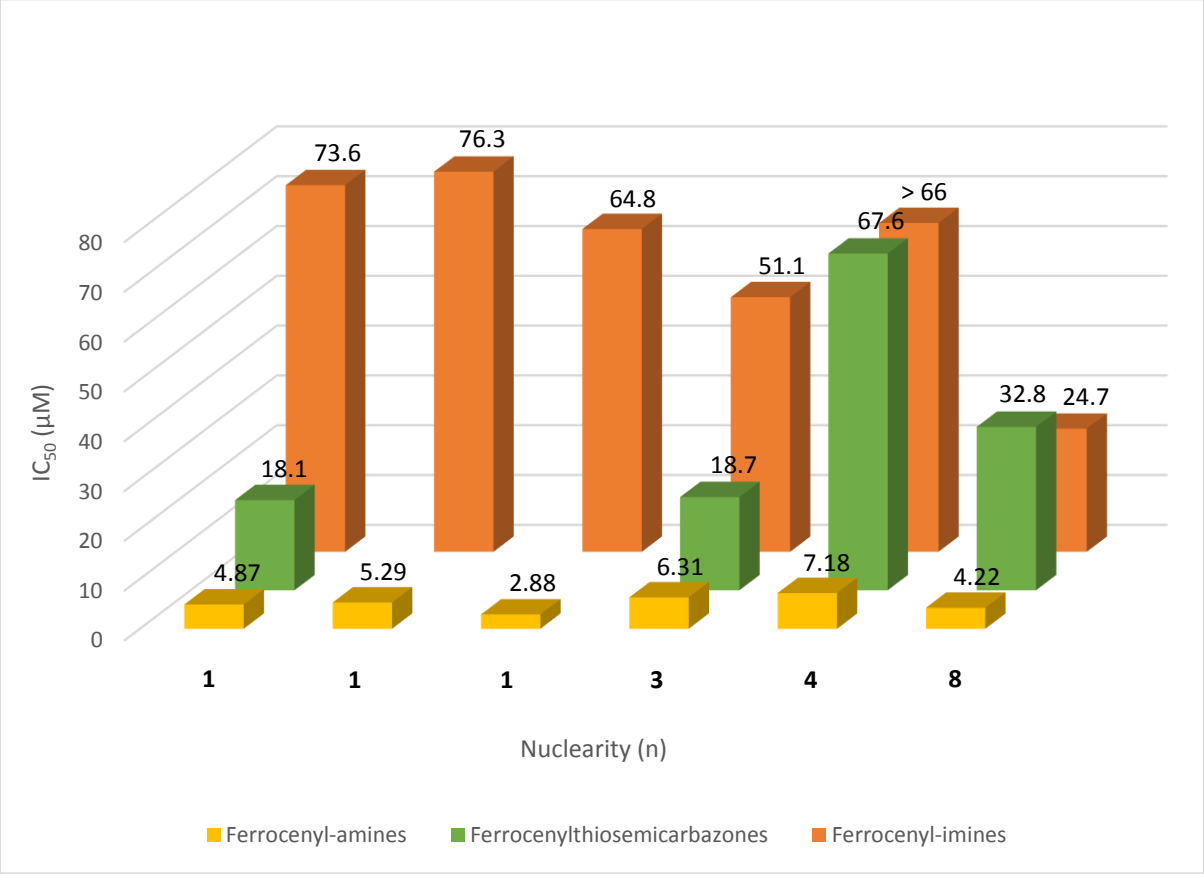

Fig. 4.4: Comparison of *in vitro* antiplasmodial activity of the ferrocenyl-imino (top), amino (bottom) and thiosemicarbazone (middle) complexes

Comparison of the IC_{50} values of the ferrocenyl-imino complexes **2.4** – **2.9** to that of the ferrocenyl-amino complexes **2.10** – **2.15** revealed that the amino complexes showed superior antiplasmodial activity. Specifically, in the case of the mononuclear complexes, the amines **2.10** – **2.12** exhibited at least a 15-fold increase in activity compared to the corresponding mononuclear imines **2.4** – **2.6**. The polynuclear amino complexes **2.13** – **2.15** exhibited at least a 5-fold increase in activity compared to the corresponding polynuclear imines **2.7** – **2.9**. This suggests that the presence of the amine moiety is favourable compared to the imine moiety as it results in greatly enhanced antiplasmodial activity.

In both series, the silicon-containing mononuclear derivatives (**2.6** and **2.12**) exhibited enhanced antiplasmodial activity compared to the carbon analogues (**2.5** and **2.11**). This trend is in agreement

with literature examples of silicon-containing compounds used in pharmacological evaluations.[21-23] The incorporation of the lipophilic silicon moiety results in an increase in the activity compared to the non-silicon analogues.[21-23] Adams and co-workers reported on the improved antiparasitic (malaria and trichomoniasis) activity of ferrocene-containing organometallic compounds by incorporation of silane moieties.[24]

In the case of the mono- and trinuclear complexes, the ferrocenylthiosemicarbazone complexes (**3.3** and **3.4**) exhibited enhanced antiplasmodial activity compared to the ferrocenyl-imino complexes (**2.4** and **2.7**), and decreased activity compared to the ferrocenyl-amino complexes (**2.10** and **2.13**). Interestingly, **3.3** and **3.4** exhibited similar and improved antiplasmodial activity compared to analogous ferrocenylthiosemicarbazone complexes reported by Stringer and co-workers.[25] The tetra- and octanuclear thiosemicarbazone complexes (**3.5** and **3.6**) displayed comparable activity to the imino complexes (**2.8** and **2.9**). Consistently for the imino, amino and thiosemicarbazone complexes, the tetranuclear complexes (**2.8**, **2.14** and **3.5**) showed the lowest antiplasmodial activity of the polynuclear complexes. This suggests that this nuclearity or molecule size is not favourable or optimum for activity.

The antiplasmodial activity of the synthesised organometallic compounds was much lower than clinically used drugs such as the organic-based chloroquine and artesunate. The results also do not compare to that of ferroquine, a very promising organometallic antiplasmodial drug candidate. Overall, the ferrocenyl-derived amino complexes **2.10** – **2.15** exhibited the highest activity, displaying IC_{50} values comparable to other organometallic complexes reported in the literature. It should be noted that there are not many examples of antiplasmodial metallodendrimers in the literature and these results are promising for the further use of similar compounds in pharmacological studies.

4.4 Experimental

4.4.1 *In vitro* Pharmacological Evaluation

4.4.1.1 *M. tuberculosis* microdilution method

The minimum inhibitory concentration (MIC) was determined using the standard broth micro dilution method, where a 10 ml culture of *Mycobacterium tuberculosis* H37RvMa::pMSP12GFP,[26] was grown to an optical density (OD_{600}) of 0.6 – 0.7 in GAST-Fe (glycerol–alanine–salts) medium pH 6.6, supplemented with 0.05% Tween-80.[27] The culture was then diluted 1:100 in GAST-Fe. The compounds to be tested were reconstituted to a concentration of 12.8 mM in DMSO. Duplicate two-fold serial dilutions of the test compound were prepared in GAST-Fe, across a 96-well micro titre plate, after which, 50 µl of the 1:100 diluted *M. tuberculosis* culture was added to each well in the serial dilution. The plate layout was a modification of the method previously described.[28] Controls used were a minimum growth control (Rifampicin at 2xMIC) a maximum growth control (5% DMSO in GAST-Fe), Rifampicin and Ethambutol. The micro titre plate was sealed in a secondary container and incubated at 37 °C with 5% CO_2 and humidification. Relative fluorescence (excitation 485nM; emission 520nM) was measured using a plate reader (FLUOstar OPTIMA, BMG LABTECH), at day 7 and day 14. The raw fluorescence data were archived and analysed using the CDD Vault from Collaborative Drug Discovery, in which, data were normalised to the minimum and maximum inhibition controls to generate a dose response curve (% inhibition), using the Levenberg-Marquardt damped least-squares method, from which the MIC_{90} was calculated.[29] The lowest concentration of drug that inhibits growth of more than 90 % of the bacterial population was considered to be the MIC_{90}.

4.4.1.2 *P. falciparum in vitro* assay

The test samples were tested in triplicate on one occasion against the chloroquine-sensitive NF54 strain. Continuous *in vitro* cultures of asexual erythrocyte stages of *P. falciparum* were maintained using a modified method of Trager and Jensen.[30] Quantitative assessment of antiplasmodial activity *in vitro* was determined via the parasite lactate dehydrogenase assay using a modified method described by Makler et al.[31] The test samples were prepared to a 20 mg/cm^3 stock solution in 100% DMSO and sonicated to enhance solubility. Samples were tested as a suspension if not completely dissolved. Stock solutions were stored at -20 °C. Further dilutions were prepared on the day of the experiment. Chloroquine (CQ) was used as the reference drug in all experiments. A full dose-response was performed for all compounds to determine the concentration inhibiting 50% of parasite growth (IC_{50} value). Test samples were tested at a starting concentration of 100 µg/cm^3, which was then serially diluted 2-fold in complete medium to give 10 concentrations, with the lowest concentration being 0.2 µg/cm^3. The same dilution

technique was used for all samples. CQ was tested at a starting concentration of 1000 ng/cm^3 against the CQS strain. The highest concentration of solvent to which the parasites were exposed had no measurable effect on the parasite viability. The IC_{50} values were obtained using a nonlinear dose-response curve fitting analysis via Graph Pad Prism v.4.0 software.

4.5 References

1. World Health Organisation, *World Health Statistics 2013*, WHO Press, Geneva, 2013.
2. P. F. Salas, C. Herrmann and C. Orvig, *Chem. Rev.,* 2013, **113**, 3450-3492.
3. A. Koul, E. Arnoult, N. Lounis, J. Guillemont and K. Andries, *Nature,* 2011, **469**, 483-490.
4. M. F. Fouda, M. M. Abd-Elzaher, R. A. Abdelsamaia and A. A. Labib, *Appl. Organomet. Chem.,* 2007, **21**, 613-625.
5. N. Lease, V. Vasilevski, M. Carreira, A. de Almeida, M. Sanaú P. Hirva, A. Casini and M. Contel, *J. Med. Chem.,* 2013, **56**, 5806-5818.
6. C. Biot, N. François, L. Maciejewski, J. Brocard and D. Poulain, *Bioorg. Med. Chem. Lett.,* 2000, **10**, 839-841.
7. I. Chopra and P. Brennan, *Tubercle Lung Dis.,* 1998, **78**, 89-98.
8. P. C. Karakousis, *Antimicrobial drug resistance,* Humana Press, New York City, 2009.
9. C. Biot, G. Glorian, L. A. Maciejewski, J. S. Brocard, O. Domarle, G. Blampain, P. Millet, A. J. Georges, H. Abessolo and D. Dive, *J. Med. Chem.,* 1997, **40**, 3715-3718.
10. G. Mombo-Ngoma, C. Supan, M. P. Dal-Bianco, M. A. Missinou, P. Matsiegui, C. L. Ospina Salazar, S. Issifou, D. Ter-Minassian, M. Ramharter and M. Kombila, *Malar. J.,* 2011, **10**, 53-63.
11. S. Müller, G. H. Coombs and R. D. Walter, *Trends Parasitol.,* 2001, **17**, 242-249.
12. C. Bacchi and N. Yarlett, *Mini Rev. Med. Chem.,* 2002, **2**, 553-563.
13. O. Heby, S. C. Roberts and B. Ullman, *Biochem. Soc. Trans.,* 2003, **31**, 415-419.
14. I. B. Müller, R. D. Gupta, K. Lüersen, C. Wrenger and R. D. Walter, *Mol. Biochem. Parasitol.,* 2008, **160**, 1-7.
15. R. Das Gupta, T. Krause-Ihle, B. Bergmann, I. B. Muller, A. R. Khomutov, S. Muller, R. D. Walter and K. Luersen, *Antimicrob. Agents Chemother.,* 2005, **49**, 2857-2864.
16. S. H. Belgorod, H. Alexander, C. E. Meidt and J. McGaley, *Chest,* 1951, **20**, 1-18.
17. W. Fox, *Chest,* 1979, **76**, 785-796.
18. E. D. Chan and M. D. Iseman, *Brit. Med. J.,* 2002, **325**, 1282-1286.
19. D. C. Greenbaum, Z. Mackey, E. Hansell, P. Doyle, J. Gut, C. R. Caffrey, J. Lehrman, P. J. Rosenthal, J. H. McKerrow and K. Chibale, *J. Med. Chem.,* 2004, **47**, 3212-3219.

20. D. A. Ralambomanana, D. Razafimahefa-Ramilison, A. C. Rakotohova, J. Maugein and L. Pelinski, *Bioorg. Med. Chem.,* 2008, **16**, 9546-9553.
21. A. K. Franz and S. O. Wilson, *J. Med. Chem.,* 2012, **56**, 388-405.
22. M. Blunder, N. Hurkes, S. Spirk, M. List and R. Pietschnig, *Bioorg. Med. Chem. Lett.,* 2011, **21**, 363-365.
23. I. Segal, A. Zablotskaya and E. Lukevics, *Chem. Heterocyc. Compd.,* 2005, **41**, 613-624.
24. M. Adams, C. de Kock, P. J. Smith, K. M. Land, N. Liu, M. Hopper, A. Hsiao, A. R. Burgoyne, T. Stringer and M. Meyer, *Dalton Trans.,* 2015, **44**, 2456-2468.
25. T. Stringer, D. Taylor, C. de Kock, H. Guzgay, A. Au, S. H. An, B. Sanchez, R. O'Connor, N. Patel and K. M. Land, *Eur. J. Med. Chem.,* 2013, **69**, 90-98.
26. G. L. Abrahams, A. Kumar, S. Savvi, A. W. Hung, S. Wen, C. Abell, C. E. Barry, D. R. Sherman, H. I. Boshoff and V. Mizrahi, *Chem. Biol.,* 2012, **19**, 844-854.
27. J. J. De Voss, K. Rutter, B. G. Schroeder, H. Su, Y. Zhu and C. E. Barry, *Proc. Natl. Acad. Sci. U. S. A.,* 2000, **97**, 1252-1257.
28. J. Ollinger, M. A. Bailey, G. C. Moraski, A. Casey, S. Florio, T. Alling, M. J. Miller and T. Parish, *PloS one,* 2013, **8**, 1-9.
29. The Collaborative Drug Discovery Database, www.collaborativedrug.com, (accessed August 2015).
30. W. Trager and J. B. Jensen, *Science,* 1976, **193**, 673-675.
31. M. T. Makler, J. M. Ries, J. A. Williams, J. E. Bancroft, R. C. Piper, B. L. Gibbins and D. J. Hinrichs, *Am. J. Trop. Med. Hyg.,* 1993, **48**, 739-741.

Chapter 5

Conclusions and Future Work

5.1 Conclusions

Ferrocene is an organometallic moiety with great potential for application in biology and chemotherapy due to its favourable chemical and physical properties. Polyamine-based dendrimers are potential bioactive moieties and possess the ability to act as drug transport and delivery scaffolds. Therefore, the main focus of this study was to prepare series ferrocenyl-derived metallodendrimers and mononuclear analogues, to characterise and evaluate their antimycobacterial and antiplasmodial activity.

Ferrocene-containing precursors were prepared by Wittig olefination, Heck cross-coupling and Schiff-base condensation reactions. The preparation of a series of ferrocenyl-imino complexes was achieved by Schiff-base condensation reactions of a ferrocenyl aldehyde with various amines. The corresponding ferrocenyl amino complexes were prepared via reductive amination reactions from the ferrocenyl aldehyde. In addition, a series of ferrocenylthiosemicarbazone complexes were synthesised by nucleophilic substitution reactions of a ferrocenyl dithiocarbamate with various amines. All precursors and complexes were characterised by various techniques such as ^{1}H, $^{13}C\{^{1}H\}$ and $^{31}P\{^{1}H\}$ NMR spectroscopy, FT-IR spectroscopy, EI- or ESI-mass spectrometry and elemental analysis.

The synthesised ferrocenyl-imino, ferrocenyl-amino and ferrocenylthiosemicarbazone metallodendrimers and mononuclear analogues were evaluated as potential antimycobacterial and antiplasmodial agents in preliminary *in vitro* assays. The compounds were screened for their antimycobacterial activity against the H37Rv strain of *Mycobacterium tuberculosis*. The tetranuclear and octanuclear ferrocenyl-imino and amino complexes (**2.8**, **2.9**, **2.14** and **2.15**) were not soluble at the required concentration and thus could not be evaluated. Two mononuclear ferrocenyl-amino complexes (**2.10** and **2.12**) as well as the tetranuclear thiosemicarbazone complex (**3.5**) were not active at the tested concentrations. The remaining ferrocenyl complexes exhibited moderate to low antimycobacterial activity in the micromolar range. The ferrocenyl-amino complexes were the least active in the antimycobacterial screening. It is noteworthy that the presence of the silicon moiety in the side chain of the mononuclear imino and amino complexes (**2.6** and **2.12**) did not have a significant effect on the antimycobacterial activity compared to their carbon analogues (**2.5** and **2.11**). In the thiosemicarbazone series, the mononuclear complex (**3.3**) and octanuclear complex (**3.6**) showed the best activity, the two displaying comparable MIC_{90} values. Again, the low solubility of the polynuclear thiosemicarbazone complexes may have hindered their antimycobacterial activity. The ferrocenyl-imino complexes were

found to exhibit the best antimycobacterial activity overall. The trinuclear imino complex (**2.7**) displayed higher activity (almost two-fold) than the mononuclear complexes (**2.4** – **2.6**), suggesting a correlation between nuclearity and antimycobacterial activity. The ferrocenyl-imino complexes displayed activity comparable to that of other organometallic complexes reported in the literature, but not comparable to clinically available antimycobacterial drugs. The overall trend observed in the antimycobacterial screening can be summarised as shown below.

ferrocenyl-imino* > *ferrocenylthiosemicarbazone* > *ferrocenyl-amino

Additionally, the compounds were evaluated for antiplasmodial activity against the chloroquine-sensitive (CQS) NF54 strain of *Plasmodium falciparum*. The tetranuclear imino complex (**2.8**) was not active at the tested concentration. The remaining complexes displayed moderate to good antiplasmodial activity in the micromolar range. In the ferrocenyl-imino series, the octanuclear complex (**2.9**) exhibited the best activity, suggesting that the antiplasmodial activity is related to high nuclearity. However, in the thiosemicarbazone series, the mono- complex and trinuclear complexes (**3.3** and **3.4**) showed the best activity. The low activity of some of the polynuclear complexes may be a result of their low solubility in the DMSO, which was used to make the stock solutions. Contrary to what was observed in the antimycobacteral screening, the silicon-containing derivatives (**2.6** and **2.12**) displayed enhanced activity compared to their carbon analogues (**2.5** and **2.11**). This trend is consistent with what is observed in the literature. Overall, the ferrocenyl-amino complexes exhibited the best antiplasmodial activity, displaying IC_{50} values in the low micromolar range. Their activity was determined to be comparable to that of other ferrocenyl-derived organometallic complexes reported in the literature. However, as seen in the antimycobacterial studies, the IC_{50} values obtained for the synthesised complexes are not comparable to that of clinically available antimalarial drugs. With regard to these ferrocenyl complexes, there seemed to be no correlation between nuclearity and antiplasmodial activity. The overall trend in activity, which is contrary to what was observed in the antimycobacterial screening, can be summarised as shown below.

ferrocenyl-amino* > *ferrocenylthiosemicarbazone* > *ferrocenyl-imino

5.2 Future Work

While some of the complexes prepared in this study exhibited promising biological activity, the activity of others may have been hindered by their physical and chemical properties. In terms of the polynuclear complexes prepared in this study, the low solubility played a major role in the determination of the biological activity. Improving the solubility and perhaps incorporating water-soluble groups to confer water-solubility, may improve the biological activity and the chemical properties in general. It has widely been observed in the literature that lipophilicity is an important factor in improving biological activity in many different microbial diseases. However, water-solubility may also be a favourable property in this regard and perhaps a good balance between lipophilicity and water-solubility would lead to new interactions in biological systems as well as aiding in permeation of cell walls and membranes.

Since the incorporation of the lipophilic silicon moiety resulted in enhanced antiplasmodial activity in this study, future synthetic work could involve the preparation and biological evaluation of carbosilane dendrimers. In order to confer water-solubility to the complexes synthesised in this project, the dendritic scaffold could be altered to incorporate water-soluble moieties. In this regard, the poly(amidoamine) (PAMAM) scaffold could be used. A series of PAMAM analogues of the synthesised complexes could be prepared and biologically evaluated, to determine the effect of the water-solubility on the activity.

In addition, the compounds that displayed good activity in the preliminary biological evaluations could be pursued in further tests. The ferrocenyl-derived amino complexes, which displayed promising activity against the chloroquine-sensitive (CQS) NF54 strain of *Plasmodium falciparum*, should be evaluated against a chloroquine-resistant (CQR) strain. Mechanistic studies such as β-haematin inhibition studies and cysteine protease inhibition studies could be performed in order to determine the possible mode of antiplasmodial action.